Intricacies of Modeling and Analysis of DC Characteristics of Single- and Multi-Channel Laterally-Gated AlGaN/GaN Heterojunction Field Effect Transistors

Mauricio Buitrago

A Thesis
In the Department of
Electrical and Computer Engineering

Presented in Partial Fulfillment of the Requirements
For the Degree of
Master of Applied Science (Electrical and Computer Engineering) at
Concordia University
Montreal, Quebec, Canada

August 2021

CONCORDIA UNIVERSITY
SCHOOL OF GRADUATE STUDIES

This is to certify that the thesis prepared

By: Mauricio Buitrago

Entitled: "Intricacies of Modeling and Analysis of DC Characteristics of Single- and Multi-Channel Laterally-Gated AlGaN/GaN Heterojunction Field Effect Transistors"

And submitted in partial fulfillment of the requirements for the degree of

Master of Applied Science (Electrical and Computer Engineering)

Complies with the regulations of this university and meets the accepted standards with respect to originality and quality.

Signed by the final examining committee:

_____ Chair
Dr. M. Z. Kabir

_____ Examiner, External to the Program
Dr. Arash Mohammadi

_____ Examiner
Dr. M. Z. Kabir

_____ Supervisor
Dr. P. Valizadeh

Approved by: _____
Dr. Yousef R. Shayan, Chair
Department of Electrical and Computer Engineering

August 25, 2021
Date of defence

_____
Dr. Mourad Debbabi, Dean
Faculty of Engineering and Computer Science

Abstract

Intricacies of Modeling and Analysis of DC Characteristics of Single- and Multi-Channel Laterally-Gated AlGaN/GaN Heterojunction Field Effect Transistors

Mauricio Buitrago

The present thesis offers a detailed description about the modeling of single- and multi-channel laterally-gated AlGaN/GaN heterojunction field effect transistors (HFETs) through device investigation in the Comsol Multiphysics® simulation environment. After two decades of research, studying GaN HFETs continues to be a very interesting area of investigation. This is because of the interest in using these devices in high frequency applications as well as low frequency power management. Laterally-gated GaN HFETs have recently drawn the attention of semiconductor devices engineers that search for obtaining higher current densities, higher linearity, better stability at higher frequencies, and better power management while increasing packing density.

The presented simulations offer an in-depth analysis of the observations made at thermal equilibrium and the results obtained for the DC characteristics of these devices, along with the comparison of these characteristics with those of the top-gated varieties. These observations demonstrate the improved effectiveness of lateral gating in controlling multiple vertically stacked 2DEG channels. Although there is improvement on several parameters like current density, linearity, and ON resistance (R_{on}), as the number of channels increases, simulations demonstrate a certain degree of degradation of drain-induced barrier lowering (*DIBL)* and knee voltage (V_{knee}). For these simulations, the devices' self-heating at higher current densities was not considered. Also, the ohmic contacts were assumed to be ideal.

Acknowledgements

First, I would like to thank my supervisor Dr. Valizadeh for his continuous support, guidance and patience, and also for his prompt responses every time I needed a feedback during this period of isolation in which we all had to work remotely. His invaluable knowledge and assistance helped me keep motivated on learning and developing a critical thinking about what is obtained from results and what is found in reported works related to this field of study.

I would also like to acknowledge my colleagues from the Reliable Electron Devices group Mehrnegar Aghayan, Yatexu Patel, and Iqbal Singh for sharing their experiences and knowledge in Comsol, which gave me ideas for improving the techniques for simulations.

Furthermore, I would like to thank CMC Microsystems support team, for solving issues with the CAD Compute Cluster, which helped me speed up simulations and served as an alternative tool to run heavy computations in parallel, specially when the complexity of the models increased.

In addition, thanks to my wife for her constant confidence and love. Finally, thanks to my parents for having taught me to follow my dreams and trust myself.

Contents

List of Figures

List of Tables

List of Abbreviations

Abbreviation	Description
2DEG	Two-dimensional electron gas
2DHG	Two-dimensional hole gas
DIBL	Drain-Induced Barrier Lowering
E-field	Electric field
E-mode	Enhancement-mode
FEM	Finite Element Method
FP	Field-Plate
GVS FOM	Gate voltage swing figure of merit
HFET	Hetero-junction field effect transistor
MIS	Metal-insulator-semiconductor
RF	Radio frequency
SCE	Short-Channel-Effects
SS	Subthreshold Swing

Chapter 1

Introduction

III-Nitride-based HFETs have been intensively investigated since 1993 [1] and have been demonstrated as one of the most suitable options for high frequency and high voltage applications. This is primarily thanks to the material properties of GaN, and many other III-Nitrides, such as high peak electron velocity, thermal stability, and wide bandgap [2]. Most of the GaN HFETs that have been developed since have either a Schottky, a p-n, or a metal-insulator-semiconductor (MIS) gate defined on the top exposed surface of the epilayer. However, more recently a number of different geometries concerning the position of the gate contact are being investigated to offer higher current densities and broader gate transconductance in order to satisfy a variety of needs including higher power density and better frequency response in applications such as 5G networks (where these devices operate at the base station side) and electric vehicles - EV (where they can operate at voltages in the order of ~600V).

1.1 III-Nitrides material properties and basics of III-Nitrides HFETs

March of the AlGaN/GaN heterostructures is primarily the result of exhaustive experimental and theoretical work on the *Wurtzite III-Nitrides* (including *GaN*, *InN*, *AlN*, and their alloys like AlGaN). When AlGaN and GaN are pseudomorphically grown one on top of the other, the result is the inherent induction of two components of polarization at the heterointerface: spontaneous and

piezoelectric. The polarization fields are responsible for induction of a high concentration of carriers at one side of the heterojunction, which in case of Ga-face tensile-strained AlGaN grown on a GaN template is the GaN layer (referred also as the channel, whereas AlGaN is known as the barrier). The vertically-confined sheet charge density in the channel is also known as the two-dimensional electron gas (2DEG) [2] [3] [4].

The *Wurtzite III-Nitrides* are part of the *noncentrosymetric compound crystals*, which have two orders of atomic layering pointing in opposite directions that are parallel to reference crystallographic axes. The wurtzite structure of GaN has the sequence of Ga and N atomic bilayers inverted along the [0001] and [000$\bar{1}$] directions, from which the *Ga-face* and *N-face* names of polarities are given to the (0001) and (000$\bar{1}$) crystalline faces, respectively. These face polarities in the pseudomorphically grown *Wurtzite III-Nitride* heterostructures are formed by the placement of a hexagonal arrangement of cations in close proximity to another one of anions forming a bilayer. For a *Ga face* GaN, Ga is on top of the {0001} bilayer. In contrast, if N is on top, it corresponds to *N face* polarity [2] [3]. This is illustrated in Figure 1.1.

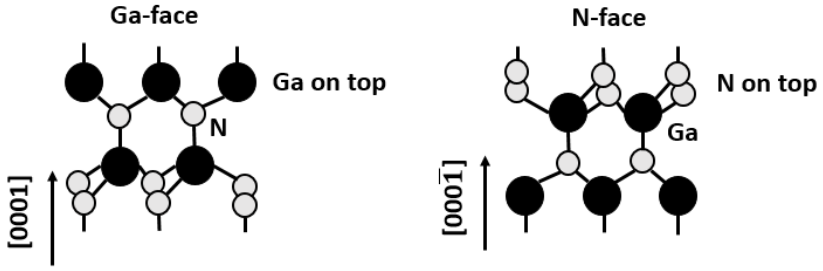

Figure 1.1 Representation of the *wurtzite* crystal structure of GaN in Ga-face and N-face [2].

The strong spontaneous and piezoelectric polarizations induced in the *Wurtzite III-Nitride* heterostructures make the carrier concentration of the 2DEG depend mainly on the properties of the materials such as the Al mole fraction (x), polarization, thickness of the barrier and channel layers, and the degree of lattice mismatch between the constituting layers. This is contrast to other

heterostructures where the dopant concentration takes the prominent role in determining the 2DEG concentration. Since Al mole fraction has a strong impact on the device performance, the expression $Al_xGa_{1-x}N/GaN$ is used rather than just AlGaN/GaN.

As mentioned earlier, the carrier concentration of the 2DEG at the heterojunction of III-Nitrides is primarily induced by the effect of the spontaneous and piezoelectric polarizations. This can be summarized mathematically by equation (1.1), where $\rho(P)$ is the concentration of polarization-induced charge carriers in C/m^2 and ∇ is de divergence of the polarization in space [3]:

$$\rho(P) = \nabla \cdot (\overrightarrow{P_{SP}} + \overrightarrow{P_{PE}}) \tag{1.1}$$

In equation (1.1), $\overrightarrow{P_{SP}}$ represents the algebraic sum of the spontaneous polarizations of the barrier and the channel and $\overrightarrow{P_{PE}}$ represents the algebraic sum of the piezoelectric polarizations of the barrier and the channel.

Figure 1.2 represents the different scenarios for the direction of the spontaneous and piezoelectric polarization vectors in pseudomorphically grown AlGaN/GaN and GaN/AlGaN Ga-face and N-face heterojunctions. One of the most common cases which also applies to this thesis is that of Ga-face AlGaN/GaN, in which the direction of both polarization vectors are the same (and opposite to the direction of the epilayer's growth). This mode of growth induces a considerably strong carrier concentration of the 2DEG in the channel layer. In contrast, when the face is changed as in Figure 1.2(b), the induced sheet charge density of the 2DEG will be reduced, which may indicate the presence of a two-dimensional hole gas instead.

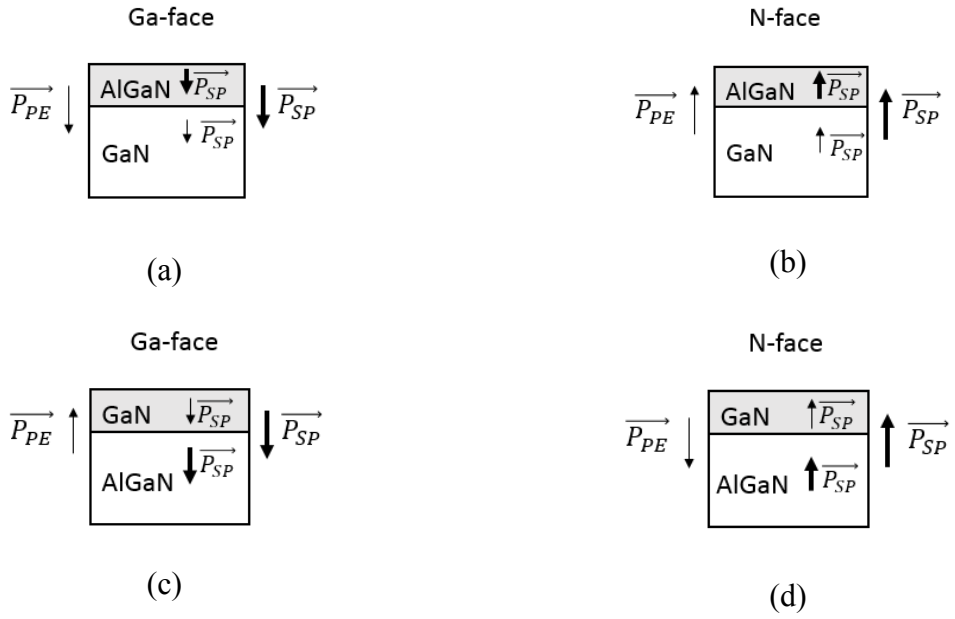

(a) (b) (c) (d)

Figure 1.2 Directions of the spontaneous and piezoelectric polarization vectors in pseudomorphically grown (a)-(b) AlGaN/GaN and (c)-(d) GaN/AlGaN heterostructures [3].

Figure 1.3 shows the schematic of a conventional top-gated AlGaN/GaN HFET along with the typical conduction-band edge bending at thermal equilibrium. The position of the fermi level (E_f) with respect to the bottom of the conduction band (E_c) at the heterojunction indicates the strong effect polarization has on the induction of a high concentration of carriers at the GaN channel layer.

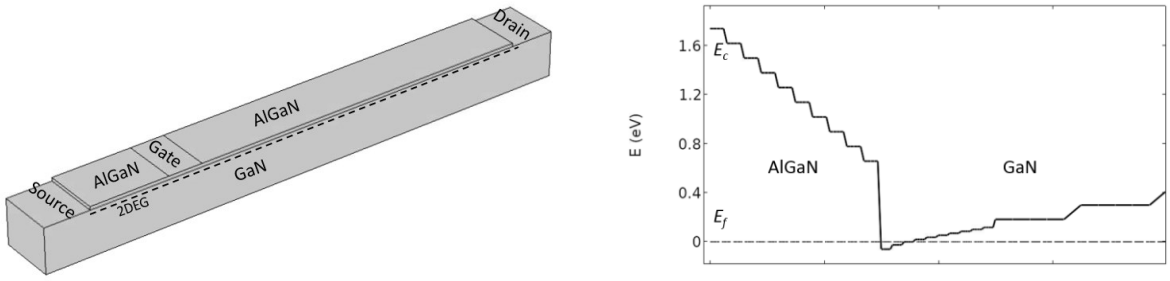

(a) (b)

Figure 1.3 (a) Schematic of a conventional top-gated pseudomorphically grown Ga-face AlGaN/GaN HFET. (b) Conduction-band edge bending at thermal equilibrium obtained by simulation of the Ga-face AlGaN/GaN HFET with Al mole fraction of 0.2. The artificial staircase observed in (b) is caused by the adopted mesh in numerical simulation. The finer the adopted mesh, the less pronounced the artificial staircase.

1.2 Limitations of conventional top-gated AlGaN/GaN HFETs

Over the past two decades, important progress in high frequency and power applications has been achieved with conventional AlGaN/GaN HFETs [5] [6] [7]. In addition, improvements in gate transconductance to achieve higher linearity have been proposed in the last ten years [8] [9], [10] [11]. However, it has also been demonstrated that this type of device faces degradation that comes from high values of electric field (E-field) next to the gate, which reduces the carrier concentration of the 2DEG and therefore the maximum drain current density [12]. Besides, experimental reports on electron-phonon scattering models demonstrate that the effective electron velocity is impacted at higher concentration of carriers in the channel, causing the gate transconductance to drop [13] [14]. Several experimental and theoretical works have demonstrated that through gating the 2DEG by a lateral E-field instead of a vertical one, the maximum values in current density, gate transconductance, and frequency response can be improved further [15] [16] [17] [18].

One of the design ideas that is showing promising results in terms of drain current density (I_D) and gate transconductance (G_m) enhancement, and higher linearity is the implementation of multiple 2DEG channels stacked vertically. This solution represents a big challenge for a top-gated AlGaN/GaN HFET topology. This is because the distance from the gate to the channels gets larger as the number of channels increases, resulting in very large negative threshold voltages (V_{TH}) and reduced values of gate transconductance as experimentally corroborated by Ma *et al.* [19], Nela *et al.* [20], and Ma *et al.* [21].

To achieve an efficient controllability of the multiple channels while fulfilling the requirements of higher current densities and higher peaks of gate transconductance along with

higher linearity, AlGaN/GaN HFETs with laterally positioned gates have been recently studied, showing promising results for their employment in high frequency and high power applications [17] [22] [19] [21] [20]. This comes also with the advantage of reduction in ON resistance (R_{on}) with the addition of the number of channels, which offers better power management at higher current densities.

1.3 Research Objectives

Since the investigation on the laterally-gated polar AlGaN/GaN HFETs is quite recent, the following objectives have been defined in order to expand the knowledge on this field:

- To explain in detail how to calculate and incorporate the AlGaN alloy parameters and the polarization parameters of AlGaN/GaN heterojunctions for realistic modeling scenarios.
- To implement the modeling of the single- and multi-channel laterally-gated AlGaN/GaN HFETs in Comsol. Two types of varieties are modeled: a hypothetical Ga-face variety devoid of polarization, whose study will serve to further highlight the role of polarization, and a second variety with realistic Ga-face polarity.
- To provide an in-depth analysis of the observations made at thermal equilibrium as well as the DC characteristics of the aforementioned novel device varieties in comparison with conventional top-gated HFETs modeled also in Comsol, addressing the benefits and drawbacks of single- versus multi-channel devices and how these characteristics may impact the implementation of the devices in real applications.

1.4 Thesis outline

This thesis is concentrated on the modeling and analysis of the DC characteristics of laterally-gated single- and multi-channel AlGaN/GaN HFETs of both cases: with the assumption of no polarization and with Ga-face polarity for different values of Al mole fraction. Chapter 2 offers a detailed explanation of how AlGaN/GaN HFETs can be modeled in Comsol Multiphysics® [23] to have a realistic scenario for simulations. This chapter also describes how to calculate the values of the physical parameters of the $Al_xGa_{1-x}N$ alloy for a given Al mole fraction (x) and gives details about the incorporation of the polarization induced fixed charge density in Comsol along with the calculation of the corresponding parameters and the values of polarization and sheet carrier concentration of the 2DEG, also for a given Al mole fraction. The same chapter contains information on the geometry, dimensions, and doping concentrations for the single- and multi-channel structures to be considered in the next two chapters and talks about the meshing strategies to take into account for getting convergence when running the computations in Comsol.

DC characteristics of the hypothetical Ga-face laterally-gated AlGaN/GaN HFETs that are devoid of polarization are presented in Chapter 3 in order to highlight the role of polarization.

For the realistic case where polarization is present, the same structure as in Chapter 3 is adapted in Chapter 4 for exposing the analysis of results of the single- and multi-channel laterally-gated Ga-face AlGaN/GaN HFETs.

Finally, Chapter 5 provides the conclusion and proposes future works.

Chapter 2

Intricacies of modeling the laterally-gated AlGaN/GaN HFET in Comsol

As outlined at the end of 0, the approach adopted in modeling the laterally-gated AlGaN/GaN HFET in Comsol was to first disable the polarization parameter often incorporated in terms of the "*Surface Charge Density,*" study the impact of this type of gating on the single-channel and the multi-channel HFETs, and then proceeding with its activation and increasing its value gradually to analyze the behavior of this type of a device structure at different levels of polarization associated with the aluminum (Al) mole fraction of the AlGaN barrier layer, also on both single- and multi-channel HFETs.

2.1 Schematic of the single-channel laterally-gated AlGaN/GaN HFET

Figure 2.1 shows the schematic of the single-channel laterally-gated AlGaN/GaN HFET explored in this thesis. Table 2.1 lists the parameters and dimensions associated with the illustrated structure in this figure. These parameters are given following the experimental work of Shinohara *et al.* [15]. Table 2.2 summarizes the doping concentrations associated with each epitaxial layer of the structure.

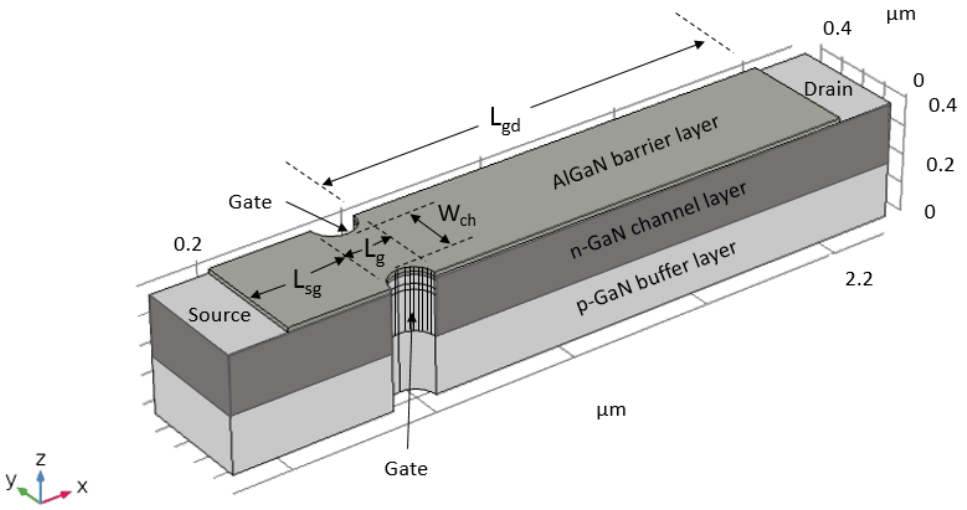

Figure 2.1 Schematic of the single-channel laterally-gated $Al_xGa_{1-x}N$/GaN HFET explored in this thesis.

Table 2.1 Structural dimensions of the single-channel laterally-gated AlGaN/GaN HFET shown in Figure 2.1.

	Dimension (nm)
AlGaN barrier layer	Thickness: **15**
GaN channel layer	Thickness: **200**
GaN buffer layer	Thickness: **200**
Source contact	Length: **200**
Drain contact	Length: **200**
Source-to-gate distance (L_{sg})	Length: **350**
Gate length (L_g)	Length: **150**
Gate-to-drain distance (L_{gd})	Length: **1500**
Channel width (W_{ch})	Width: **250** (for the hypothetical polarization-less HFET structure) **150** for the real Ga-face HFET structure

The difference in channel widths (W_{ch}) listed in Table 2.1 for the two varieties of the laterally-gated AlGaN/GaN HFETs comes from the impact a realistic Ga-face polarity has on the effectiveness of the lateral gates to deplete the 2DEG. As it will be shown in Chapter 4, the wider the W_{ch} the more challenging would be the depletion of the channel by using exclusively lateral E-fields.

Table 2.2 Doping concentrations of the epitaxial layers in the single-channel laterally-gated AlGaN/GaN HFET structure shown in Figure 2.1.

	Doping concentration (cm^{-3})
AlGaN barrier layer for the hypothetical polarization-less structure[1]	10^{18} n-type - Uniformly doped
AlGaN barrier layer for the realistic Ga-face structure	Top 14 nm: 10^{15} n-type – Uniformly doped Bottom 1nm: $\sim 10^{20}$ n-type – Uniformly doped[2]
GaN channel layer	10^{14} n-type - Uniformly doped
GaN buffer layer	10^{18} p-type - Uniformly doped
Source and drain contacts	10^{20} n-type – Uniformly doped 4nm below the ohmic contacts followed by a Gaussian profile with its peak at a Projected Range (R_p) of 4nm and a standard deviation or "straggle" (ΔR_p) of about 1nm.

[1] Details about the incorporation of polarization and the choice of the doping concentration values are explained in section 2.3.

[2] The exact value of the 1-nm AlGaN barrier doping concentration for the realistic Ga-face polarity depends on the Al-mole fraction (x). Details are given in section 2.3. Values for $x = 0.1$ and 0.2 are listed in Table 2.4

In terms of simulations for achieving a close to ideal contact, it was tested and confirmed that the position of the source and drain's ohmic contacts can be either at the level of the GaN channel layer as in Figure 2.1, where a 4nm-thick highly doped (10^{20} cm^{-3}) n-type region is defined below each ohmic contact followed by a Gaussian profile with its peak at a Projected Range (R_p) of 4nm and a standard deviation (straggle) (ΔR_p) of about 1nm, or at the same level of the AlGaN barrier layer, where heavily doped (10^{20} cm^{-3}) n-type GaN regions are defined for source and drain from the top of AlGaN up to several nanometers below the heterojunction in order to assure contact with the 2DEG. This was confirmed by successfully testing both approaches without any tangible change among the simulated DC characteristics.

The gates are defined as vertical, cylindrical pillars from the top of the AlGaN barrier layer up to the bottom of the GaN channel layer. They are Schottky contacts with a metal work function ($q\Phi_M$) of 5.2 eV, which corresponds to Platinum.

2.2 Introduction of alloy III-Nitride material parameters

After defining the geometry of the structure, another important step to complete in Comsol is the definition of material parameters. By default, the software includes several materials such as GaN. However, since the material parameters of the $Al_xGa_{1-x}N$ alloy depend on the Aluminum mole fraction (x) [2] [3] [4], it is necessary to calculate and incorporate them for any given value of x. For the structure depicted in Figure 2.1, the value used for aluminum mole fraction was either 0.28, 0.1, or 0.2. The latter two cases where specifically used in simulations reported in Chapter 4, while the first in simulations of Chapter 3.

For these values of *x,* the following parameters were calculated using the expressions extracted from the work of Ambacher *et al.* [2] [4] according to the application of Vegard's law [3]. With the purpose of offering a clear explanation, the calculations of the parameters for x = 0.28 are shown next to each equation. Following this, Table 2.3 summarizes the values of these parameters for the three previously mentioned values of Al mole fraction.

- **Bangap Energy ($E_{g\text{-}AlGaN}$):**

$$\boldsymbol{E_{g-AlGaN}}(x) = xE_{g-AlN} + (1-x)E_{g-GaN} - x(1-x)b, \tag{2.1}$$

where b is the bowing parameter of value $b = 1.0\ eV$ [24]. Therefore, using the corresponding bandgaps for AlN and GaN, and neglecting the effect of bowing, from equation (2.1):

$$\boldsymbol{E_{g-AlGaN}}(x = 0.28) = (0.28)(6.13\ eV) + (1-0.28)(3.42\ eV),$$

$$\boldsymbol{E_{g-Al_{0.28}Ga_{0.72}N}} = 4.178\ eV.$$

- **Electron affinity ($q\chi_{AlGaN}$):**

$$q\boldsymbol{\chi}_{AlGaN}(x) = xq\boldsymbol{\chi}_{(AlN)} + (1-x)q\boldsymbol{\chi}_{(GaN)}. \tag{2.2}$$

Using the corresponding values of electron affinity for AlN and GaN, equation (2.2) will give:

$$q\boldsymbol{\chi}_{AlGaN}(x = 0.28) = (0.28)(0.6) + (1-0.28)(4.1),$$

$$q\boldsymbol{\chi}_{Al_{0.28}Ga_{0.72}N} = 3.12\ eV.$$

- **Static relative permittivity ($\mathcal{E}_{AlGaN}$):**

$$\boldsymbol{\varepsilon}_{AlGaN}(x) = -0.5\ x + 9.5, \tag{2.3}$$

After replacing the value of x = 0.28 in equation (2.3), the value of static relative permitivity will be:

$$\boldsymbol{\varepsilon}_{Al_{0.28}Ga_{0.72}N} = 9.36.$$

- **Effective conduction and valence band density of states (N_c *and* N_v respectively):**

These parameters depend on the effective mass of electrons (m_n^*) and holes (m_p^*) and the temperature of the lattice [3] and are given by:

$$\boldsymbol{N}_c = 2\left(\frac{2\pi m_n^* kT}{h^2}\right)^{3/2}, \tag{2.4}$$

$$\boldsymbol{N}_v = 2\left(\frac{2\pi m_p^* kT}{h^2}\right)^{3/2}, \tag{2.5}$$

where k is the *Boltzmann* constant, equal to 1.38×10^{-23} J/K; T is the temperature in Kelvin, which at room temperature is ~300K; and h is the *Planck's* constant, equal to 6.63×10^{-34} J · s.

In order to calculate the values of the effective mass of electrons and holes, the *virtual crystal approximation* applied in *Vegard's law* dictates that the alloy's carrier effective mass is related to the masses of the parent semiconductors (in this case AlN and GaN), by the following expression [3]:

$$\frac{1}{m^*_{Al_xGa_{1-x}N}(x)} = \frac{x}{m^*_{AlN}} + \frac{1-x}{m^*_{GaN}} \ . \tag{2.6}$$

Using the data from [3] and [25], the values of effective mass for electrons in AlN and GaN are $m^*_{n-AlN} = 0.4m_0$ and $m^*_{n-GaN} = 0.2m_0$ respectively, and the values of effective mass for holes in AlN and GaN are $m^*_{h-AlN} = 7.26m_0$ and $m^*_{h-GaN} = 0.8m_0$ respectively, where $m_0 = 9.1 \times 10^{-31}\ kg$ is the rest mass of electron. Therefore, from equation (2.6), the effective mass of electrons and holes in $Al_{0.28}Ga_{0.72}N$ are respectively:

$$m^*_{n-Al_{0.28}Ga_{0.72}N} = 0.232\ m_0,$$

and

$$m^*_{h-Al_{0.28}Ga_{0.72}N} = 1.066\ m_0.$$

Following this calculation, from equations (2.4) and (2.5), the effective conduction band density of states and the effective valence band density of states at $T = 300\ K$ are respectively:

$$\boldsymbol{N_c} = 2.77 \times 10^{18}\ cm^{-3},$$

and

$$\boldsymbol{N_v} = 2.75 \times 10^{19}\ cm^{-3}.$$

- **Electron mobility (μ_n) and hole mobility (μ_p):**

Expectedly, the values reported for low-field electron and hole mobilities in $Al_xGa_{1-x}N$ alloys are sparse and variable within a range. There are several experimental reports on Hall measurements of very low electron mobilities in AlGaN at different Al mole fractions: from $\mu_n=35\ cm^2/V{\cdot}s$ with $x=0.09$ and carrier concentration of $5 \times 10^{18}\ cm^{-3}$ [26], or $\mu_n=50\ cm^2/V{\cdot}s$ with $x=0.75$ and carrier concentration of $10^{18}\ cm^{-3}$ [27],to $\mu_n=80\ cm^2/V{\cdot}s$ with $x=0.3$ and carrier concentration of $3 \times 10^{18}\ cm^{-3}$ [28]. Regarding the low-field hole mobility, values of $\mu_p=9\ cm^2/V{\cdot}s$ at $x=0.08$ and carrier concentration of $1.48 \times 10^{19}\ cm^{-3}$ [29], and $\mu_p=2.7\ cm^2/V{\cdot}s$ at $x=0.3$ and hole concentration of $2.2 \times 10^{17}\ cm^{-3}$ [30] have been reported. All these reported measurements were made at room temperature. It is important to note that since the 2DEG is formed in GaN, the value set for mobility in the AlGaN barrier layer may not have a big impact on the results of simulations unless a parallel channel is formed in the AlGaN barrier. Taking into consideration the mentioned reported values, the low-field electron and hole mobilities for $x = 0.28$ were respectively set in Comsol as:

$$\boldsymbol{\mu_n} \approx 80\ cm^2/V \cdot s,$$

$$\boldsymbol{\mu_p} \approx 10\ cm^2/V \cdot s.$$

Table 2.3 Parameters of the $Al_xGa_{1-x}N$ barrier layer used to model the AlGaN/GaN HFET in the Semiconductor module of Comsol.

Parameter	Value (x=0.1)	Value (x=0.2)	Value (x=0.28)
Bandgap Energy ($E_{g\text{-}AlGaN}$)	3.691 eV	3.962 eV	4.178 eV
Electron affinity ($q\chi_{AlGaN}$)	3.75 eV	3.4 eV	3.12 eV
Permitivity ($\mathcal{E}_{AlGaN}$)	9.45	9.4	9.36
Effective conduction band density of states (N_c)	2.41×10^{18} cm^{-3}	2.61×10^{18} cm^{-3}	2.77×10^{18} cm^{-3}
Effective valence band density of states (N_v)	2.05×10^{19} cm^{-3}	2.39×10^{19} cm^{-3}	2.75×10^{19} cm^{-3}
Electron mobility (μ_n)	40 cm^2/V·s	80 cm^2/V·s	80 cm^2/V·s
Hole mobility (μ_p)	10 cm^2/V·s	10 cm^2/V·s	10 cm^2/V·s

2.3 Incorporation of polarization in the laterally-gated AlGaN/GaN heterostructure

- Hypothetical Ga-face polarity with no polarization

As mentioned at the beginning of this chapter, to further highlight the role of polarization in functioning of the laterally-gated single- and multi-channel AlGaN/GaN HFETs, in a hypothetical case to be reported in Chapter 3, the inclusion of polar charge was not considered at the AlGaN/GaN heterojunction. This was done by keeping the parameter known in Comsol as "*Surface Charge Density*" deactivated. In this case, in absence of polarization, the AlGaN barrier layer has been highly doped to the level of 10^{18} cm^{-3} in order to let modulation doping take effect by having electron accumulation at the GaN side of the heterojunction in the form of the 2DEG

[3]. This type of hypothetical structure which is elaborated further below can be seen in resemblance to what is known as a pseudomorphically grown AlGaN/GaN epilayer in N-face.

In N-face AlGaN/GaN heterostructures, the direction of the spontaneous and piezoelectric polarization vectors ($\overrightarrow{P_{SP}}$ and $\overrightarrow{P_{PE}}$, respectively) is normal to the heterointerface and in the same direction of the growth (positive) [4]. This can be appreciated in Figure 2.2.

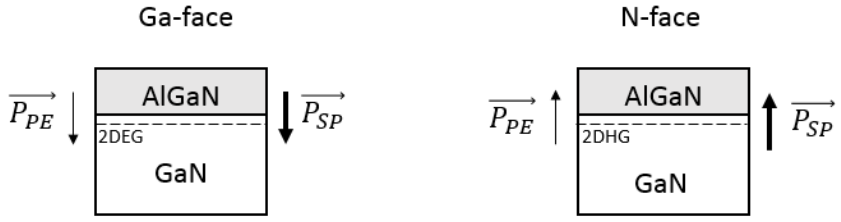

Figure 2.2 Representation of the direction of the spontaneous and piezoelectric polarization vectors ($\overrightarrow{P_{SP}}$ and $\overrightarrow{P_{PE}}$, respectively) in pseudomorphically grown AlGaN/GaN Ga-face and N-face heterostructures.

While in the Ga-face the spontaneous and piezoelectric polarizations support the induction of a substantial 2DEG in GaN behind the conduction band discontinuity (ΔE_c), in N-face the opposite direction of the polarization components results in the induction of a much weaker 2DEG concentration, in addition to yielding possibility for the induction of a two-dimensional hole gas (2DHG). The latter of which according to the calculations presented in section 2.2 in terms of lacking a positive valence band discontinuity (ΔE_v) seems unlikely.

- **Realistic Ga-face polarity**

To achieve a functional Ga-face AlGaN/GaN heterostructure that gives the appropriate value of sheet charge density corresponding to well-known predictions of [2] and [4], there are two methods that can be employed in Comsol to effectively incorporate the effect of the spontaneous and piezoelectric polarization. The first method consists of activating the parameter

called "*Surface Charge Density*," which is placed at the junction between AlGaN and GaN and then assigning to it the value of polarization induced charge that corresponds to the specific Al mole fraction (x) and the calculated sheet charge density of the 2DEG [2] [4]. The second method does not use the "*Surface Charge Density*" parameter but the scheme of doping known as "*delta doping,*" [3] [31], which consists of having a highly doped 1nm-thickness of the AlGaN barrier layer at its bottom, just above the heterojunction, and allows the induction of a large 2DEG concentration at the GaN side of the heterojunction. Equivalently, this 1nm-AlGaN doping concentration is set up so that the calculated sheet charge density of the 2DEG, which depends on Al mole fraction (x) is obtained in the simulation.

The value to be set up for the "*Surface Charge Density [C/m^2]*" parameter, which is used in the first method mentioned in the previous paragraph, is calculated based on the expressions provided by Ambacher *et al.* [2] [4], where this parameter is referred to as the "*Polarization Induced Sheet Charge (σ) [C/m^2].*" This parameter depends on both the spontaneous and piezoelectric polarization vectors ($\overrightarrow{P_{SP}}$ and $\overrightarrow{P_{PE}}$, respectively) as described in equation (2.7) [2] [4]. The fact that both polarization vector magnitudes are added together in this expression is because the vectors happen to be in the same direction as described previously, which occurs when AlGaN is grown over GaN causing the epitaxial layers to be under tensile strain,

$$\sigma(P_{SP} + P_{PE}) = \{P_{SP}(barrier) - P_{SP}(channel)\} + \{P_{PE}(barrier) - P_{PE}(channel)\}$$
$$= \sigma(P_{SP}) + \sigma(P_{PE}). \quad (2.7)$$

The two terms at the right side of equation (2.7) can be obtained from the expressions of equations (2.8) and (2.9) [2] [4] for the spontaneous polarization (P_{SP}) and the piezoelectric polarization (P_{PE}), respectively:

$$P_{SP}(x) = (-0.052x - 0.029)\ \frac{C}{m^2}\ , \tag{2.8}$$

$$P_{PE}(x) = 2\{r(x) - 1\}\left\{\frac{a_0(x) - a(GaN)}{a_0(x)}\right\} \times \left\{e_{31}(x) - e_{33}(x)\frac{C_{13}(x)}{C_{33}(x)}\right\}\frac{C}{m^2}\ . \tag{2.9}$$

From equation (2.8), the x-independent term referred to as $P_{SP}(channel)$ is not taken into account for the device modeled in this thesis. This is because what we are interested in is the discontinuity of the spontaneous polarization vector across the AlGaN/GaN heterointerface.

In equation (2.9), $r(x)$ represents the degree of relaxation. For AlGaN pseudomorphically grown on GaN and for $0 \leq x < 0.38$, $r(x) = 0$, which applies for the device modeled in this thesis. $a_0(x)$ (obtained by equation (2.10)) and $a(GaN)$ (whose value is $3.189 \times 10^{-10}\ m$) are the length of the edge of the hexagonal plane (*lattice constant*) in the wurtzite crystal structure of the AlGaN alloy of composition *x* and GaN channel layer, respectively. $e_{31}(x)$ and $e_{33}(x)$ are the piezoelectric coefficients of $Al_xGa_{1-x}N$, while $C_{13}(x)$ and $C_{33}(x)$ are the elastic constants. They can be calculated using the expressions of equations (2.11) to (2.13) [2] [4].

$$a_0(x) = (-0.077x + 3.189) \times 10^{-10}\ m, \tag{2.10}$$

$$e_{ij}(x) = \left[e_{ij}(AlN) - e_{ij}(GaN)\right] x + e_{ij}(GaN)\ \frac{C}{m^2}, \tag{2.11}$$

$$C_{13}(x) = (5x + 103)\ GPa\ , \tag{2.12}$$

$$C_{33}(x) = (-32x + 405)\ GPa\ . \tag{2.13}$$

The piezoelectric constants $e_{ij}(AlN)$ and $e_{ij}(GaN)$ are experimentally provided in different reports [32] [33] [34] and their values differ 15% and 35% for e_{33} and e_{31}, respectively. All the calculations made in the present thesis are made with the values of piezoelectric constants

reported by Bernardini *et al.* [32]. For the specific case of Al mole fraction of 0.28, after applying equations (2.7) to (2.13), the value obtained for the *Polarization Induced Sheet Charge (σ)* is:

$$\sigma_{P_{SP}+P_{PE}}(x = 0.28) = \ 0.025\ C/m^2\ ,$$

which is the value to be set up in Comsol as the "*Surface Charge Density.*" When running a simulation under Equilibrium, the value of the sheet carrier concentration of the 2DEG (*or Sheet Charge Density*) is close to the one obtained by calculation. This calculation is explained in the next paragraph.

The sheet carrier concentration of the 2DEG, $n_s(x)$, depends on several parameters of the heterostructure and can be calculated from the expression of equation (2.14) [2] [4]:

$$n_s(x) = \frac{\sigma(x)}{q} - \left(\frac{\epsilon_0 \epsilon(x)}{d_{AlGaN}\ q^2}\right)\left[q\phi_b(x) + E_f(x) - \Delta E_c(x)\right], \tag{2.14}$$

where $\sigma(x)$ is the polarization induced sheet charge calculated from equation (2.7), q is the charge of an electron with absolute value equal to $1.6 \times 10^{-19}\ C$, ϵ_0 is the permittivity of the vacuum equal to $8.85 \times 10^{-14}\ F/cm$, $\epsilon(x)$ is the static relative permittivity of $Al_xGa_{1-x}N$ given by equation (2.3), d_{AlGaN} is the thickness of the AlGaN barrier, $q\phi_b(x)$ is the Schottky barrier of the gate calculated by equation (2.15) [2] [4], $E_f(x)$ is the fermi level with respect to the bottom of the conduction band of GaN at the heterointerface obtained by equation (2.16) [2], and $\Delta E_c(x)$ is the conduction band discontinuity at the heterojunction and can be calculated from equation (2.18) [2] [4]. Accordingly,

$$q\phi_b(x) = (1.3x + 0.84)eV\ , \tag{2.15}$$

$$E_f(x) = E_0(x) + \frac{\pi\hbar^2}{m_n^*(x)} n_s(x)\ , \tag{2.16}$$

where the first energy subband of the 2DEG, $E_0(x)$, is obtained from equation (2.17) [2]. $\hbar$ represents the modified Planck's constant with expression $\hbar = {}^{h}/_{2\pi}$, and $m^*(x)$ is the effective mass of electrons obtained from equation (2.6). For $E_0(x)$ and $\Delta E_c(x)$, we have,

$$E_0(x) = \left\{ \frac{9\pi\hbar q^2}{8\epsilon_0\sqrt{8m^*(x)}} \frac{n_s(x)}{\epsilon(x)} \right\}^{2/3}, \tag{2.17}$$

$$\Delta E_c(x) = 0.7[E_g(x) - E_g(0)] \ . \tag{2.18}$$

Equations (2.14) and (2.16) are mutually dependent, for which an iterative method must be used to find $n_s(x)$ [35]. The way the iterative method was implemented is as follows:

1. An initial value of zero (*0 eV*) is assigned to $E_f(x)$ in equation (2.14) to calculate $n_s(x)$.
2. The calculated value of $n_s(x)$ is then used in equation (2.16) to obtain a new $E_f(x)$.
3. The new value of $E_f(x)$ is then used in equation (2.14).
4. Repeat steps 2 and 3 in a loop until the most recent value of $n_s(x)$ equals within a margin of error the one obtained in the preceding cycle.

It is worth mentioning that equation (2.14) is formulated considering a Schottky barrier of a gate positioned at the top of AlGaN. Although the device modeled in this thesis has lateral gates, comparisons between the values of $n_s(x)$ calculated using equation (2.14) and those obtained experimentally in many reports allows us to take comfort in the accuracy of the way we have incorporated polarization in our calculation, a factor which is independent of the way the gate is placed.

As mentioned at the beginning of this section, the second method that can be used to incorporate the realistic Ga-face polarity makes use of *delta doping* to induce the calculated sheet

carrier concentration of the 2DEG, $n_s(x)$. The doping concentration of the 1-nm AlGaN thickness close to the heterointerface is set up so that the calculated $n_s(x)$ is obtained in the simulation at thermal equilibrium. According to the observation made in Comsol, in the case of Al mole fraction of 0.28, the doping concentration of the 1-nm AlGaN region that induces the calculated $n_s(x = 0.28)$ of $1.18 \times 10^{13}\ cm^{-2}$ is $1.3 \times 10^{20}\ cm^{-3}$. For the case of x = 0.1 and 0.2, which are the values used in this thesis for simulations of the realistic Ga-face AlGaN/GaN HFETs, the calculated values for $n_s(x)$ within the delta doped layer are listed in Table 2.4.

Table 2.4 Sheet carrier concentration of the 2DEG ($n_s(x)$) obtained from equation (2.14) along with the 1-nm delta-doped AlGaN-region doping concentration used to achieve the corresponding $n_s(x)$ for x = 0.1 and 0.2 by simulation at thermal equilibrium of the realistic Ga-face AlGaN/GaN HFETs.

Al-mole fraction (x)	**$n_s(x)$ [cm^{-2}]**	**1nm-AlGaN-region doping [cm^{-3}]**
0.1	2.23×10^{12}	3×10^{19} – n-type uniformly doped
0.2	7.45×10^{12}	8.2×10^{19} – n-type uniformly doped

2.4 Schematic of the multi-channel laterally-gated AlGaN/GaN HFET

Figure 2.3 shows the schematic of the multi-channel laterally-gated AlGaN/GaN HFET modeled in this thesis. Table 2.5 and 2.6 list the dimensions and doping concentrations of the epitaxial layers, respectively. The depicted device has a total of four channels, for quad-channel AlGaN/GaN HFET.

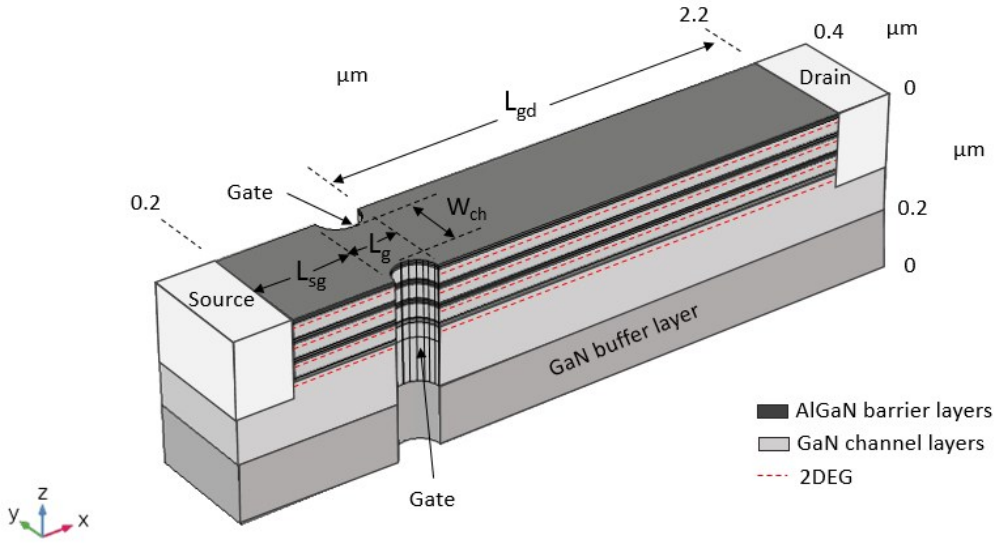

Figure 2.3 Schematic of the multi-channel (quad-channel) laterally-gated $Al_xGa_{1-x}N$/GaN explored in this thesis.

Table 2.5 Structural dimensions of the quad-channel laterally-gated AlGaN/GaN HFET structure shown in Figure 2.3.

	Dimension (nm)
AlGaN barrier layer	Thickness: **15**
Top and middle two GaN channel layers	Thickness: **50** for the hypothetical polarization-less structure **100** for the realistic Ga-face structure[3]
Bottom GaN channel layer	Thickness: **200**
GaN buffer layer	Thickness: **200**
Source contact	Length: **200**
Drain contact	Length: **200**
Source-to-gate distance (L_{sg})	Length: **350**
Gate length (L_g)	Length: **150**

[3] If not specified, the shown value applies for both heterostructures.

Gate-to-drain distance (L_{gd})	Length: **1500**
Channel width (W_{ch})	Width: **250** for the hypothetical polarization-less structure **150** for the realistic Ga-face structure[4]

Table 2.6 Doping concentrations of the epitaxial layers in the quad-channel laterally-gated AlGaN/GaN HFET structure shown in Figure 2.3.

	Doping concentration (cm^{-3})
Top and middle two AlGaN barrier layers for the hypothetical polarization-less structure	Top half: 10^{15} n-type - Uniformly doped Bottom half: 10^{18} n-type - Uniformly doped[5]
Bottom AlGaN barrier layer for the hypothetical polarization-less structure	10^{18} n-type - Uniformly doped
AlGaN barrier layers for the realistic Ga-face structure	Top 14 nm: 10^{15} n-type – Uniformly doped Bottom 1nm: $\sim 10^{20}$ n-type – Uniformly doped[6]
GaN channel layers	10^{14} n-type - Uniformly doped
GaN buffer layer	10^{18} p-type - Uniformly doped
Source and Drain Contacts	10^{20} n-type – Uniformly doped GaN regions

[4] As mentioned in section 2.1 for the single-channel device, the difference in W_{ch} for the two varieties of the laterally-gated AlGaN/GaN HFETs comes from the impact a realistic Ga-face polarity has on the effectiveness of the lateral gates to deplete the 2DEG, which is described in detail in Chapter 4.

[5] The difference in doping concentrations for the AlGaN barrier layers in the hypothetical polarization-less structure comes from the effort to achieve comparable levels of sheet charge densities between channels in order to assure their simultaneous control from the lateral gates. The details of the choice of these doping techniques are explained in section 3.1.2.

[6] The exact value of the 1-nm AlGaN barrier doping concentration for the realistic Ga-face polarity depends on the Al-mole fraction (x). Values for x = 0.1 and 0.2 are listed in Table 2.4.

The source and drain ohmic contacts to the 2DEG were achieved by having a heavily doped ($10^{20}\ cm^{-3}$) n-type GaN regions for both source and drain from the top all the way to the bottom channel, assigning an ohmic contact at the top for these.

The gates are defined the same way as in the equivalent single-channel structure, being Schottky contacts with a metal work function ($q\Phi_M$) of 5.2 eV and defined as a cylindrical metal contacts from the top of the top channel's AlGaN barrier up to the bottom of the bottom channel's GaN channel layer.

2.5 Meshing strategy for the laterally-gated AlGaN/GaN HFET

To make the Finite Element Method (FEM) work properly, the 3-D modeling of semiconductors in Comsol requires a specific type of elements (*triangular*) to build the mesh in the *x-y* plane and also a technique known as *swept mesh* to build the solid, which consists on reproducing (or sweeping) the mesh created in the 2-D plane along the *z-axis* (or vertical direction) to form the solid in 3-D [36]. For this, the "*user-controlled mesh*" option must be selected.

A mesh with triangular elements was defined at the top of the structure and then swept into the wafer. The number of triangular elements in the mesh defined in the *x-y* plane as well as that of the vertical elements during the swept mesh along the *z-axis* was tuned in order to assure acceptable time of computations without impacting the reliability of results (in other words to achieve *grid independence*). The vertical swept mesh (along the *z-axis*) was split in different regions defined within the AlGaN barrier, the GaN channel layer, and the GaN buffer layer, which offered the flexibility to distribute the number of elements vertically depending on the region. The

areas with the maximum number of elements are those close to the heterointerface and in the proximity of the gates. An example for the case of single-channel HFET is shown in Figure 2.4.

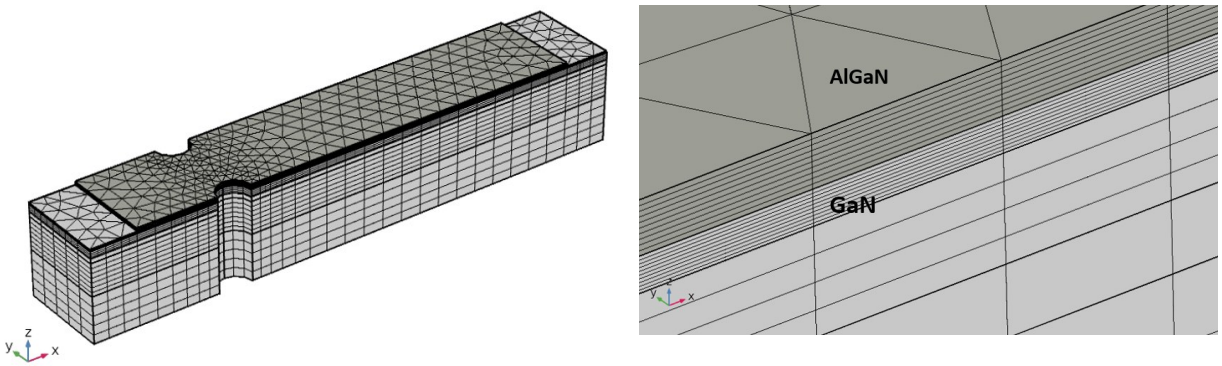

(a) (b)

Figure 2.4 An example of mesh distribution for the single-channel laterally-gated AlGaN/GaN HFET. (a) The entire structure and (b) magnified view of the AlGaN/GaN heterointerface.

It should be mentioned that this meshing technique combined with the strategy used for initial conditions can make the computations achieve a faster convergence. As an example for explaining the role of initial conditions, consider when the computation needs to be run for obtaining the $I_D - V_{GS}$ characteristics (drain current vs. gate-to-source voltage). In such a case, it is recommendable to use very low values of V_{GS} as initial conditions and then ramp it up with relatively small steps (e.g. 0.1V or 0.25V). Alternatively, during the process of trying to achieve convergence, the values of the doping concentrations of the epilayers can also be ramped up when layers need to be heavily doped.

Chapter 3

Comparison of the DC characteristics of the laterally- and top-gated AlGaN/GaN HFETs in absence of polarization-induced 2DEG

In Chapter 2, the details of how to setup in Comsol for properly modeling the laterally-gated $Al_xGa_{1-x}N$/GaN HFETs both in absence and presence of polarization were explained. This chapter shows the characteristics of the hypothetical polarization-less laterally-gated AlGaN/GaN HFETs and its comparison to the conventional top-gated AlGaN/GaN HFETs. The goal is to illustrate both under thermal equilibrium condition and upon application of the DC bias possible gains and losses from replacing the traditional top-gated structure with a lateral gate, where for simplifying the situation polarization is hypothetically assumed to be absent.

3.1 Thermal equilibrium observations

3.1.1 Single-channel laterally-gated AlGaN/GaN HFET in absence of polarization

For the device of specifications indicated in section 2.1 of the previous chapter, Figure 3.1 shows the conduction-band edge bending across the heterojunction at thermal equilibrium for both the laterally-gated and the top-gated AlGaN/GaN HFETs, where hypothetically polarization is absent. For the given dimensions, the position of E_f in regard to the bottom of E_c represents a much weaker polarization induced 2DEG for the top-gated structure, yielding in this case a positive V_{TH}, hence an enhancement mode (e-mode) characteristics.

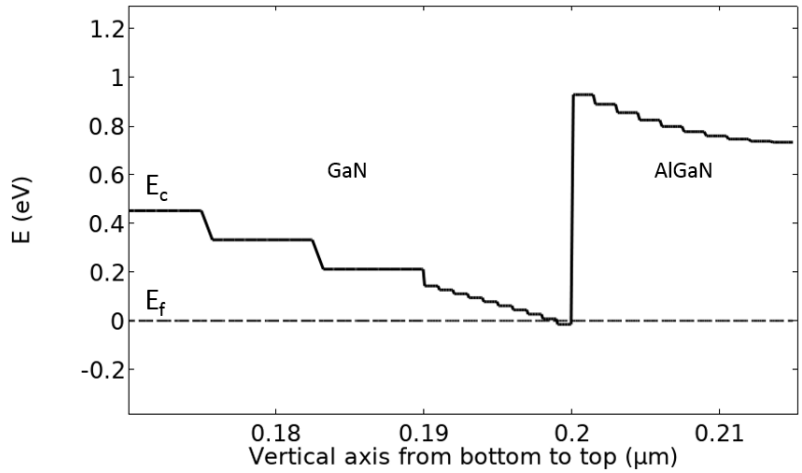

(a)

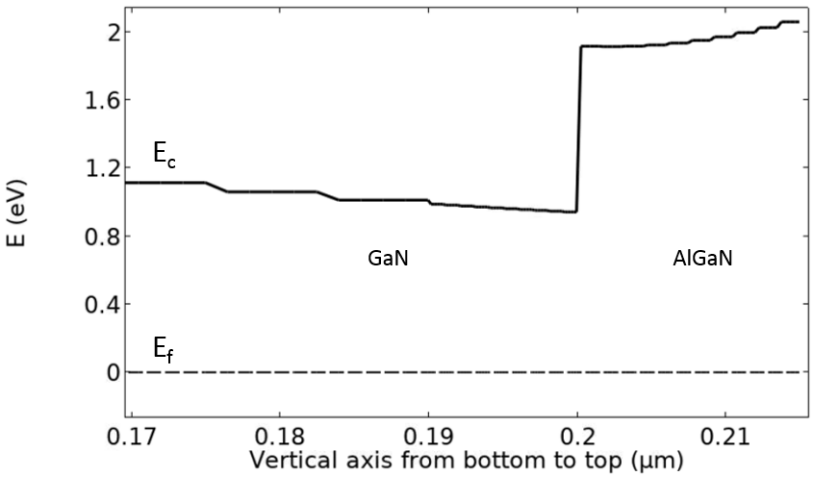

(b)

Figure 3.1 Conduction-band edge bending across the heterojunction in the gated region at thermal equilibrium for (a) the laterally-gated and (b) the top-gated AlGaN/GaN HFETs with the assumption of no polarization[7].

Figure 3.2 presents an observation on the vertical profile of E-field in the gated region among the two varieties of top- and laterally-gated AlGaN/GaN HFETs with the assumption of no polarization. The difference in the variation of E-field across the GaN channel layer among the

[7] The artificial staircase variation in different profiles presented in this thesis is caused by the rough meshing imposed by heavy computational demands of the required 3-D numerical simulations.

two structures is due to the presence of the Schottky contact of the gate at the top in the top-gated device, which has a stronger effect in this structure at thermal equilibrium on the depletion of the 2DEG (as also observed in Figure 3.1). Expectedly, this is not evidenced in areas outside the gated region, (e.g. the source and drain access regions), where the vertical E-field profile is similar to that of the laterally-gated AlGaN/GaN HFET.

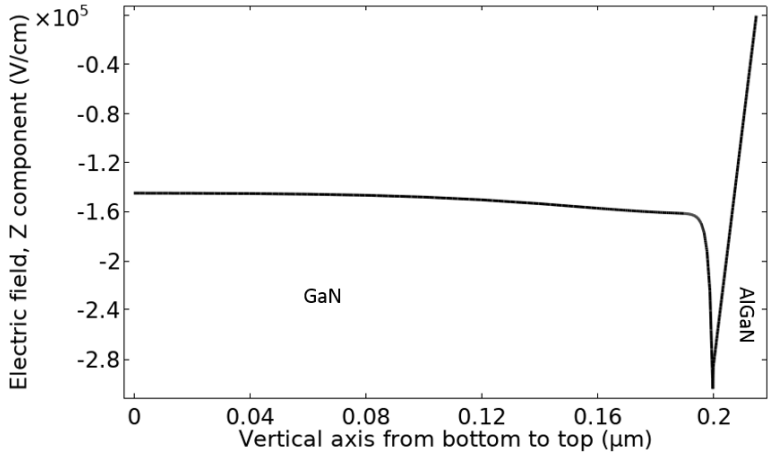

(a)

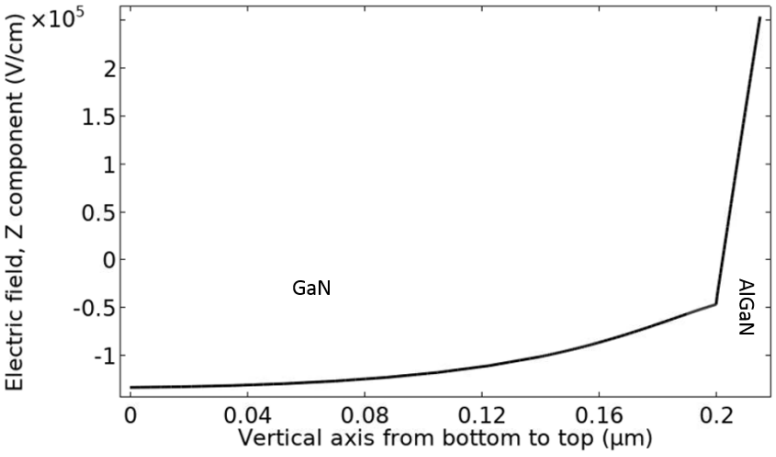

(b)

Figure 3.2 Vertical profile of the E-field across the heterojunction in the gated area at thermal equilibrium for (a) the laterally-gated and (b) the top-gated AlGaN/GaN HFETs with the assumption of no polarization.

Regarding the profile of the E-field at thermal equilibrium along the channel, Figure 3.3 shows the schematic of the aforementioned laterally-gated AlGaN/GaN HFET indicating the

locations where this lateral profile was assessed. Specifically for this device type, the longitudinal (or lateral) E-field was read from source to drain, at the heterojunction for two cases: 1) in the middle of the distance between the two gates (in other words in the middle of the channel width ($\frac{W_{ch}}{2}$)), and 2) near one of the gates (at 1nm of distance). While the laterally-gated AlGaN/GaN HFET shows little variation of its lateral E-field in the gated region when it is measured at $\frac{W_{ch}}{2}$ (Figure 3.4(a)), the variation increases near the gates, which is expected due to the presence of the metal contact of the gates (Figure 3.4(b)). The peaks in Figure 3.4(b) may be explained by the circular geometry of the gates in association with the roughness of the mesh and the non-uniform distance from the gates (along the gate length (L_g)) to the reference cut line (in red in Figure 3.3). In contrast, the lateral profile of the E-field in the studied top-gated AlGaN/GaN HFET has a much stronger variation in the gate region at the middle of the channel width compared to the laterally-gated device and it keeps the same shape along the width of the device due to the presence of the gate at the top.

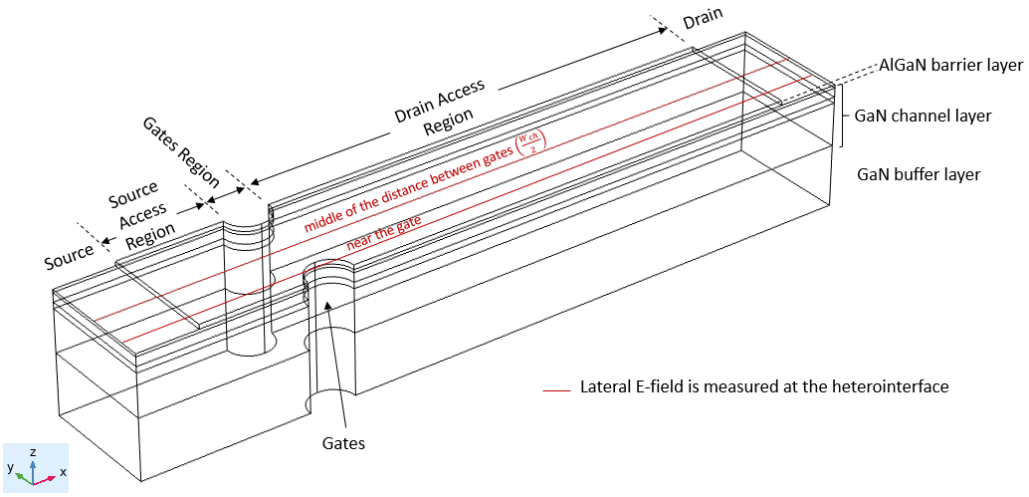

Figure 3.3 Schematic of the single-cannel laterally-gated AlGaN/GaN HFET showing the regions and points where the lateral profile of E-field was measured.

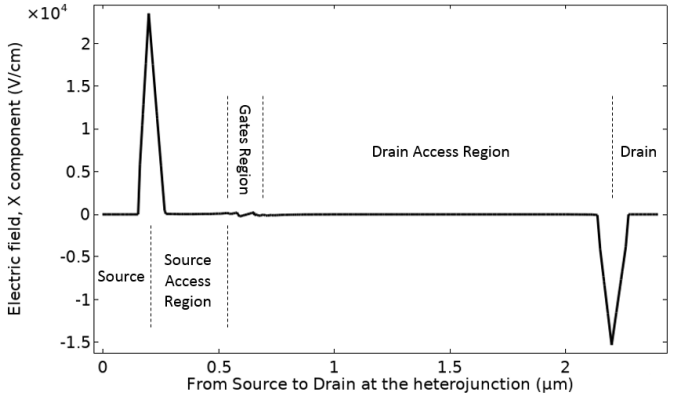

(a)

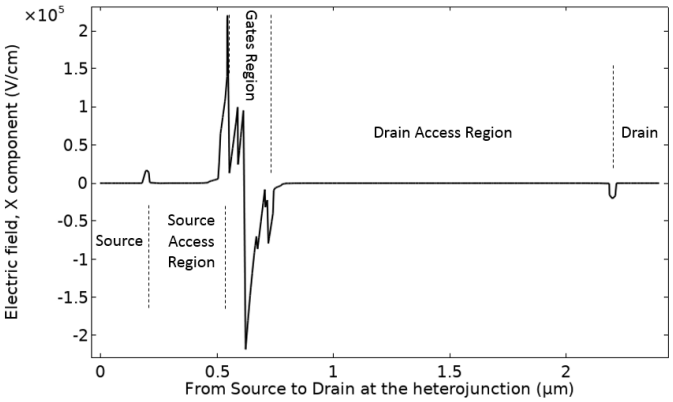

(b)

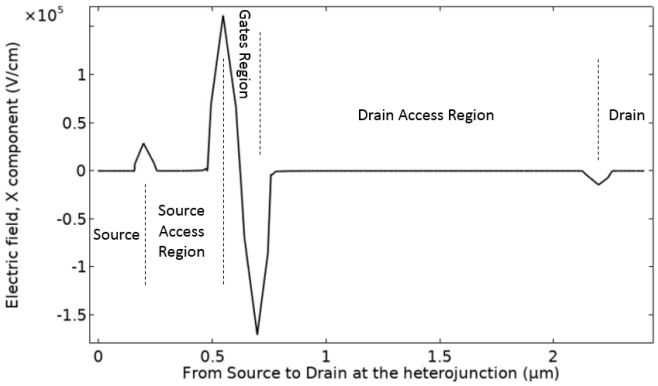

(c)

Figure 3.4 Lateral profile of the E-Field at thermal equilibrium taken at the heterojunction for the single-channel laterally-gated AlGaN/GaN HFET with the assumption of no polarization, measured at (a) the middle of the distance between gates and (b) close to one of the gates. (c) Lateral profile of the E-Field for the top-gated AlGaN/GaN HFET with the assumption of no polarization.

Although for the moment assessed in our simulations in absence of polarization and application of bias, the reduction of the E-field peak at the drain edge of the gate shown in Figure 3.4(a) for the laterally-gated AlGaN/GaN HFET has been also experimentally reported to offer an advantage over top-gated AlGaN/GaN HFETs in realizing higher channel breakdown voltage [15] [22]. It is worth highlighting that this lower value of the peak of E-field in the drain access region obtained with the laterally-gated AlGaN/GaN HFET is achieved without the need of a Field-Plate (FP), which is a well-known technique used in top-gated GaN FETs, requiring the definition of an additional electrode over the drain access region where the high E-Field exists. This Field-Plate solution comes with drawbacks such as increased number of steps in the microfabrication process and degradation of frequency response due to additional parasitic capacitances [37].

3.1.2 Multi-channel laterally-gated AlGaN/GaN HFET in absence of polarization

As already indicated in Chapter 2, a multi-channel structure has two or more parallel channels positioned vertically with adding multiple barrier and channel layers to the AlGaN/GaN epilayer, keeping the same channel width (W_{ch}), gate length (L_g), and source and drain access regions (L_{sg} and L_{gd}, respectively) for each channel. The multi-channel devices explored in this thesis have up to four channels.

The simplest way to start building the multi-channel HFET is to first set up a dual-channel structure by adding one AlGaN/GaN heterojunction on top of the single-channel device described in section 3.1.1.

To assure a simultaneous control of the parallel channels by the lateral gates in the dual-channel structure, it was necessary to maintain comparable levels of sheet charge density between both channels. This was achieved through the following techniques: by doping the bottom half of

the AlGaN barrier layer of the top channel (i.e. the top half is undoped or n-type doped to 10^{15} cm^{-3}, while the bottom half is n-type doped to 10^{18} cm^{-3}), while the AlGaN barrier of the bottom channel was uniformly doped to 10^{18} cm^{-3}, and by incorporating a 2nm-thin layer of AlN on the top of the AlGaN barrier of the bottom channel. Whereas normally AlN is used as spacer between the barrier and the channel layers in AlGaN/GaN HFETs to avoid the Coulombic scattering [3], here it is used as an insulator between the two channels to avoid much of an impact on charge distribution the top channel may have on the bottom one. The presence of this AlN layer can be appreciated in the band diagram of Figure 3.5(c).

Figure 3.5(a)-(b) show the impact of adding such an AlN layer in the hypothetical polarization-less dual-channel laterally-gated AlGaN/GaN HFET. In contrast to Figure 3.5(a), where no AlN is used, Figure 3.5(b) shows that the sheet charge density in the bottom channel improves by 24.6%, essentially moving towards that of the top channel in setting the parity between the two.

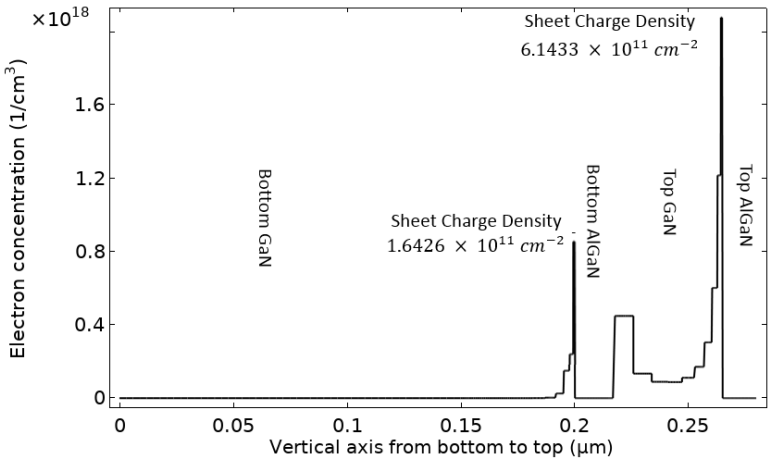

(a)

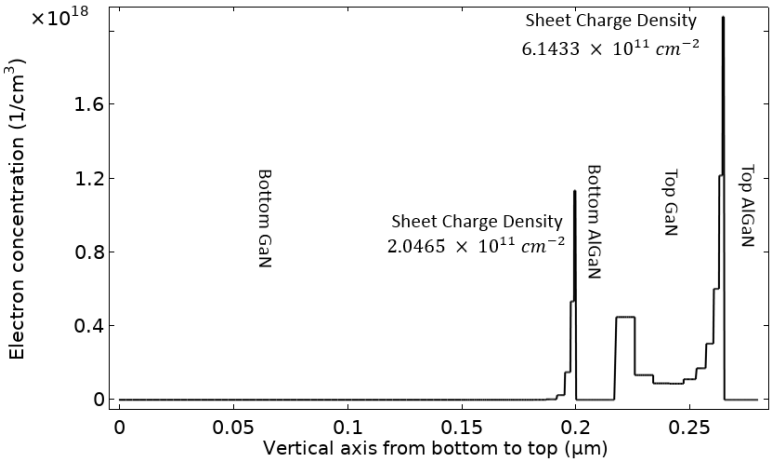

(b)

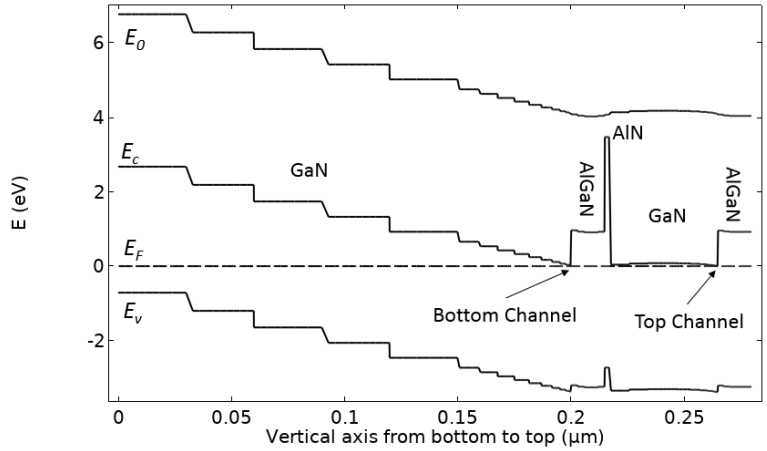

(c)

Figure 3.5 (a)-(b) Electron concentration along with sheet charge densities and (c) energy band diagram at thermal equilibrium read at the gated area and at $W_{ch}/2$ for the laterally-gated dual-channel AlGaN/GaN HFET with assumption of no polarization (a) without AlN and (b)-(c) with AlN on the top of the bottom AlGaN. E_0, E_c, E_F, and E_v are the energy levels of vacuum, the bottom of the conduction band, the fermi level, and the top of the valence band, respectively.

To achieve the triple- and quad-channel polarization-less laterally-gated AlGaN/GaN HFETs, the indicated technique of doping only half of the AlGaN barrier of the top channel in the dual-channel device was implemented on the AlGaN barrier layers of the third and fourth channels. In addition, AlN interlayers were incorporated on top of the AlGaN barriers of the second and third

channels. As in the case of what was shown in Figure 3.5, the result is the successful establishment of parity also for the third and the fourth channels.

More details about the reasons behind the choice of the specific channels layers thicknesses and barriers doping techniques are given in section 3.2, where the effort to maintain the same threshold voltage (V_{TH}) during the process of adding more channels is described. Figure 3.6 shows the electron concentration profile and band diagram of the hypothetical polarization-less quad-channel laterally-gated AlGaN/GaN HFET structure modeled in this thesis.

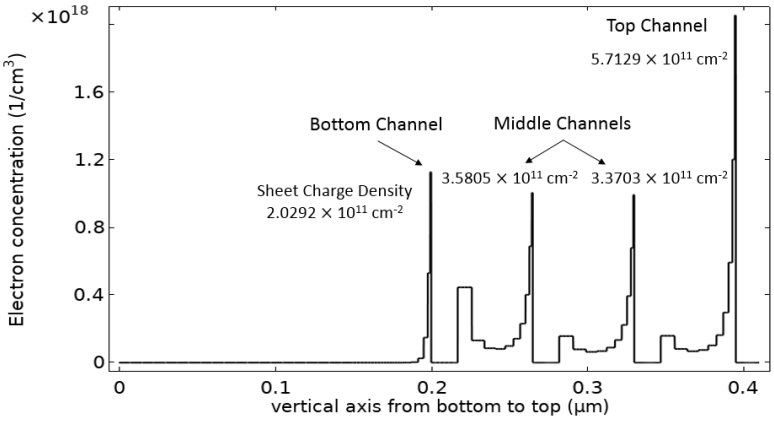

(a)

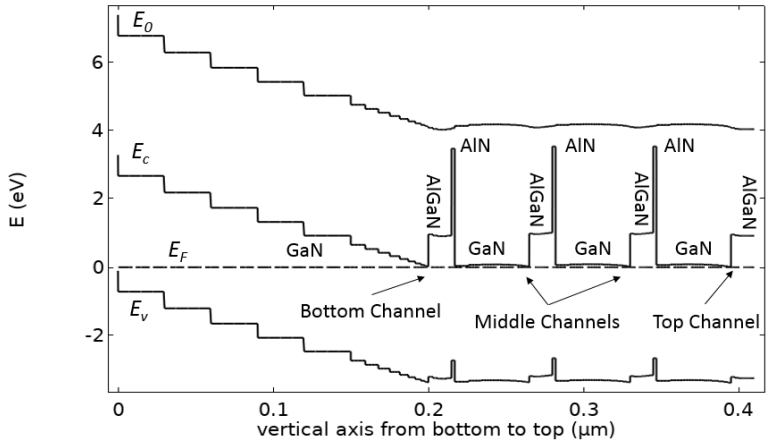

(b)

Figure 3.6 (a) Electron concentration profile along with the sheet carrier concentration of the 2DEG and (b) energy band diagram at thermal equilibrium read at the gated area and at $W_{ch}/2$ for the quad-channel laterally-gated AlGaN/GaN HFET in absence of polarization.

According to these observations, three types of channels are identified: The top channel, with a $n_s = 5.71 \times 10^{11}$ cm^{-2}, which is influenced primarily by the surface at the top; the middle channels, whose n_s is approximately the same ($\approx 3.4 \times 10^{11}$ cm^{-2} in average); and the bottom channel, which is mostly influenced by the buffer and thickness of the bottom channel layer, having a $n_s = 2.03 \times 10^{11}$ cm^{-2}. The values of the sheet charge densities are obtained by integrating the electron concentration (N) along the region where the 2DEG exists at each channel:

$$n_s(cm^{-2}) = \int_a^b N\ (cm^{-3})\ dz\ , \tag{3.1}$$

where a and b are the limits of integration defined according to the extent of z (vertically) in the region where the 2DEG is formed in each GaN channel layer.

From Figure 3.6(a), the peaks of the electron concentration for the middle channels may indicate a lower value in sheet charge density than in the bottom channel. However, the higher values of sheet charge density in the middle channels are caused by the larger area occupied by N in the same range of integration (i.e. a to b). The whole structure gives a sum total sheet charge density among the four channels of 1.47×10^{12} cm^{-2}, offering an expected current density and gate transconductance enhancements compared to the single-channel device.

Another important observation to make from the band diagram in Figure 3.6(b) is the presence of the valence band (E_v) discontinuity. The reason of this discontinuity is that the values of electron affinity ($q\chi$) and bandgap (E_g) of this specific $Al_{0.28}Ga_{0.72}N$/GaN heterostructure make the AlGaN barrier bandgap not to completely overlap that of GaN, which represents the type of band lineup shown in Figure 3.7, known as *Type-II* or *staggered bandgap* [3].

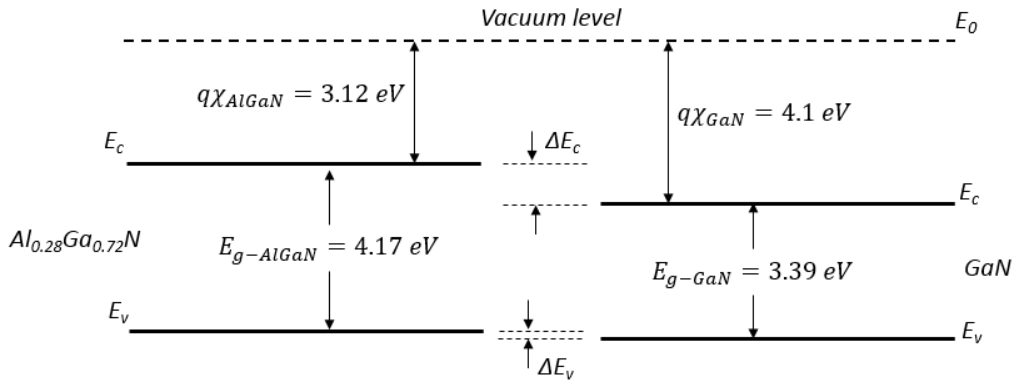

Figure 3.7 Band lineup (*staggered bandgap* or *Type-II*) of the $Al_xGa_{1-x}N$/GaN heterostructure for Al-mole fraction (*x)* = 0.28.

As reported in Chapter 2, such values of $E_{g\text{-}AlGaN}$ and $q\chi_{AlGaN}$ are obtained from using the Al mole fraction (*x*) of 0.28 on the equations (2.1) and (2.2), respectively.

For reference, the given values for GaN by Comsol and also confirmed by [3] and [25] are:

$$q\chi_{GaN} = 4.1\ eV$$

$$E_{g-GaN} = 3.39\ eV$$

Also, from the band diagram in Figure 3.6(b), it is worth noting that the bottom of the conduction band at the heterojunction (E_c) of the four channels is practically at the same level in regards to the fermi level (E_f), which not only supports the observation made earlier about the similarity of the sheet charge density of the 2DEG in the four channels but also demonstrates that the lateral control of the channels is made by the gates to the same extent. This can be evidenced also in the electric potential profile, where the four channels are practically at the same potential (Figure 3.8).

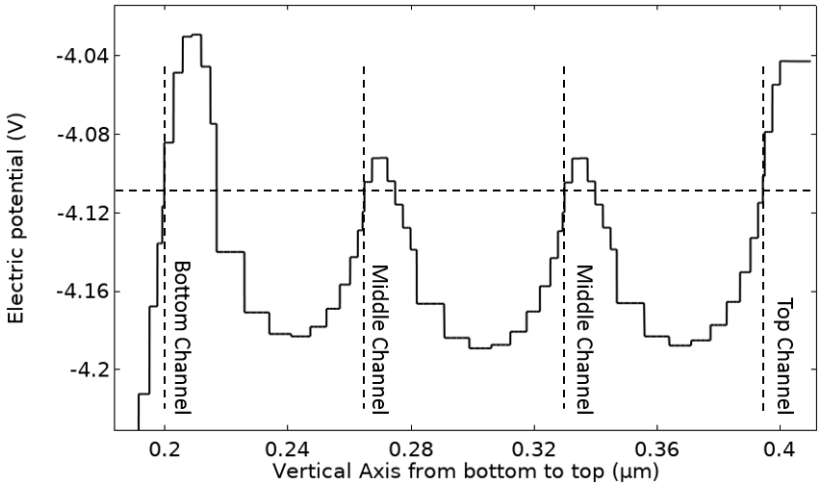

Figure 3.8 Vertical profile of the electric potential at thermal equilibrium of the hypothetical polarization-less quad-channel laterally-gated AlGaN/GaN HFET at the gated area and at $W_{ch}/2$. (By default, the initial value for electric potential in Comsol is set to -4 V).

Figure 3.9 shows the E-field profiles for the hypothetical polarization-less quad-channel laterally-gated AlGaN/GaN HFET. The vertical E-field profile follows the pattern observed in the single-channel (Figure 3.2(a)) for every channel, where the E-field is not constant within the highly doped parts of the AlGaN barriers. This happens specifically for the whole barrier of the bottom channel, which is uniformly doped to 10^{18} cm^{-3}, and also for the bottom half of the AlGaN barriers in the middle and top channels, whose doping concentration is also set to 10^{18} cm^{-3}, whereas their top half are undoped or lightly doped to 10^{15} cm^{-3} (inducing a constant E-field on such top half). This parity between channels is achieved because from one side the presence of the undoped top half of the AlGaN barrier layers in the middle and top channels helps diminish the parallel channel that may exist in the barrier layers and affects the induced 2DEG under the heterojunction, and from the other side the doped bottom half of these AlGaN barriers makes their depletion share a higher proportion of carriers with the 2DEG, producing a higher charge density on each channel. The small spikes in the middle channels are due to the presence of the AlN spacers on the top of the AlGaN barriers. Also, thanks to the half doping technique in the middle and top channels, E-

field peaks are reduced due to the presence of the undoped top half of the AlGaN barriers, which improve the Schottky contact quality of the gates [3], promising an improvement in gate transconductance for the entire structure.

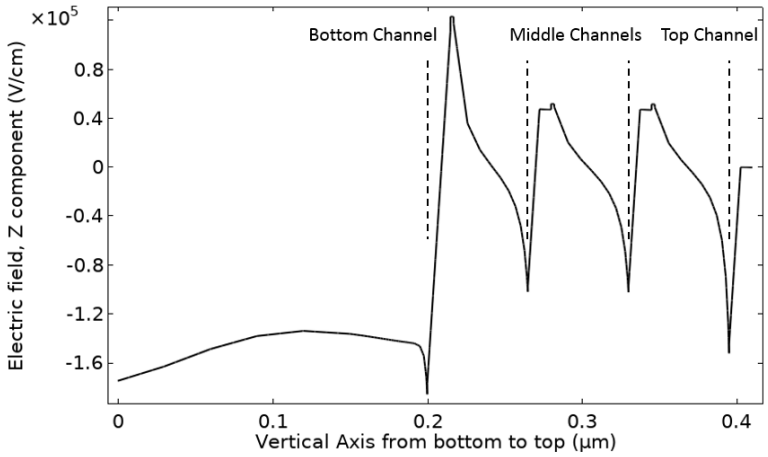

(a)

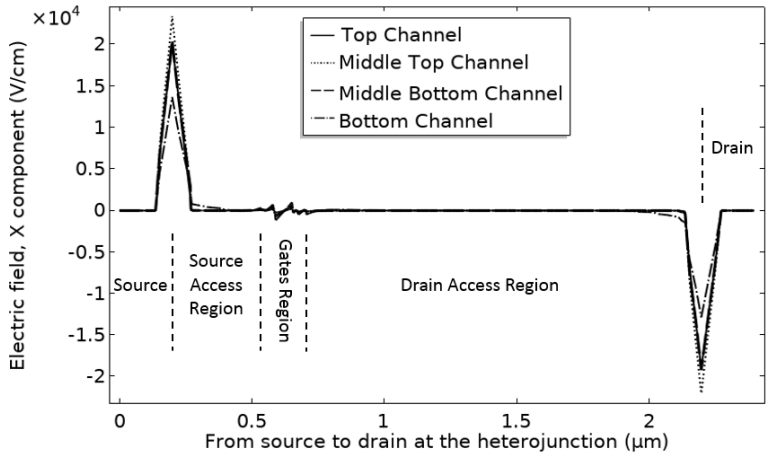

(b)

Figure 3.9 Electric field profiles of the hypothetical polarization-less quad-channel laterally-gated AlGaN/GaN HFET measured (a) vertically at the gated region and (b) laterally from source to drain at the heterojunction.

It should also be pointed out that, from the lateral profiles of E-field in Figure 3.9(b), it is observed that the peak of the E-field at the gated area does not increase with the incorporation of

additional channels if compared to the lateral E-field profile of the hypothetical polarization-less single-channel laterally-gated AlGaN/GaN HFET presented earlier in Figure 3.4(a), which may indicate an advantage in terms of current density enhancement without compromising the breakdown characteristics.

3.2 Transfer characteristics

During the study and characterization of a transistor, its DC characteristics show how the device behaves at a specific range of terminal bias. One important piece of this DC assessment comes in the form of studying the variation of drain current (I_D) with the gate-to-source voltage (V_{GS}), when drain-to-source voltage (V_{DS}) has a finite value. The change in V_{GS} results in an I_D output, which will form an I_D - V_{GS} curve that represents the transfer characteristics. This curve gives insight into the details such as the threshold voltage of the transistor (V_{TH}), and when *Log* (I_D) vs V_{GS} is plotted, it also provides an assessment of the Drain-Induced Barrier Lowering (*DIBL*), Subthreshold Swing (*SS*), off-state current, and I_{ON}/I_{OFF} ratio. In addition to the $I_D - V_{GS}$ curve, the *gate transconductance* (G_m) can be obtained using also V_{GS} as input, which results in the $G_m - V_{GS}$ curves. Looking into all these characteristics, which will be described in detail, make us capable of qualifying the transistor for a specific application in digital, high frequency, and/or high voltage circuits.

3.2.1 Single-channel laterally-gated AlGaN/GaN HFET in absence of polarization

Figure 3.10 shows the transfer characteristics for the single-channel laterally-gated AlGaN/GaN HFET of Figure 2.1 in comparison to that of a top-gated AlGaN/GaN HFET of the same doping concentrations and dimensions, where equally no polarization is taken into account.

As indicated in Chapter 2, in these cases: gate length (L_g) is of 150 nm, channel width (W_{ch}) is of 250 nm, source-to-drain distance (L_{sd}) is of 2 µm, and gate-to-drain distance (L_{gd}) is of 1.5 µm.

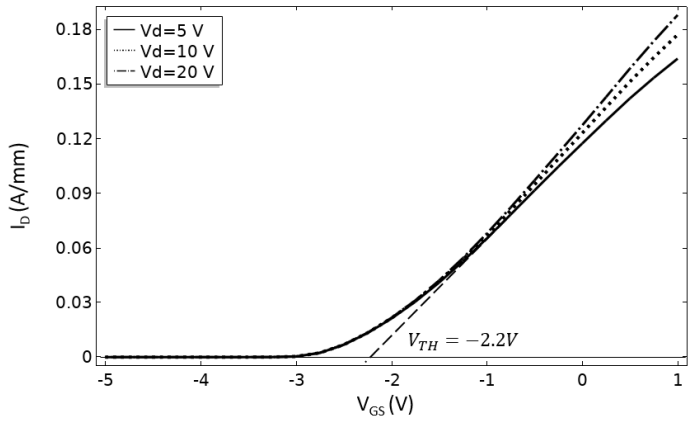

(a)

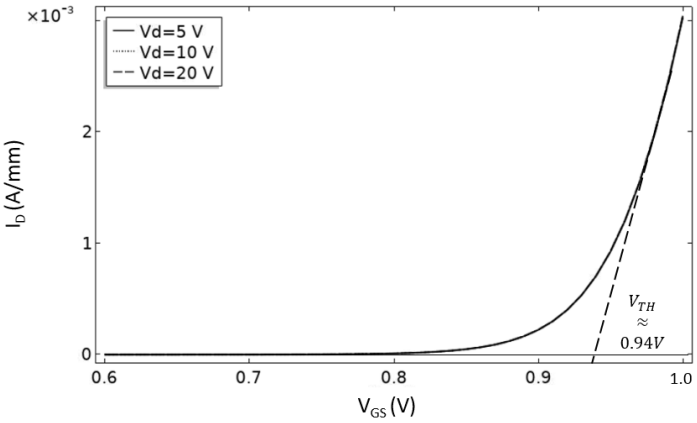

(b)

Figure 3.10 Transfer characteristics of (a) the laterally-gated single-channel and (b) the top-gated AlGaN/GaN HFETs with the same dimensions and doping concentrations, where in neither case polarization has been considered.

The transfer characteristics for the top-gated heterostructure (Figure 3.10(b)) show a lower current density and a positive threshold voltage compared to the case of the laterally-gated device (Figure 3.10(a)). As indicated earlier in this chapter, this is caused by the Schottky barrier of the gate at the top, which is closer to the heterojunction along the entire width of the transistor. This impacts the induction of the 2DEG at thermal equilibrium to take on a much lower value (6.4187

$\times 10^{-5}$ cm^{-2}) in contrast to that of the hypothetical polarization-less laterally-gated AlGaN/GaN HFET (7.0198×10^{11} cm^{-2}).

The definition of current density in A/mm is based on W_{ch}, which is taken as the distance between gates for the case of laterally-gated AlGaN/GaN HFET or the width of the gate for the case of top-gated structure. The value of this quantity is 250 nm for both devices. It is important to note that in general for laterally-gated devices the value of W_{ch} is not used to the same level of accuracy to that of the top-gated structures. This is because in the case of the former, the 2DEG is already laterally depleted at thermal equilibrium as shown by Figure 3.11, which makes the real W_{ch} to shrink. In addition, this depletion is furthered when a negative V_{GS} is applied.

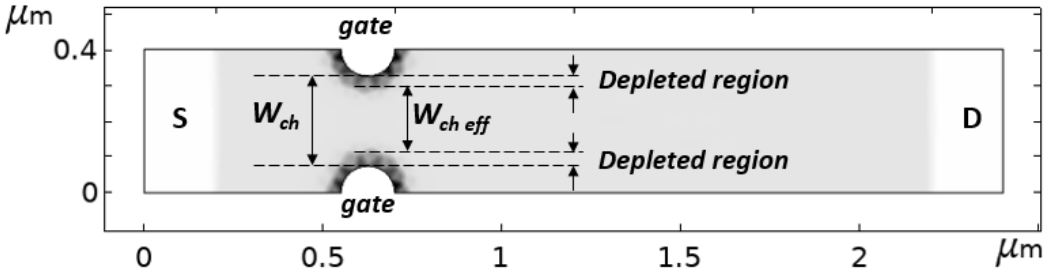

Figure 3.11 2-D profile of the electron concentration at thermal equilibrium taken 1nm below the heterojunction of the laterally-gated single-channel AlGaN/GaN HFET with the assumption of no polarization (Top view). The shaded region around the gates represents the depletion of the 2DEG, which affects the channel width (W_{ch}).

Looking into the subthreshold performance presented in terms of the *Log* I_D vs V_{GS} characteristics (Figure 3.12), the off-state current density at a low V_{DS} (0.3 V – 0.4 V) is observed to be on low side ($I_D < 10^{-9}$ A/mm). Although gate leakage has not accurately factored into the simulation, the off-state current density seems to indicate how high or low the expected channel leakage is.

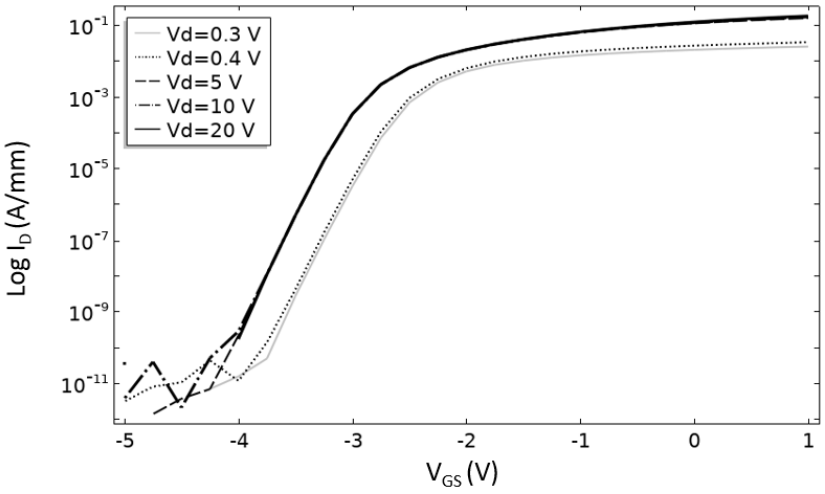

Figure 3.12 Subthreshold characteristics for the hypothetical polarization-less single-channel laterally-gated AlGaN/GaN HFET for V_{DS} in saturation (5 V, 10 V, 20 V) and in the linear regime (0.3 V, 0.4 V).

Additionally, *Drain-Induced Barrier Lowering* (DIBL) indicates the degree of impact the drain-to-source voltage (V_{DS}) has on the controllability of the channel, which must be as small as possible [3]. This means that the lower the *DIBL*, the less impact V_{DS} has on the electrostatic control of the gate. In general, *DIBL* worsens (or becomes higher) due to Short-Channel-Effects (SCE) when shrinking the gate length (L_g) further [38]. *DIBL* can be calculated in terms of the shift of V_{TH} per volt change in V_{DS}:

$$DIBL_{(mV/V)} = \frac{V_{TH}^{sat} - V_{TH}^{lin}}{V_{DS}^{sat} - V_{DS}^{lin}}, \tag{3.2}$$

where V_{TH}^{sat} is the threshold voltage at V_{DS} in saturation (V_{DS}^{sat}) and V_{TH}^{lin} is the threshold voltage at V_{DS} in the linear regime (V_{DS}^{lin}). For the hypothetical polarization-less single-channel laterally-gated AlGaN/GaN HFET exposed in this chapter of the thesis: $V_{TH}^{sat} = -2.2\,V$, $V_{TH}^{lin} = -2.4\,V$, for a $V_{DS}^{sat} = 20\,V$, and a $V_{DS}^{lin} = 0.4\,V$, respectively, which gives *DIBL = 10.2 mV/V*. The

threshold voltages are defined by the intersection with the V_{GS} axis of the extrapolated $I_D - V_{GS}$ characteristics (see Figure 3.10(a) and 3.13 for V_{TH}^{sat} and V_{TH}^{lin}, respectively).

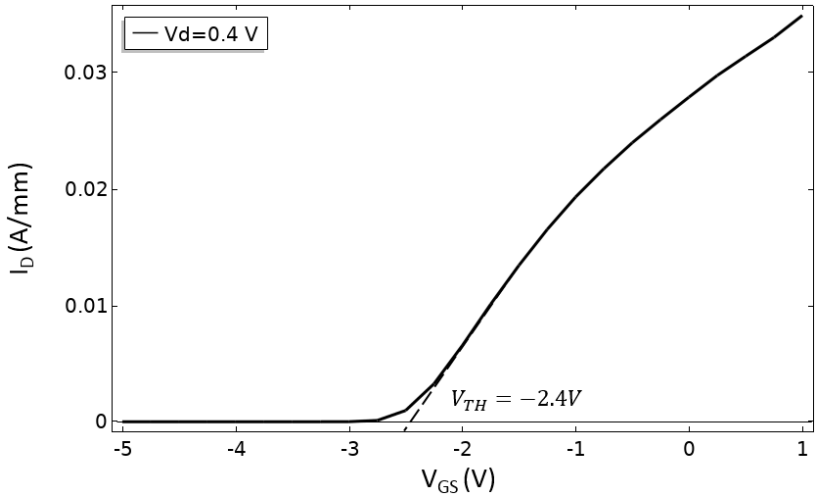

Figure 3.13 Transfer characteristics for the hypothetical polarization-less single-channel laterally-gated AlGaN/GaN HFET for V_{DS} in the linear regime (0.4 V).

Figure 3.12 can also be used to calculate *DIBL* by taking a region from the subthreshold zone where the curves corresponding to V_{DS}^{sat} and V_{DS}^{lin} are parallel, then reading the shift in V_{GS} and dividing this difference between the change in V_{DS} (Equation (3.3)).

$$DIBL_{(mV/V)} = \frac{\Delta V_{GS}}{V_{DS}^{sat} - V_{DS}^{lin}} \tag{3.3}$$

For example, if the region corresponding to I_D = 10^{-7} A/mm is chosen, then $\Delta V_{GS} = 3.55\,V - 3.35\,V = 0.2\,V$, which gives *DIBL = 10.2 mV/V*.

For the case of the polarization-less top-gated AlGaN/GaN HFET, using Figure 3.14 and the same method described above, *DIBL* is observed to take on values that are smaller than those of the laterally-gated structure. This difference may be caused by the geometry of the gate, which for the case of the former has a constant distance to the 2DEG along the entire width of the channel and therefore a more uniform channel control, whereas for the case of the latter the effect of the

lateral gates over the channel might be diminished at the middle of the channel width, where the distance from the gates is larger.

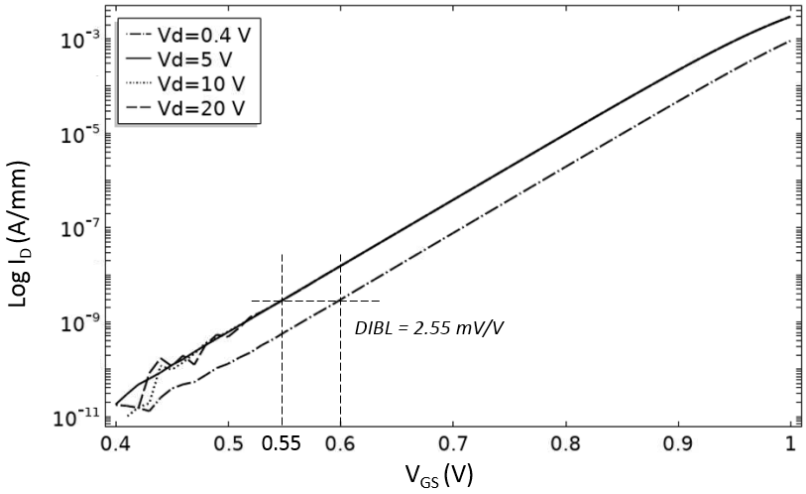

Figure 3.14 Subthreshold characteristics for the polarization-less top-gated AlGaN/GaN HFET for V_{DS} in saturation (5 V, 10 V, 20 V) and in the linear regime (0.4 V).

These results show that, although *DIBL* for the laterally-gated device is larger than that of the top-gated variety, the former still offers a superb electrostatic dominance of the gate over the channel. It has to be kept in mind that the presented results as a consequence of lack of attention to the gate leakage are however optimistic [3].

In addition to reading DIBL, from Figure 3.12 it is possible to extract the Subthreshold Swing (*SS*) characteristic of the device. This value, which is the inverse of the slope of the transfer characteristics in the subthreshold regime in the plot of *Log* I_D vs V_{GS}, defines how fast a device can switch between its ON and OFF states and is measured in mV/dec, or by the needed reduction of V_{GS} below V_{TH} to achieve a 10 times reduction on drain current [3]. In terms of this metric, the smaller the *SS*, whose minimum value for Boltzman controlled channels is theoretically *60 mV/dec* at room temperature [3], the faster the device. As per Figure 3.12, *SS = 160 mV/dec*, which is a relatively small value.

The subthreshold response of the polarization-less top-gated AlGaN/GaN HFET exposed in Figure 3.14, gives *SS = 70mV/dec*, which is ~56% smaller than that of the laterally-gated device. Agreeing with our earlier observations made on sheet charge density, this means that the lateral E-field used in the latter is not as effective as the vertical E-field induced by a gate at the top at least when polarization is absent.

The relatively small value of *160 mV/dec* reported for the polarization-less single-channel laterally-gated AlGaN/GaN HFET discussed above might have been produced thanks to the low leakage current, which has been reported to be also the cause of high I_{ON}/I_{OFF} ratios [39]. For this device, the I_{ON}/I_{OFF} extracted also from Figure 3.12 is > 10^6, which indicates an excellent channel control. It is worth mentioning that both *SS* and I_{ON}/I_{OFF} ratio are very stable along a wide range of V_{DS}, from its linear regime (0.3 V) to deep saturation (~20 V).

One of the discoveries made during the exploration of the polarization-less laterally-gated AlGaN/GaN HFET in the present chapter, is that not only the AlGaN barrier layer doping but also the GaN channel layer thickness play important roles in shifting the value of V_{TH}. The impact of the AlGaN barrier doping was explored in the single-channel device and is explained in this section whereas that of the GaN channel thickness is explained later in section 3.2.2. A well-known challenge that is faced by polar Ga-face AlGaN/GaN HFETs is the achievement of enhancement-mode (normally-off) devices. This is due to the polarization induced 2DEG, which causes these transistors to have a negative threshold voltage.

In the hypothetical case of no polarization, for the single-channel AlGaN/GaN HFET of this work, when having the following structure:

$$n\text{-}Al_xGa_{1-x}N\ (15nm)\ /\ n\text{-}GaN\ (200nm)\ /\ p\text{-}GaN\ (200nm),$$

and with the following doping concentrations:

n-AlGaN: 10^{18} cm^{-3}, *n-GaN*: 10^{14} cm^{-3}, and *p-GaN*: 10^{18} cm^{-3},

the V_{TH} takes the value of $-2.2\ V$ as in Figure 3.10(a).

However, when only half of the AlGaN barrier is doped, that is, when the bottom half of AlGaN is set to 10^{18} cm^{-3} while its top half is set to 10^{15} cm^{-3}, the carrier concentration below the heterojunction becomes five orders of magnitude smaller than that of a fully-doped AlGaN structure to the level of 10^{18} cm^{-3}. Consequently, the threshold voltage shifts to the right by 2.68V, getting a new $V_{TH} \approx 0.48\ V$ as shown in Figure 3.15.

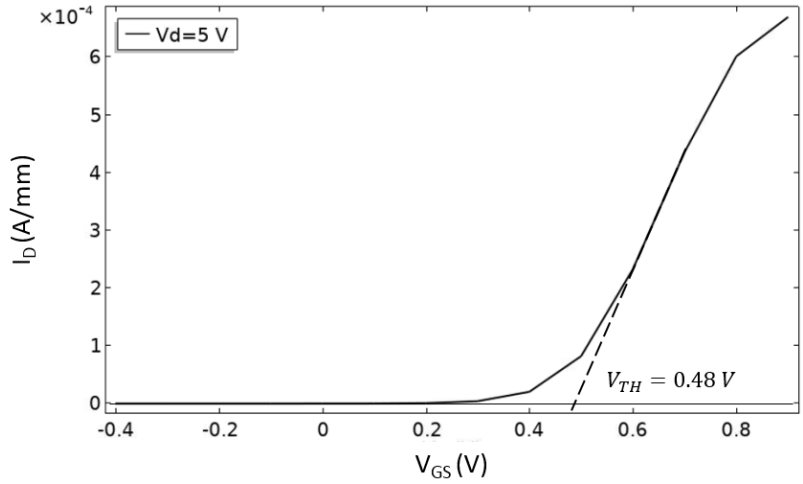

Figure 3.15 Transfer characteristics of the polarization-less single-channel laterally-gated AlGaN/GaN HFET with only the bottom half of AlGaN doped.

This may be explained by the fact that by having a thinner part of AlGaN doped, the effect of the lateral gates gets stronger over the charge carriers in the barrier at thermal equilibrium, making the depleted barrier layer stop sharing the carriers with the 2DEG.

3.2.2 Multi-channel laterally-gated AlGaN/GaN HFET in absence of polarization

One of the challenges faced by the multi-channel HFETs is to maintain the same threshold voltage as the single-channel device, as experimentally corroborated by Erine *et al.* [22]. Maintaining the same V_{TH} allows the multi-channel HFET to offer an enhancement in current

density and gate transconductance without changing the design of the circuit in charge of providing the gate-to-source voltage (V_{GS}). For investigation purposes on the simultaneous and efficient controllability of several channels, this challenge was also explored during the modeling of the dual-, triple, and quad-channel laterally-gated AlGaN/GaN HFETs described in this chapter.

When a second channel is added to the single-channel device, while keeping the AlGaN barrier layer of the bottom channel fully doped, the thickness of the GaN channel layer and the doping of the AlGaN barrier layer in the top channel play important roles in determining the threshold voltage. In the case when the AlGaN barrier layer of the top channel is fully doped, it is necessary to have GaN channel layer of the top channel of the same thickness as that of the bottom channel's. This is to avoid impacting the V_{TH} obtained in the single-channel device. Figure 3.16 presents a successful example of this design strategy.

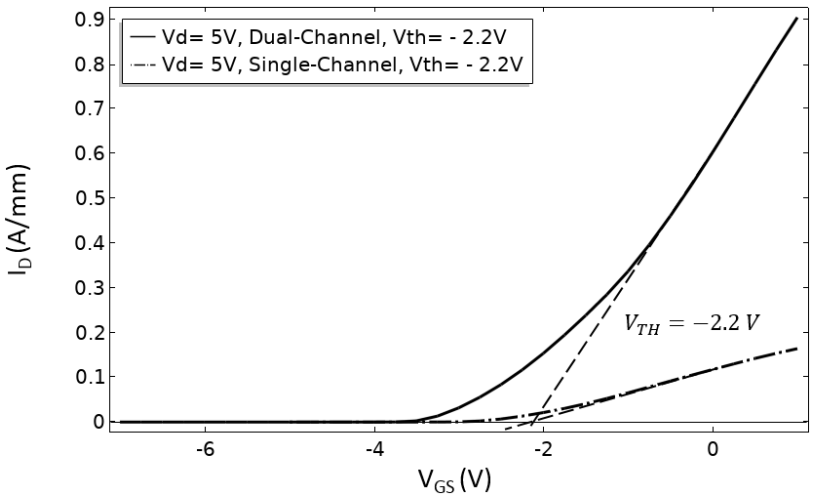

Figure 3.16 Transfer characteristics of single- and dual-channel polarization-less laterally-gated AlGaN/GaN HFETs using fully-doped AlGaN barrier and GaN thickness = 200 nm in both channels of the dual-channel device.

This outcome can be explained by the fact that since channels are gated laterally instead of from the top, it is necessary to assure the same electric potential on both channels in order to have

an almost simultaneous depletion from the vertically-defined gate pillars. This can be achieved if channels are far enough apart in order to avoid interference between channels' potentials. This is satisfied by having an undoped GaN channel layer thick enough at the top channel. For example, in the case of the explored polarization-less dual-channel laterally-gated AlGaN/GaN HFET, if the top channel's GaN channel layer were thinner than 200 nm, and keeping the top channel's AlGaN barrier layer fully doped to 10^{18} cm^{-3}, the electric potential at the top channel would have started to become higher. This is observed to effectively induce an unbalance between the gate controllability of the two channels. This can be observed in Figure 3.17, where in the electric potential profile at thermal equilibrium, under such circumstances we see a difference between the potential of the two channels.

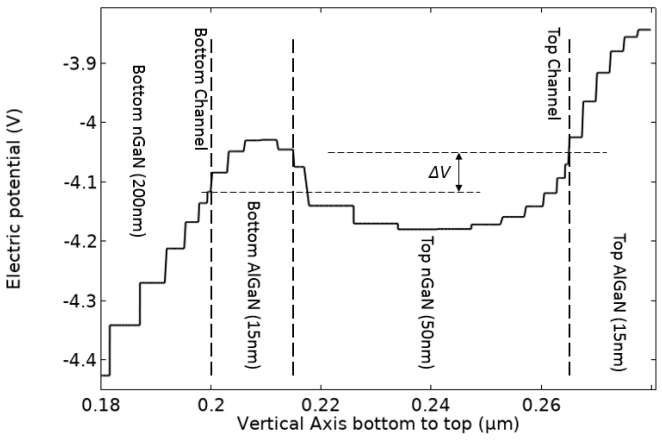

(a)

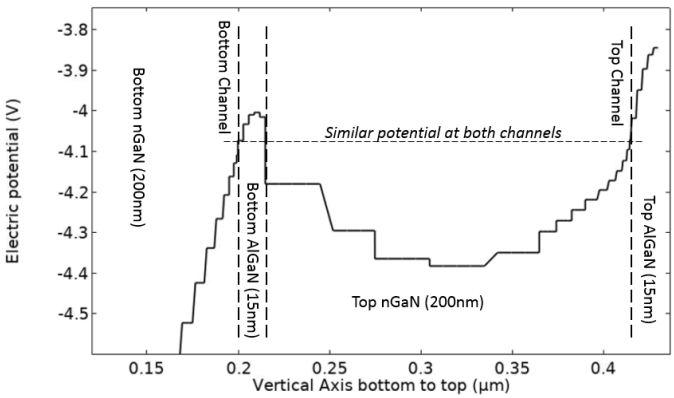

(b)

Figure 3.17 Electric potential profile from bottom to top for the polarization-less dual-channel laterally-gated AlGaN/GaN HFET at the gated region when both the top and the bottom AlGaN barriers are fully doped with (a) top GaN = 50 nm and (b) top GaN = 200 nm. The electric potential between channels is different in (a).

However, if half of the top AlGaN barrier is doped (i.e. doping only the bottom half of it to the level of 10^{18} cm^{-3}, while having the top half doped to 10^{15} cm^{-3}), we see opening of the possibility to reduce the top GaN thickness to 25% of that of the bottom GaN in order to maintain V_{TH} parity. In this case, since the bottom GaN is 200 nm thick, then the top GaN will be only 50 nm.

Reducing the thickness of the GaN channel layer of the top channel, although of some material growth incentive, comes at the cost of reduction in current density, which for the case of our example contracts by almost 39% at a drain-to-source bias of 5V compared to the case when the AlGaN barrier of the top channel is fully doped (Figure 3.18). This reduction in current density may be explained by the less doping concentration of the barrier, which reduces the number of carriers transferred to the 2DEG in the top channel when of course polarization is hypothetically assumed to be absent.

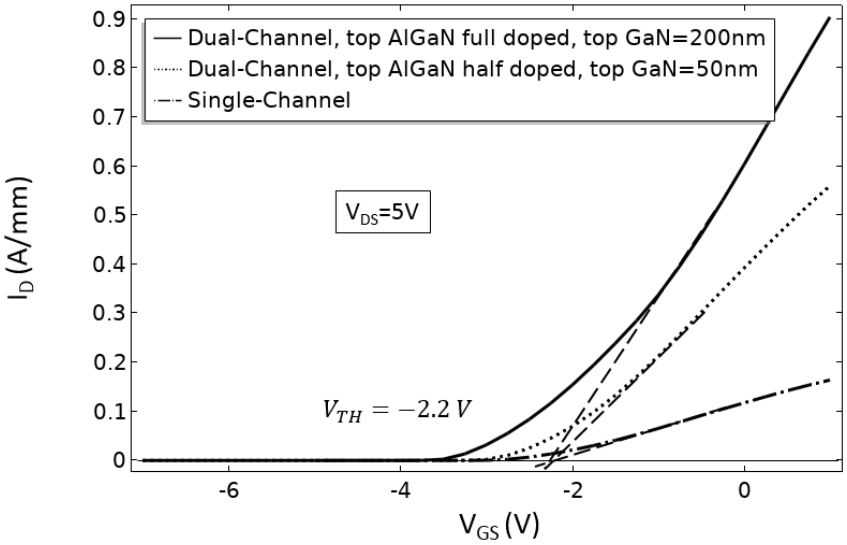

Figure 3.18 Transfer characteristics of the polarization-less dual-channel laterally-gated AlGaN/GaN HFETs for both cases: 1) top channel's AlGaN barrier fully doped with GaN channel thickness of 200 nm and 2) top channel's AlGaN barrier half doped with GaN channel thickness of 50 nm.

Additionally, by having the top AlGaN barrier half doped and the top GaN channel layer thickness set to only 50 nm, the same electric potential is achieved in both channels. As indicated earlier, this effectively assures simultaneous gating of both channels from the lateral gates (Figure 3.19).

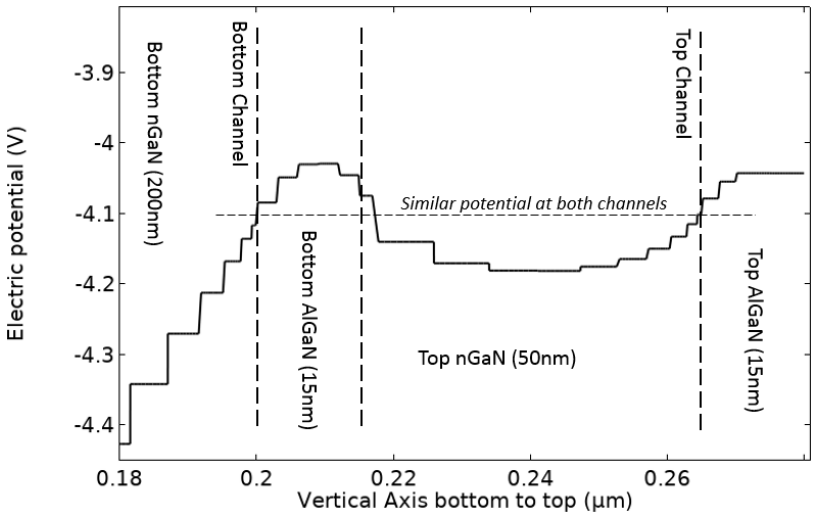

Figure 3.19 Electric potential profile for the polarization-less dual-channel laterally-gated AlGaN/GaN HFET using half doping in the AlGaN barrier and 50-nm-thickness for the GaN channel layers at the top channel.

Having achieved the transfer characteristics of Figure 3.18 for the dual-channel structure, the next step on building the multi-channel device was to add the third and fourth channels following the same pattern of the dual-channel in order to maintain V_{TH} among the additional channels. With that goal in mind, the quad-channel configuration includes the top and the middle channels' AlGaN barriers only bottom-half heavily doped, while GaN channel layers of the same thickness and AlN spacers between channels' structures are incorporated:

4th ch (top): ***bottom half AlGaN doped (15nm) / GaN (50nm) / AlN(2nm)***
3rd ch: ***bottom half AlGaN doped (15nm) / GaN (50nm) / AlN(2nm)***
2nd ch: ***bottom half AlGaN doped (15nm) / GaN (50nm) / AlN(2nm)***
1st ch (bottom): ***full AlGaN doped (15nm) / GaN (200nm) / p-GaN (200nm)***

Figure 3.20 shows the transfer characteristics for the single-, dual-, triple-, and quad-channel devices, where shifting of V_{TH} is avoided, while higher current density is achieved with each additional channel. According to the presented data, increase of 243% on current density with dual-channel, 462% with triple-channel, and 680% with quad-channel at V_{GS} = 1 V is observed.

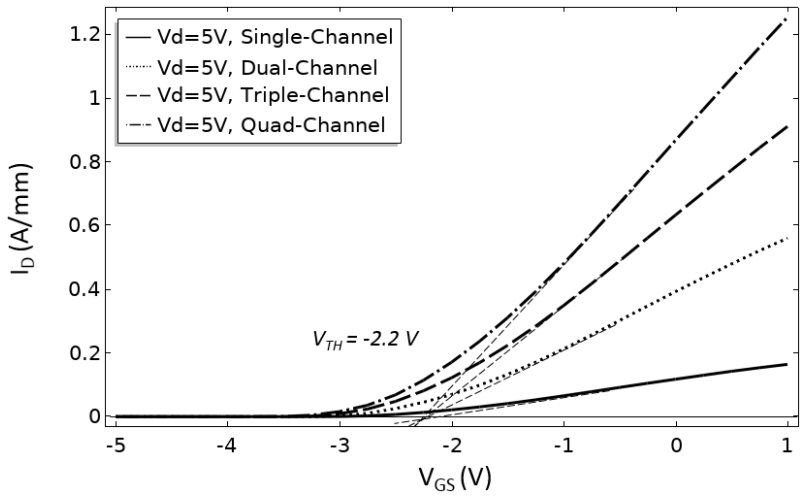

Figure 3.20 Transfer characteristics from the single- to the quad-channel hypothetical polarization-less laterally-gated AlGaN/GaN HFETs at V_{DS} = 5 V.

As expected from the structure, in terms of *Log* I_D vs V_{GS}, the multi-channel structure shows stability on its low off-current, keeping it under 10^{-9} A/mm for lower values of V_{DS}, in the linear

regime of operation. This can be appreciated in Figure 3.21. Another interesting observation is that the V_{DS} dependence increases for V_{DS} values in the saturation region (e.g. from 5V to 20V) with the number of channels. This seems to be because the effect of the buffer layer below the bottom channel structure is diminished the more channels are added to the device, and this can also be appreciated from the output characteristics to be presented in section 3.3, where the saturation region shifts to the right with the increase in the number of the channels.

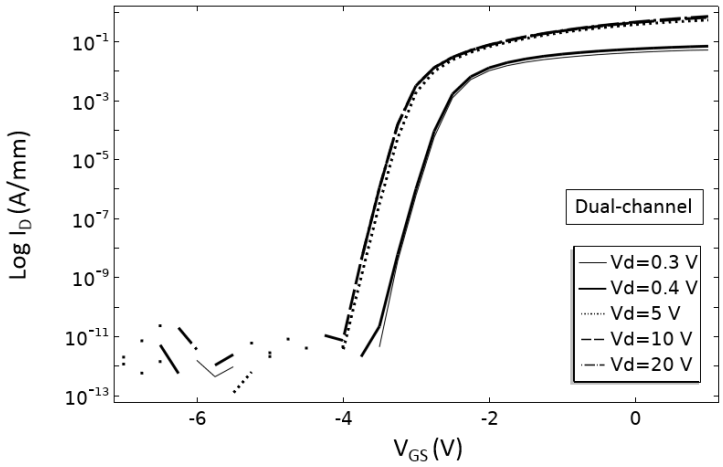

(a)

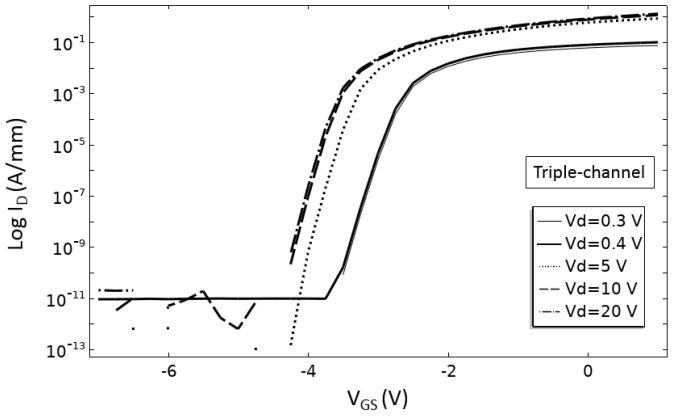

(b)

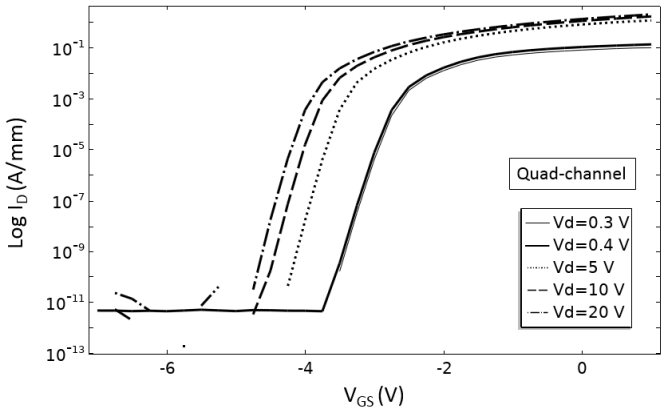

(c)

Figure 3.21 Subthreshold characteristics for the polarization-less (a) dual-, (b) triple-, and (c) quad-channel laterally-gated AlGaN/GaN HFETs.

In terms of the Drain-Induced Barrier Lowering (*DIBL*), the more channels are added the larger the DIBL. Considering the same $V_{DS}^{sat} = 20\,V$ and $V_{DS}^{lin} = 0.4\,V$ as in the single-channel (section 3.2.1) for comparison (where DIBL is *10.2 mV/V*), the values of DIBL extracted from Figure 3.21 are *20.4 mV/V*, *40.8 mV/V*, and *61.2 mV/V* for the dual-, triple-, and quad-channel structures, respectively, meaning an almost linear dependence of DIBL on the number of channels (Figure 3.22). Although there is more presence of the drain voltage on the controllability of the channels, *DIBL* for the hypothetical polarization-less quad-channel laterally-gated AlGaN/GaN HFET is still below the values reported for conventional single-channel top-gated GaN HFETs (~*92 mV/V*) [40]. However interesting, this promising result in light of lacking of appreciation of all the involved mechanisms in SCEs should be celebrated with caution.

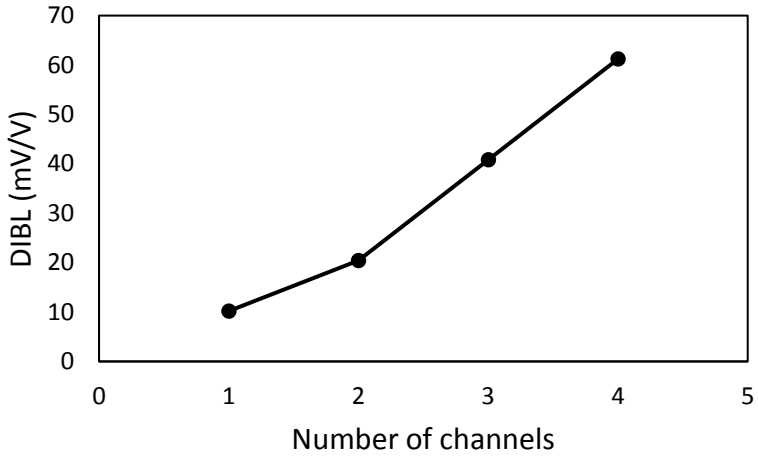

Figure 3.22 DIBL dependence on the number of channels for the laterally-gated multi-channel AlGaN/GaN HFET in absence of polarization.

Regarding the subthreshold slope (*SS*), the multi-channel structure offers a better value than that of the single-channel device. From Figure 3.21, *SS* can be extracted as *100 mV/dec* for the dual-, triple, and quad-channel HFETs, which represents a reduction of 37.5% compared to that of the single-channel laterally-gated AlGaN/GaN HFET exposed in the previous section (Figure 3.23).

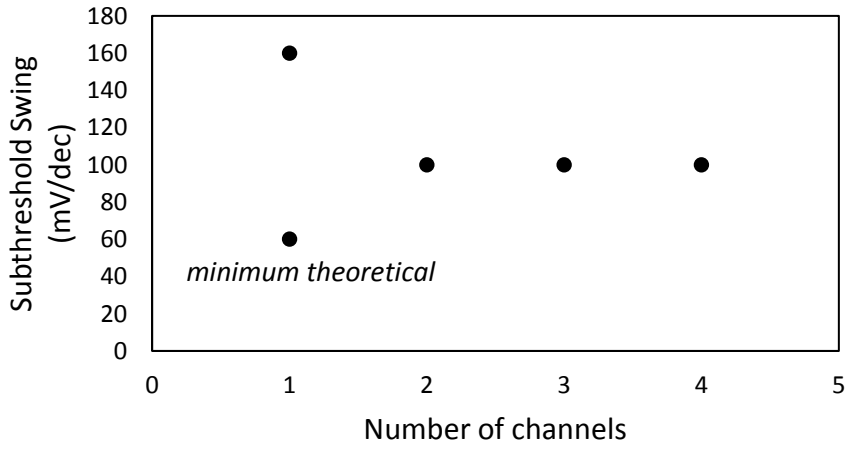

Figure 3.23 Subthreshold swing dependence on the number of channels for the laterally-gated multi-channel AlGaN/GaN HFET in absence of polarization.

3.3 Output characteristics

3.3.1 Single-channel laterally-gated AlGaN/GaN HFET in absence of polarization

Figure 3.24(a) shows the output characteristics of the polarization-less single-channel laterally-gated AlGaN/GaN HFET modeled in this chapter. The device exhibits a relatively early current density saturation at a $V_{DS} \approx 2.2\ V$ for $V_{GS} = 1V$. This value of V_{DS} known also as the knee voltage (V_{knee}), is the drain bias at which the drain current starts saturation [41] and can be extracted from the output characteristics by intersecting the tangents of the linear and the saturation regions. Compared to the simulated polarization-less top-gated AlGaN/GaN HFET modeled with the same dimensions as the laterally-gated structure (Figure 3.24(b)), the value of the knee voltages for both structures are comparable at the same V_{GS}. Although the difference is small (0.3V), it is still an improvement offered by the laterally-gated HFET that can possibly be exploited by digital applications.

The aforementioned low V_{knee} is related to a low ON resistance (R_{on}), which is the resistance of the device in ON state and needs to be as low as possible in order to limit power dissipation. Its value can also be extracted from the output characteristics by looking at the linear region, also called the resistive region by designers [42], and using the expression of equation (3.4):

$$R_{on} = \frac{\Delta V_{DS}}{\Delta I_D} \tag{3.4}$$

From Figure 3.24(a) in the linear regime, for $V_{GS} = 0\ V$, $\Delta V_{DS} = 0.1\ V$, and $\Delta I_D = 7.5\ mA/mm$, the calculated *ON* resistance $R_{on} \approx 13.33\ \Omega \cdot mm$ for the polarization-less laterally-gated AlGaN/GaN HFET and from Figure 3.24(b), for $V_{GS} = 1\ V$, $\Delta V_{DS} = 0.1\ V$, and $\Delta I_D = 0.297\ mA/mm$, the calculated *ON* resistance $R_{on} \approx 336\ \Omega \cdot mm$ for the top-gated variety.

Another parameter to extract from Figure 3.24 is the output conductance (g_o), defined as the variation of drain current with the drain-to-source voltage at a constant gate-to-source voltage in the saturation regime of operation, that is the slope of the curve in saturation, which is the inverse of the output resistance [43], calculated as:

$$g_o = R_o^{-1} = \frac{\partial I_D}{\partial V_{DS}} \Big|_{V_{GS}} . \tag{3.5}$$

Ideally, this slope tends to zero in the saturation region to offer stability in radio-frequency operation. However, Short-Channel Effects (SCE) may cause it to increase with V_{DS}. In general, and compared to the output characteristics of the modeled planar HFET in Figure 3.24(b), the polarization-less laterally-controlled AlGaN/GaN HFET discussed in this chapter shows a very low or almost zero slope for most of the V_{GS} values, starting to present some increase at $V_{GS} = 1V$.

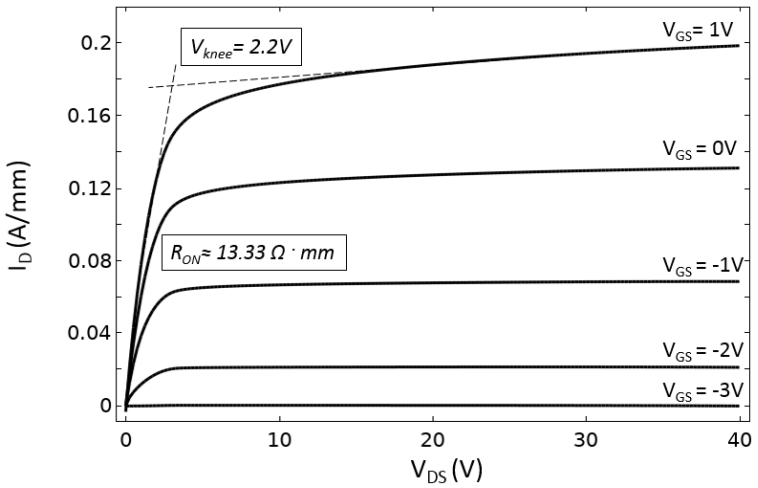

(a)

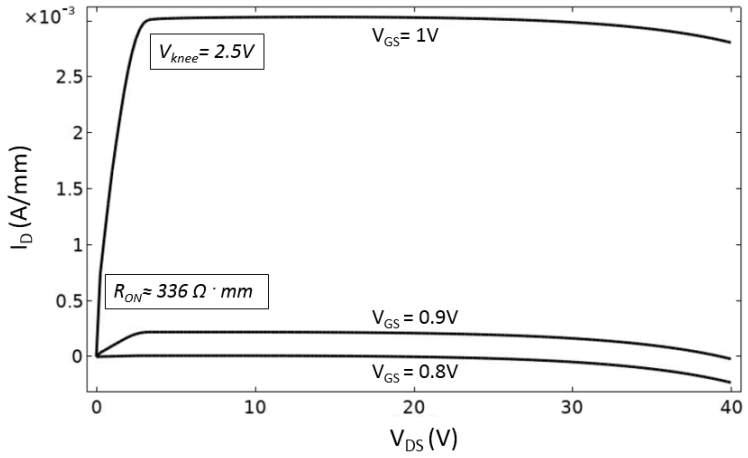

(b)

Figure 3.24 Output characteristics of the single-channel (a) laterally-gated and (b) a top-gated AlGaN/GaN HFETs modeled with the same parameters in absence of polarization.

3.3.2 Multi-channel laterally-gated AlGaN/GaN HFET in absence of polarization

Figure 3.25 shows the output characteristics for several values of V_{GS} for the dual-, triple-, and quad-channel laterally-gated AlGaN/GaN HFETs for which hypothetically polarization has been set off. Figure 3.26 shows the output characteristics at $V_{GS} = -1\ V$ of the four structures on the same graph for easier comparison. As more channels are added, current density in saturation gets higher by ~3.5x for two channels, ~7.1x for three channels, and ~12x for four channels. Surprisingly, the presented enhancements in current density per additional channel is higher than one might expect (i.e. 3.5x, 7.1x, and 12x, instead of 2x, 3x, or 4x for the dual-, triple-, and quad-channel devices, respectively). This could possibly be due to differences among the 3-D distribution of the electric field and hence drift-velocity among these devices.

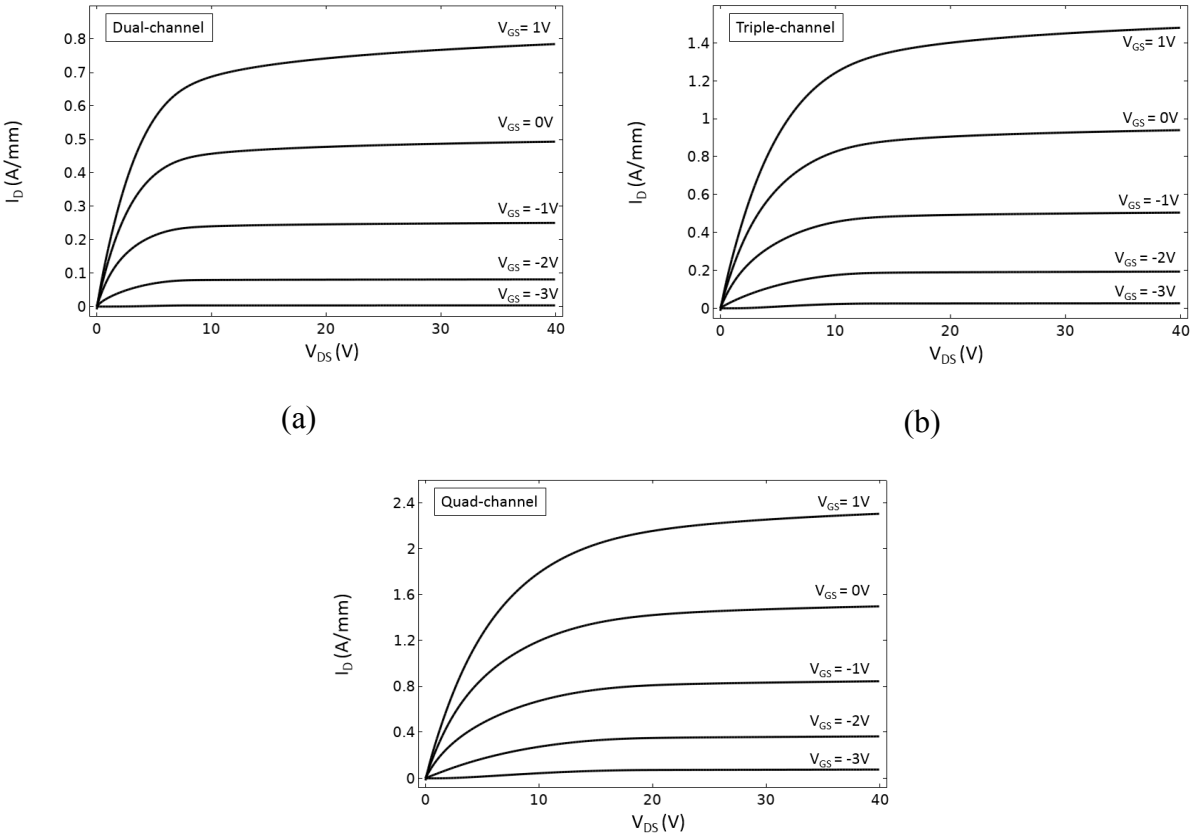

Figure 3.25 Output characteristics for the (a) dual-, (b) triple, and (c) quad-channel laterally-gated AlGaN/GaN HFET modeled in this chapter with the assumption of no polarization.

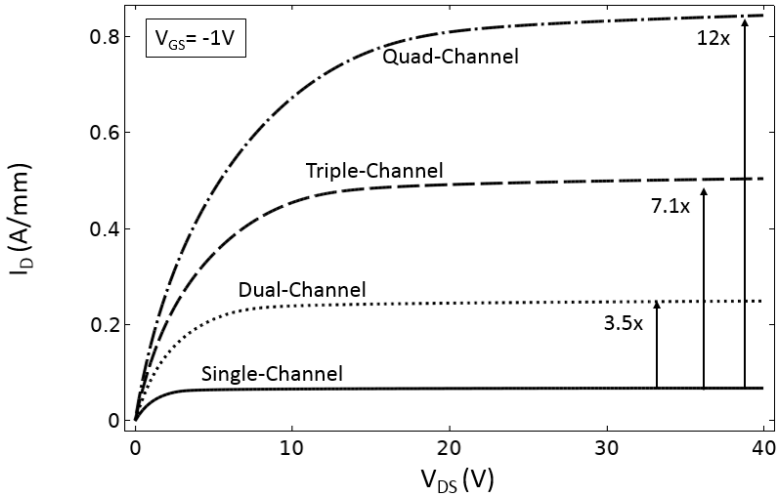

Figure 3.26 Output characteristics at $V_{GS} = -1\,V$ for the single-, dual-, triple-, and quad-channel laterally-gated AlGaN/GaN HFETs presented in Figure 3.25.

As can be deduced from Figure 3.25 and 3.26, R_{on} becomes smaller as more channels are added. Compared to the single-channel structure, where $R_{on} \approx 13.33\ \Omega \cdot mm$ and using the same V_{GS} (0 V) and V_{DS} (0.1 V) in the linear region, the dual-, triple-, and quad-channel structures give $6.6\ \Omega \cdot mm$, $4.58\ \Omega \cdot mm$, and $3.5\ \Omega \cdot mm$, respectively, which indicates a better power management at higher current densities and represents an attenuation with respect to the single-channel device of *2.02* (*~2*), *2.9* (*~3*), and *3.8* (*~4*) times when using two, three, and four channels, respectively. This almost linear dependence of R_{on} attenuation on the number of channels is shown by Figure 3.27.

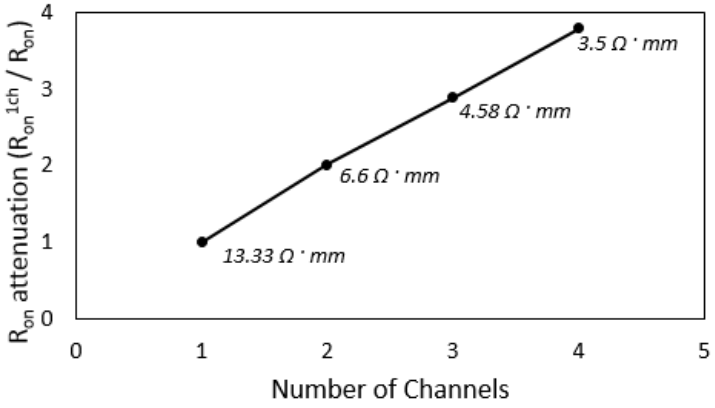

Figure 3.27 R_{on} attenuation dependence on the number of channels for the multi-channel laterally-gated AlGaN/GaN HFET in absence of polarization. R_{on} gets smaller by 2.02, 2.9, and 3.8 times with respect to the value of the single-channel HFET.

In terms of knee voltage (V_{knee}), compared to the simulated polarization-less laterally-gated single-channel AlGaN/GaN HFET, the number of additional channels tends to degrade the value of V_{knee}, which sets an alert in terms of designing when drain current and gate transconductance enhancement are needed but the maximum knee voltage tolerated by a specific circuit is below the one offered by this multi-channel HFET.

Another important feature of the simulated polarization-less multi-channel laterally-gated AlGaN/GaN HFETs is that the low output conductance (g_o) achieved in the single-channel variety is kept in the multi-channel ones.

3.4 Gate transconductance

3.4.1 Single-channel laterally-gated AlGaN/GaN HFET in absence of polarization

To study the gate transconductance (G_m) response of the device, multiple V_{DS} values need to be considered in order to evaluate its behavior under both the linear and the saturation operation regimes. The V_{DS} values in the linear regime are those values for which V_{DS} is much smaller than $V_{GS} - V_{TH}$, for $V_{GS} > V_{TH}$ [3]. For example, from the output characteristics (Figure 3.24(a)), and knowing that $V_{TH} = -2.2\ V$ (Figure 3.10(a)), one can choose either the curve for $V_{GS} = 0\ V$ or $V_{GS} = 1\ V$ and take $V_{DS} \ll V_{GS} - V_{TH}$, which is $V_{DS} \ll 2.2\ V$ or $V_{DS} \ll 3.2\ V$. Considering one order of magnitude smaller as a proper value for V_{DS} in the linear regime, then it could be $V_{DS} = 0.22\ V$ or $V_{DS} = 0.32\ V$, respectively. Taking the output characteristics for $V_{GS} = 0\ V$, then part of the linear regime around *0.2 V* is as shown in Figure 3.28, which suggests that one could use V_{DS} values between *0.1 V* and *0.5 V*.

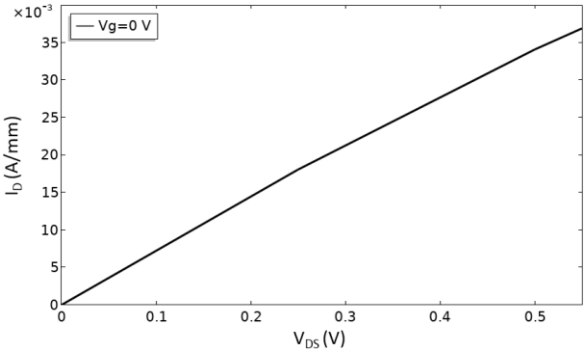

Figure 3.28 Part of the linear regime of the output characteristics at $V_{GS} = 0\ V$ for the single-channel laterally-gated AlGaN/GaN HFET in absence of polarization.

Figure 3.29 shows the G_m - V_{GS} characteristics of the simulated polarization-less single-channel laterally-gated AlGaN/GaN HFET for V_{DS} values under the linear and the saturation regimes. In comparison to a polarization-less single-channel top-gated AlGaN/GaN HFET, whose gate transconductance response is exposed in Figure 3.30, the peak on G_m becomes broader for V_{DS} under the saturation regime, getting to its maximum at $V_{GS} \approx 0.25\,V$ for $V_{DS} = 20\,V$. In this comparison of course it is quite relevant to remember that for the top-gated variety essentially no 2DEG was formed given the same layer structure. The mentioned broader range of V_{GS} is used to evaluate the linearity of the device and can also be used to compare its performance against the top-gated HFETs through the figure of merit (FOM) called gate voltage swing (GVS), which is defined as the V_{GS} range for which the gate transconductance is greater than or equal to 80% of its peak [16]. In the case of the simulated single-channel laterally-gated AlGaN/GaN HFET in absence of polarization, the value of GVS at $V_{DS} = 5V$ (Figure 3.29) improves by 407% compared to the polarization-less top-gated variety (Figure 3.30), which indicates a much better response in terms of linearity. This broader gate transconductance helps reduce the distortion in applications that require enhanced linear characteristics for power amplification [44].

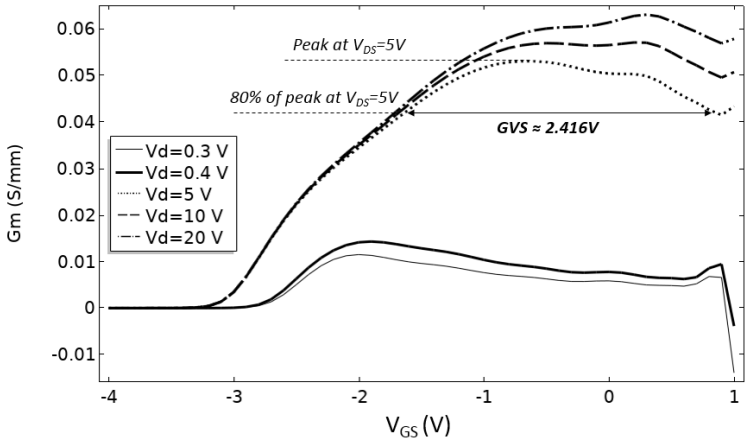

Figure 3.29 Gate transconductance (G_m) vs V_{GS} for the single-channel laterally-gated AlGaN/GaN HFET in absence of polarization. V_{DS} = 0.3 V and 0.4 V are in the linear regime.

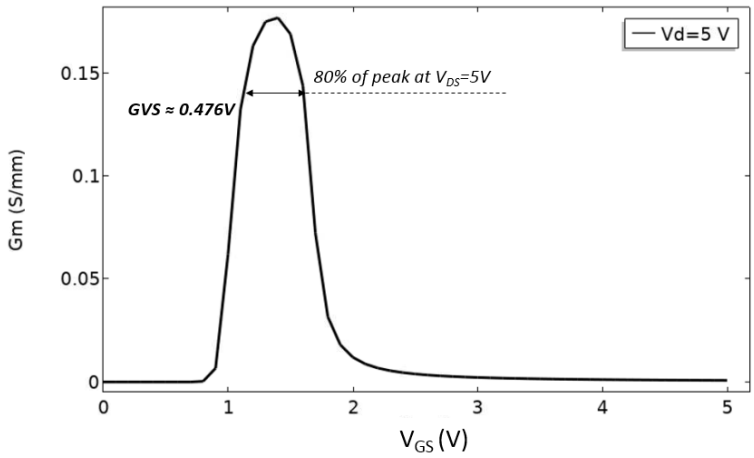

Figure 3.30 Gate transconductance vs V_{GS} for a top-gated single-channel AlGaN/GaN HFET in absence of polarization with the same dimensions as the laterally-gated variety modeled in this chapter. L_g=150nm and W_{ch}=250nm.

Also, the gate transconductance for the laterally-gated variety has a more gradual transition to its maximum value than in the case of the top-gated HFET, whose gate transconductance is generally presented by a bell-shaped profile (Figure 3.30) with a peak and then a rapid degradation at more positive values of V_{GS}, which is known to be caused in part by the leakage of channel's carrier population into the barrier layer [3].

3.4.2 Multi-channel laterally-gated AlGaN/GaN HFET in absence of polarization

Figure 3.31 shows the gate transconductance characteristics for the multi-channel structures from dual- to quad-channel polarization-less laterally-gated AlGaN/GaN HFETs modeled and discussed in this chapter for several V_{DS} values under both the linear and the saturation regimes. Not only the trend on gradual transfer characteristics observed in the previous section for the single-channel laterally-gated variety is maintained but also the enhancement on peak and broader G_m (higher VGS FOM) is assured with the addition of more channels. This is an indication of the simultaneous effect of the gate-induced electric field on the parallel channels.

Gate transconductance is even broader at higher drain biases, which enhance the linearity of the device for being used in power amplifier applications [44]. Since gate transconductance should be as high as possible to offer either the needed gain in analog applications or the fastest transition between ON and OFF states in digital applications [3], this is another reason to believe that the studied multi-channel structure can be deemed promising.

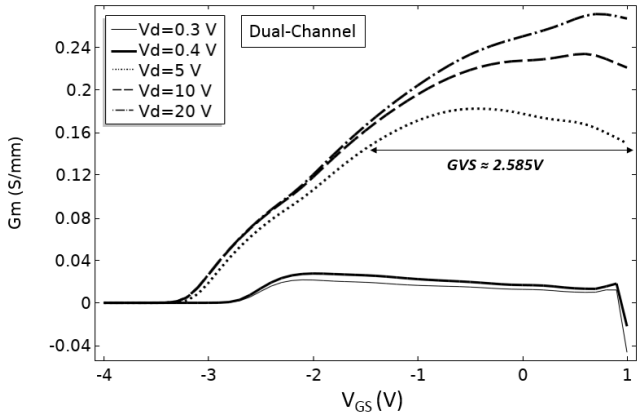

(a)

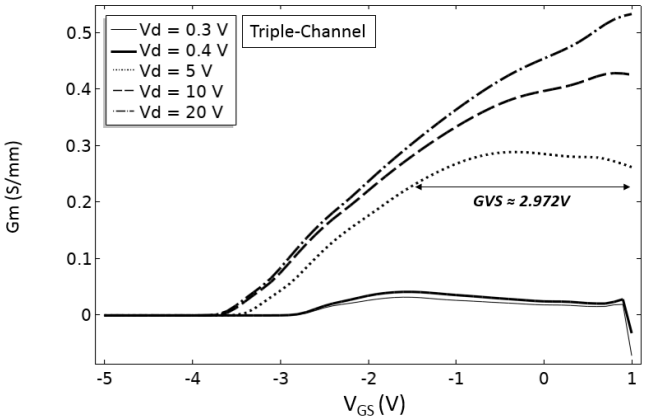

(b)

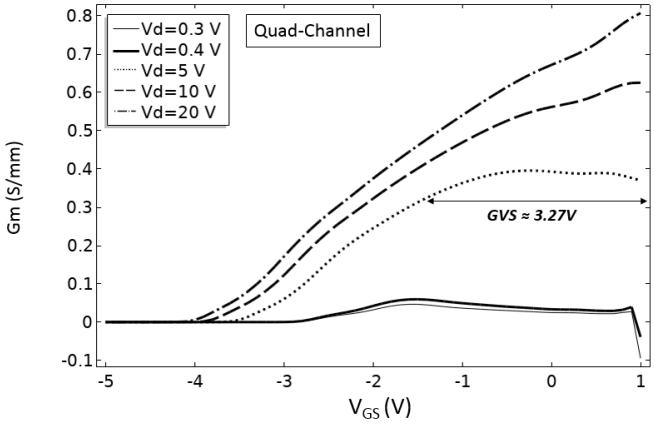

(c)

Figure 3.31 Gate transconductance vs V_{GS} for several values of V_{DS} of the (a) dual-, (b) triple-, and (c) quad-channel laterally-gated AlGaN/GaN HFET in absence of polarization. V_{DS} in the linear region are defined at 0.3 V and 0.4 V.

For better comparison on the effect of the number of channels on gate transconductance, Figure 3.32 has the plots of G_m vs V_{GS} at $V_{DS} = 20\ V$. The enhancement of G_m by 4.3x, 8.4x, and 12.3x in the dual-, triple-, and quad-channel devices, respectively, demonstrates that, on the one hand the gate transconductance enhancement scales almost linearly with the number of channels (Figure 3.33), and on the other hand the efficiency of the gates' control is maintained with respect to the equivalent single-channel device; a feature that is critical for high-power and high-frequency applications.

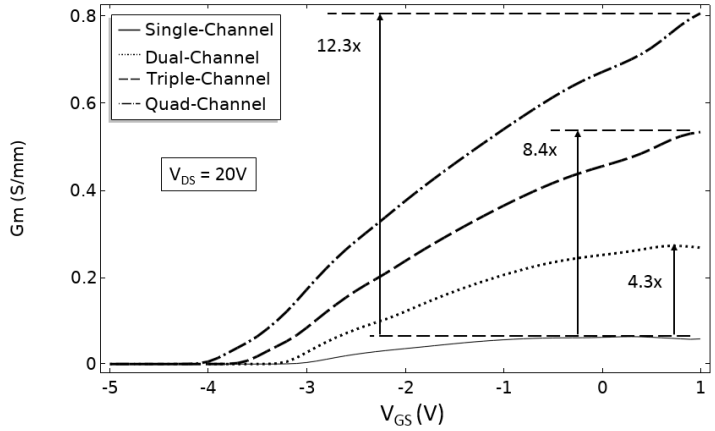

Figure 3.32 Gate transconductance vs V_{GS} at V_{DS} = 20 V for the single-, dual-, triple-, and quad-channel laterally-gated AlGaN/GaN HFETs with the assumption of no polarization.

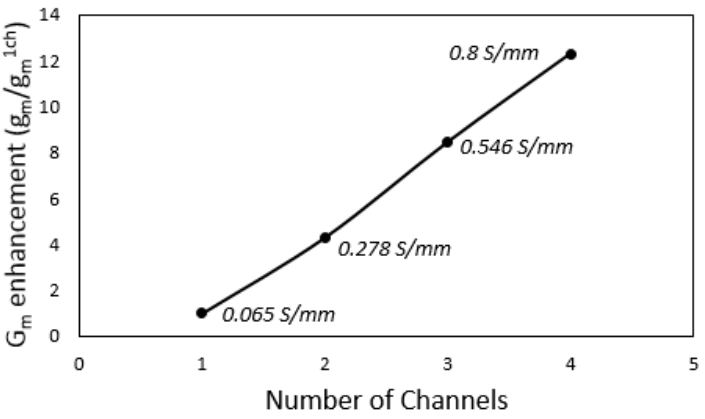

Figure 3.33 Gate transconductance enhancement dependence on the number of channels in the multi-channel laterally gated AlGaN/GaN HFET with the assumption of no polarization. V_{DS} = 20V and V_{GS} = 1V.

3.5 Chapter conclusions

- The polarization-less single-channel top-gated AlGaN/GaN HFET compared to the laterally-gated one presents a much weaker polarization induced 2DEG, which yields a positive V_{TH}.
- A simultaneous control of multiple channels stacked vertically can be achieved by lateral gates. Also, by assuring a similar electric potential among the channels, the shift of the threshold voltage is avoided.
- The single- and multi-channel laterally-gated varieties alleviate the peak of the electric field present in the gated area of the top-gated devices, representing an advantage of the former to achieve higher breakdown voltages.
- The enhancement in current density, gate transconductance, and the gate voltage swing figure of merit as well as the attenuation in ON resistance obtained in laterally-gated multi-channel AlGaN/GaN HFETs make these structures promising for applications that require high linearity and high power operation.

- The *DIBL* and the V_{knee} degrade in the laterally-gated varieties with the increase in the number of channels. This may represent a limitation for high voltage applications in the case of the former and for low voltage operation in the case of the latter.
- Although the subthreshold swing in the single-channel laterally-gated variety is not as good as that of the top-gated one, it improves in the multi-channel laterally-gated devices and keeps almost constant, indicating little degradation despite the increase in the number of channels.
- Linear dependences on the number of channels were identified for the gate transconductance enhancement and the ON resistance attenuation.

Chapter 4

Comparison of the DC characteristics of the laterally-gated and top-gated Ga-face AlGaN/GaN HFETs

In chapter 2, details about the incorporation of N- and Ga-face polarities in AlGaN/GaN HFETs for simulation purposes in Comsol were given. Following this description, in chapter 3 the DC characteristics of the laterally-gated single- and multi-channel N-face AlGaN/GaN HFETs, or to be more precise hypothetical HFETs without consideration of polarization, were exposed along with the comparison with the counterpart top-gated device variety. This chapter looks into the DC characteristics of the realistic Ga-face laterally-gated single- and multi-channel AlGaN/GaN HFETs where polarization is accurately appreciated.

The geometries for the single- and multi-channel laterally-gated Ga-face AlGaN/GaN HFETs are the same as those considered in chapter 2 (and are shown in Figure 2.1 and 2.3, respectively). The dimensions are those listed in Table 2.1 for the single-channel Ga-face HFET and in Table 2.5 for the multi-channel variety. The doping concentrations of the epilayers are listed in Table 2.2, 2.4, and 2.6. To achieve the calculated carrier concentration of the 2DEG ($n_s(x)$) for the single- and multi-channel Ga-face HFETs in Comsol, the method employed has been the second one mentioned in the *Realistic Ga-face polarity* subsection of section 2.3, which consists of implementation of *delta doping* by highly doping the 1nm-thickness of the AlGaN barrier layer closest to the heterojunction. The values of the semiconductor parameters for the $Al_xGa_{1-x}N$ barrier, which according to the description provided in chapter 2 depend on the Al mole fraction (x), are

listed in Table 2.3. For the purpose of this chapter, for which case Ga-face polarity applies, the values of *x* used for simulations are 0.1 and 0.2.

4.1 Thermal equilibrium observations

4.1.1 Single-channel laterally-gated Ga-face AlGaN/GaN HFET

Figure 4.1 shows the conduction-band edge bending at the gated area and $\frac{W_{ch}}{2}$ across the heterojunction at thermal equilibrium for the laterally-gated (Figure 4.1(a)-(b)) and the top-gated (Figure 4.1(c)-(d)) HFETs with Ga-face polarization and for the two different Al mole fractions of 0.1 and 0.2. The observed differences on the position of E_f with respect to E_c makes the sheet carrier concentration of the 2DEG stronger in the gated area for the laterally-gated variety. The geometry of the Schottky contact of the gate causes the AlGaN barrier to have a more pronounced depletion for the top-gated variety. The aforementioned observation contributes to the difference in threshold voltage (V_{TH}) among the two devices varieties even given the same Al mole fraction of the barrier. For the case of $x = 0.2$, although E_f sets above E_c compared to the case of $x = 0.1$ in the top-gated variety, its position is even higher in the laterally-gated device, predicting a more negative V_{TH} for the latter. As expected, this means that the value of V_{TH} in the laterally-gated HFET can be tuned by changing the distance between gates, also known as channel width (W_{ch}), assuring a faster depletion of the 2DEG from the lateral E-field when W_{ch} is smaller [15] [16] [17] [22].

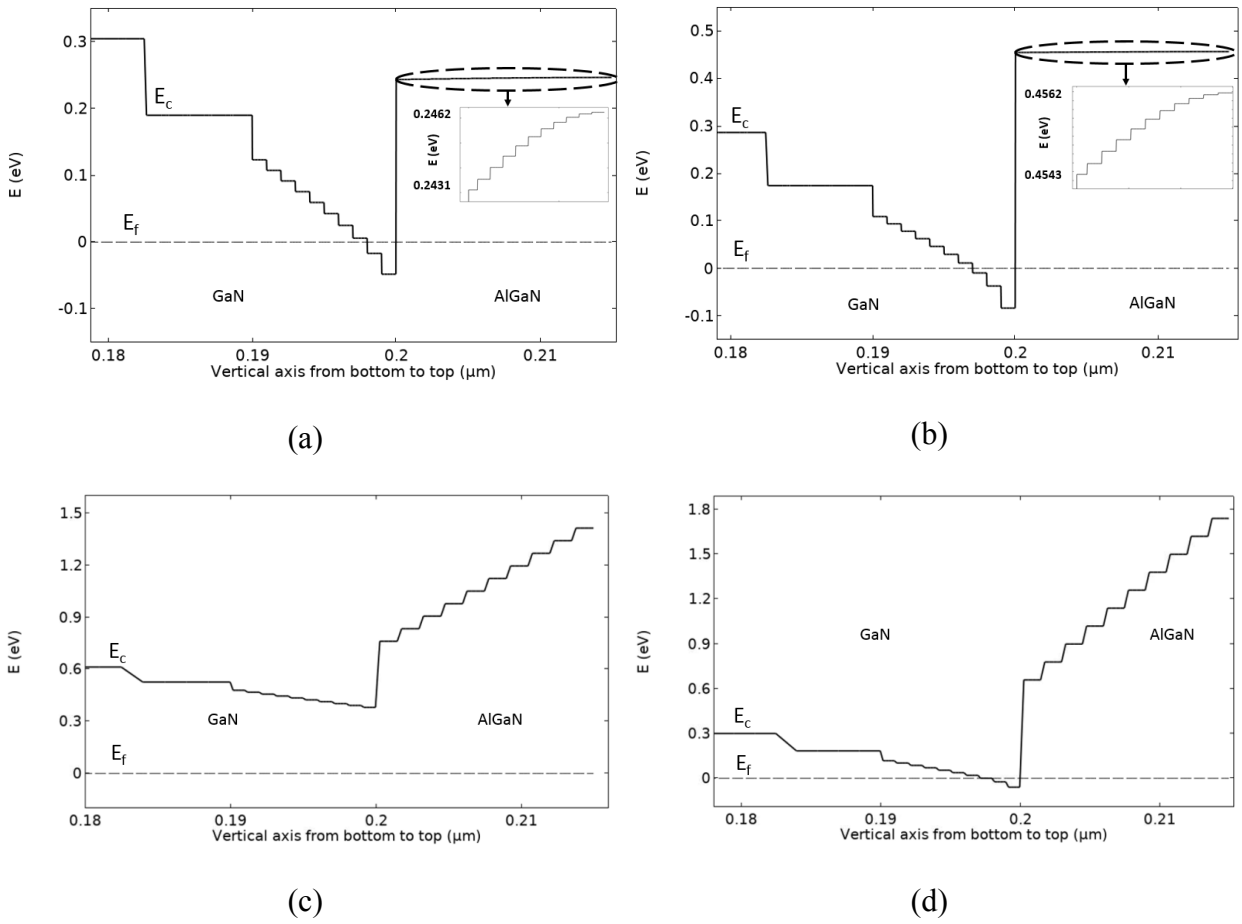

Figure 4.1 Conduction-band edge bending across the heterojunction in the gated area at thermal equilibrium for the (a)-(b) laterally-gated and (c)-(d) the top-gated Ga-face AlGaN/GaN HFETs at two different Al mole fractions of (a),(c) 0.1 (b),(d) 0.2.

In terms of the vertical E-field with respect to the heterojunction, the value of polarization as well as the position of the gates have an impact on its distribution profile and peak. Figure 4.2 presents the vertical profile of the electric field measured at the gated region of the aforementioned two device varieties: the laterally- and the top-gated AlGaN/GaN HFETs, and at two different Al mole fractions (x = 0.1 and x = 0.2). For x = 0.1, the induced charge carrier concentration of the 2DEG at the gated area of the top-gated variety is not strong enough to produce a peak of the E-field at the heterojunction (Figure 4.2(c)). For Al mole fraction of 0.2, the induced carrier concentration of the 2DEG is stronger than the case of x = 0.1, being capable of inducing also a

peak of E-field in the top-gated HFET despite of the presence of the Schottky barrier at the top. The peak of E-field is even higher on the laterally-gated variety, where the Schottky contacts are not as close as the top gate to the region where the electric field is measured, in which case the distance is $\frac{W_{ch}}{2}$.

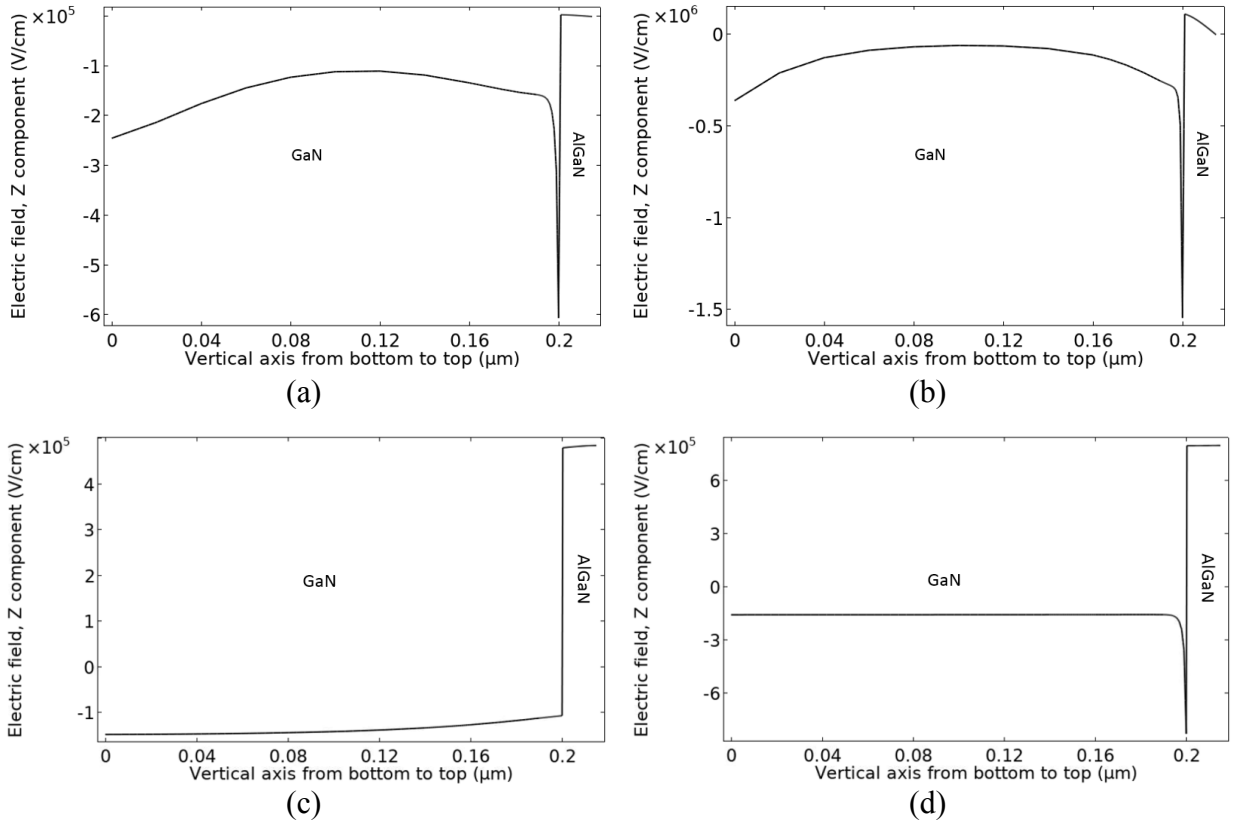

Figure 4.2 Vertical profile of the E-field across the heterojunction in the gated area at thermal equilibrium for (a)-(b) the laterally-gated and (c)-(d) the top-gated Ga-face AlGaN/GaN HFETs at two different Al mole fractions of (a),(c) 0.1 and (b),(d) 0.2.

Another characteristic that can be studied under thermal equilibrium is the profile of the E-field along the length of the device channel from source to drain at the heterojunction, which we refer to as lateral E-field. For its measurement, the same schematic shown by Figure 3.3 is used. Accordingly, two cut lines are set from source to drain, but one is positioned at $\frac{W_{ch}}{2}$, whereas the

other is placed near one of the lateral gates, specifically at 1nm of distance. Figure 4.3 presents the profile of the lateral E-field at thermal equilibrium for both device varieties: the laterally-gated (Figure 4.3(a)-(d)) and the top-gated (Figure 4.3(e)-(f)) Ga-face HFETs at the two different Al mole fractions (Figure 4.3(a),(c),(e) for $x = 0.1$ and Figure 4.3(b),(d),(f) for $x = 0.2$). According to Figure 4.3, the earlier observation of the negligible variation of the E-field at the gated area and at $\frac{W_{ch}}{2}$ in the laterally-gated variety compared to the top-gated device is replicated for the Ga-face polarization. This observation demonstrates again that the main reason for this negligible variation is the position of the Schottky contact of the gates, regardless of the induced charge density of the 2DEG or in other words, regardless of the Al mole fraction and consideration of polarization. This also indicates that with or without polarization laterally-gated AlGaN/GaN HFETs provide an alternative for alleviating the E-field peak present in the drain access region of the top-gated AlGaN/GaN HFETs, without the need for incorporating a Field-Plate (FP) to improve the breakdown voltage as mentioned in Chapter 3.

The increase on the peak of the E-field observed near the gates in the case of the laterally-gated Ga-face HFET (Figure 4.3(c) and (d)) was also observed for the hypothetical polarization-less HFET in Figure 3.4(b). This demonstrates that these peaks are caused predominantly by the closeness of the gates to the heterojunction. Additionally, as indicated earlier the several peaks in Figure 4.3(c) and (d) are caused by the mesh roughness in defining the circular cross-section of the gate pillars.

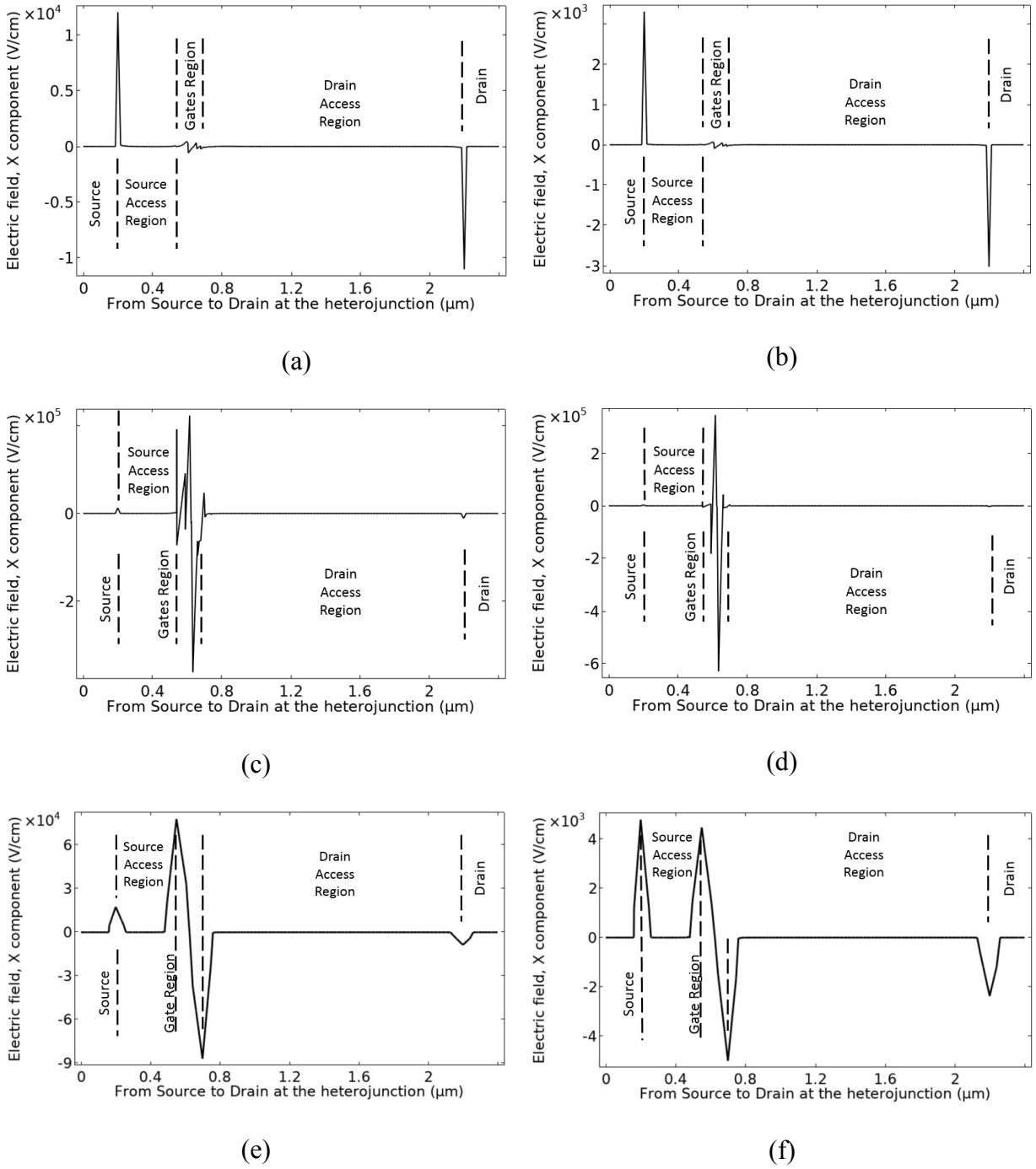

Figure 4.3 Lateral profile of the E-Field at thermal equilibrium taken at the heterojunction for the single-channel laterally-gated Ga-face AlGaN/GaN HFET measured at (a),(b) $\frac{W_{ch}}{2}$ and (c),(d) close to one of the gates. (e),(f) Lateral E-Field profile for the Ga-face top-gated AlGaN/GaN HFET. (a),(c),(e) for $x = 0.1$ and (b),(d),(f) for $x = 0.2$.

4.1.2 Multi-channel laterally-gated Ga-face AlGaN/GaN HFET

The multi-channel Ga-face AlGaN/GaN HFET built for investigation has the same geometry as that used in Chapter 3 which has been shown in Figure 2.3. As in the case of the polarization-less laterally-gated AlGaN/GaN HFET, the multi-channel Ga-face HFET was achieved by starting to position one additional AlGaN/GaN heterojunction on the top of the single-channel device explained in section 4.1.1 and keeping the same W_{ch}, L_g, L_{sg}, and L_{gd} in order to complete a dual-channel device. Then, other two similar AlGaN/GaN heterojunctions were added on the top to finally obtain a quad-channel Ga-face HFET.

As mentioned at the beginning of this chapter, to achieve the calculated carrier concentration of the 2DEG ($n_s(x)$) for the Ga-face AlGaN/GAN HFET in Comsol, keeping up with delta doping strategy to implement polarization, the 1nm-thickness of the AlGaN barrier layer at the heterojunction is heavily doped. One may assume that the doping values for the AlGaN barrier's 1nm thickness listed in Table 2.4 for a single-channel device can be configured in a straight forward manner to all the channels in the multi-channel structure. However, simulations at thermal equilibrium demonstrate that using the same doping value does not give exactly the expected values of $n_s(x)$ in every channel when there are two or more channels. This difference may be produced by the fact that the carrier concentration of the 2DEG in a channel can be affected by the electric potential of neighbor channels. Table 4.1 lists the values of doping concentration for the 1nm-thickness of the AlGaN barrier in the quad-channel Ga-face AlGaN/GaN HFET. It is worth mentioning that the average of these doping concentration values is close to the one used in the single-channel Ga-face HFET for the two cases of Al mole fraction.

Table 4.1 Sheet carrier concentration of the 2DEG ($n_s(x)$) obtained from equation (2.14) along with the 1-nm-AlGaN-region doping concentration used to achieve the corresponding $n_s(x)$ for x = 0.1 and 0.2 by simulation at thermal equilibrium of the quad-channel Ga-face AlGaN/GaN HFET.

Al-mole fraction (x)	$n_s(x)$ **[$\times$ 10^{12} cm^{-2}]**	**1nm-AlGaN-region n-type uniformly doping [$\times$ 10^{19} cm^{-3}]**			
		Channel 1 (bottom)	Channel 2	Channel 3	Channel 4 (top)
0.1	2.23	3.5	3.1	3.1	2.6
0.2	7.45	9	8.6	8.6	7.8

Figure 4.4(a) and (b) illustrate the electron concentration profiles along with the sheet charge densities obtained at thermal equilibrium from simulations after setting up the doping concentrations of the AlGaN barriers' 1nm-thickness for the quad-channel laterally-gated Ga-face AlGaN/GaN HFET and for the two Al mole fractions of 0.1 and 0.2.

The three types of channels (bottom, middle, and top channels) are identified for each case of Al mole fraction from Figure 4.4(a) and (b). The reported values of the sheet charge densities are very close among the channels, which produces a symmetry in the position of the fermi level (E_f) with respect to the bottom of the conduction band (E_c) at the heterojunctions along the whole structure of four channels (Figure 4.4(c) and (d)). This indicates a concurrent depletion of the four 2DEGs by the lateral E-fields. The total sheet charge densities for the two cases of Al mole fractions in this multi-channel Ga-face HFET adds up to 8.93×10^{12} cm^{-2} and 2.99×10^{13} cm^{-2}, when x = 0.1 and 0.2, respectively. Expectedly, these values are higher than those obtained in Chapter 3 for the case of the multi-channel AlGaN/GaN HFET where polarization was not considered.

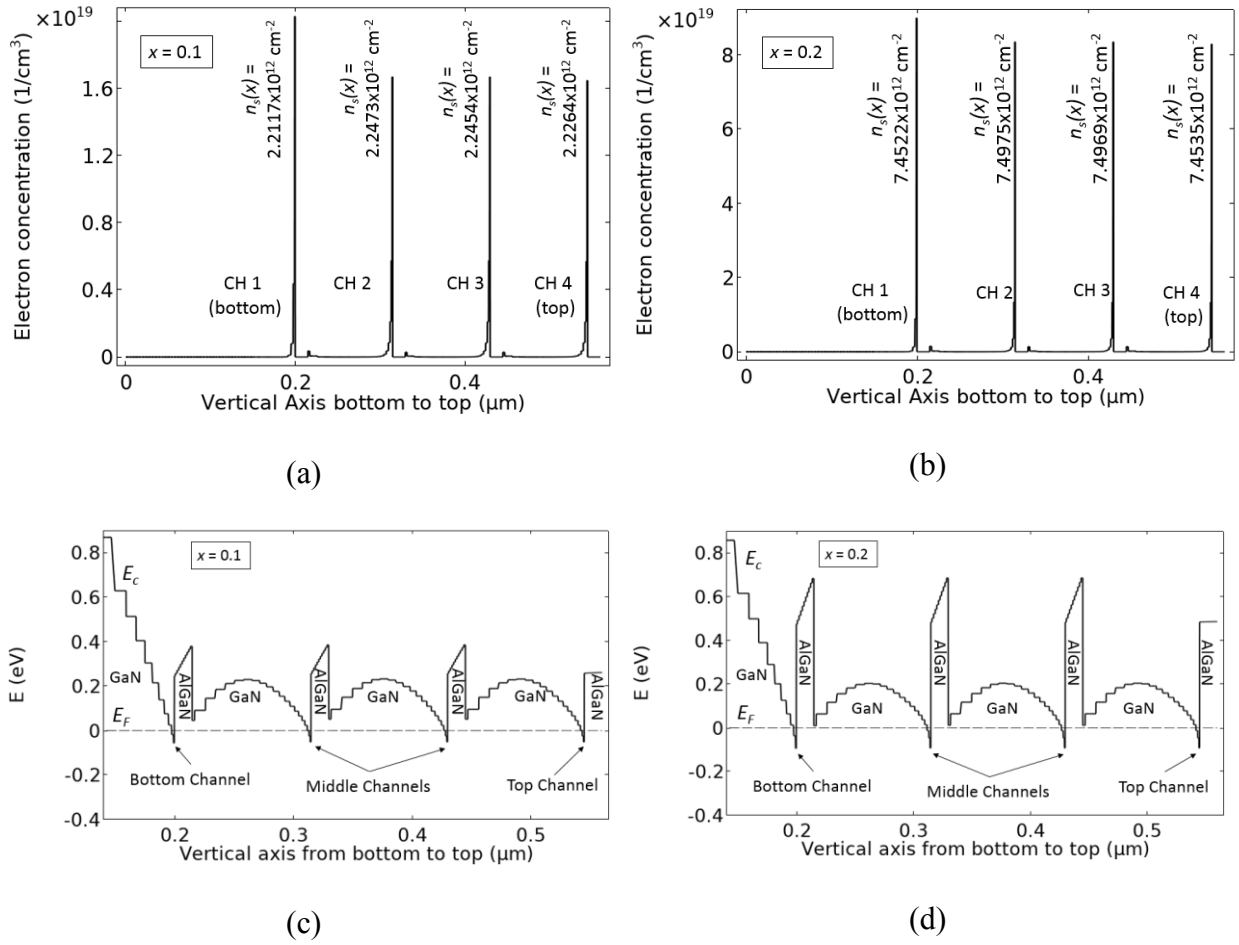

Figure 4.4 (a)-(b) Electron concentration profiles along with the carrier concentration of the 2DEGs at thermal equilibrium obtained from simulation and (c)-(d) conduction band edge at thermal equilibrium for the quad-channel laterally-gated Ga-face AlGaN/GaN HFET for the two Al mole fractions of (a),(c) 0.1 and (b),(d) 0.2.

Another observation that supports the concurrent depletion of the four 2DEGs in this multi-channel Ga-face HFET is that of the electric potential profile taken vertically across the entire structure in the gated area at thermal equilibrium. This is shown by Figure 4.5, where the four channels are at the same potential regardless the Al mole fraction.

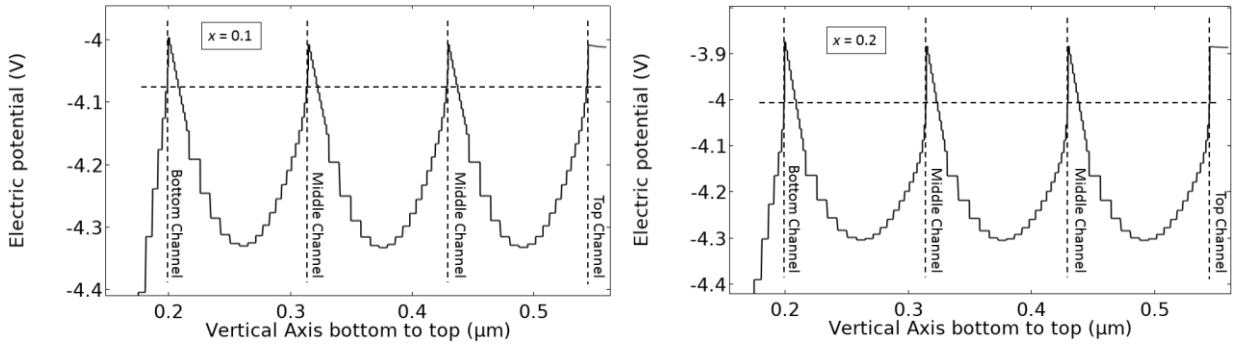

(a) (b)

Figure 4.5 Vertical profile of the electric potential at thermal equilibrium of the quad-channel laterally-gated Ga-face AlGaN/GaN HFET at the gated area and at $\frac{W_{ch}}{2}$. (By default, the initial value for electric potential in Comsol is set to -4 V).

The profiles of the E-field taken vertically at the gated area and laterally from source to drain at each heterojunction of the multi-channel heterostructure are presented in Figure 4.6. Vertically, the E-field at each heterojunction has a similar profile to that of the single-channel Ga-face variety given in Figure 4.2, which may serve as a reference when additional channels are added. Furthermore, the peaks of the E-fields for the four channels are very similar, which also demonstrates the symmetry in terms of concurrent control by the lateral gates.

Regarding the lateral E-field at each heterojunction, its profile keeps the same pattern showed by the single-channel at the gated area, where the variation of the E-field is very low, indicating that the multi-channel Ga-face is also a very good alternative to alleviate the E-field peaks present at the gate edge of the drain access region in the top-gated AlGaN/GaN HFETs, while current density and gate transconductance are expectedly enhanced.

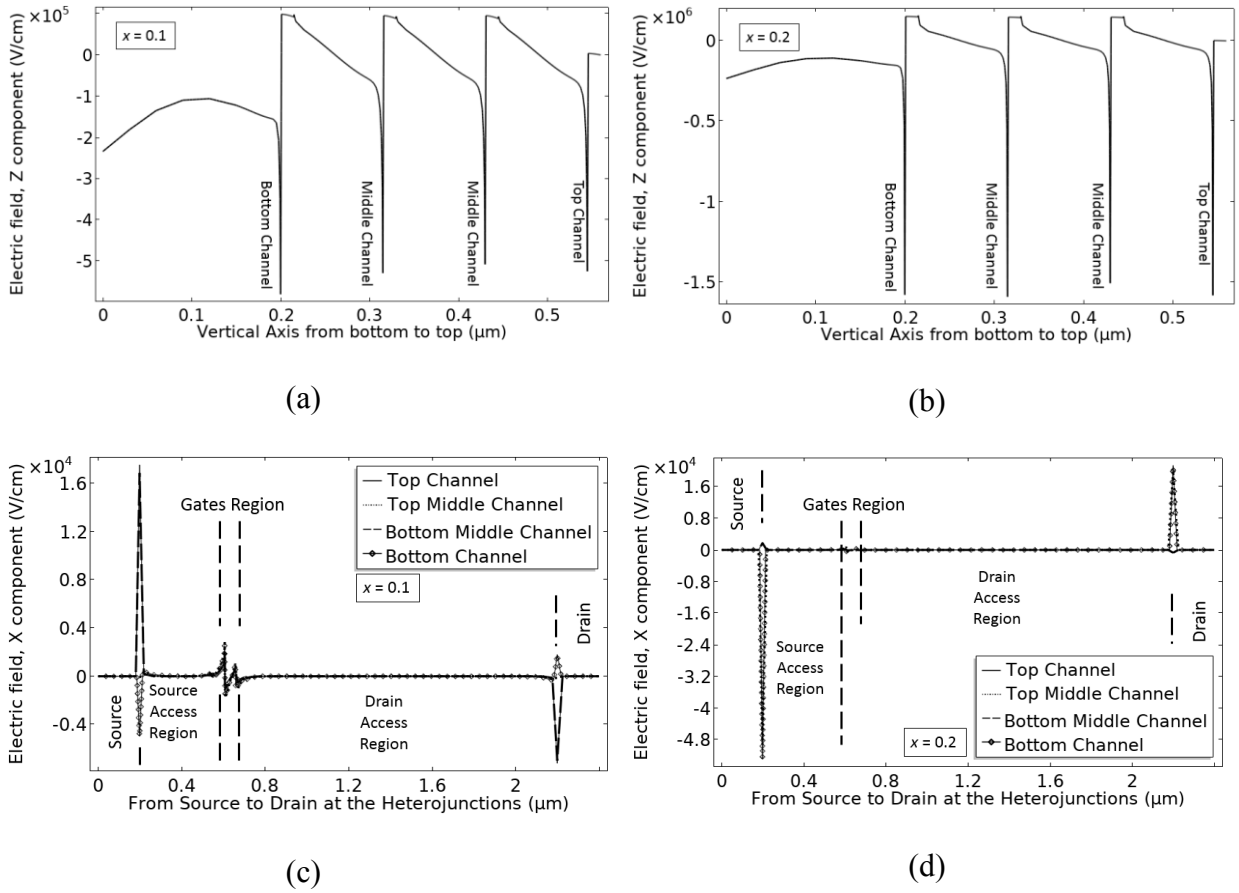

Figure 4.6 Electric field profiles of the quad-channel laterally-gated Ga-face AlGaN/GaN HFET measured (a)-(b) vertically at the gated region and at $\frac{W_{ch}}{2}$ and (c)-(d) laterally from source to drain at the heterojunctions.

4.2 Transfer characteristics

4.2.1 Single-channel laterally-gated Ga-face AlGaN/GaN HFET

Figure 4.7 shows the transfer characteristics of the single-channel laterally- and top-gated Ga-face AlGaN/GaN HFETs for the two values of Al mole fraction (0.1 and 0.2) for comparison.

The threshold voltages obtained in the laterally-gated Ga-face variety are considerably more affected by the Al mole fraction. This situation exacerbates by the wider the W_{ch} when the more challenging would be the depletion of the 2DEG by the lateral E-field, which has been

experimentally corroborated by Odabasi *et al.* [16], Nikoo *et al*. [17], Santoruvo *et al.* [18], and Erine *et al.* [22]. These experimental works support the results obtained here by simulation and confirm the assertiveness of the methods used to achieve the calculated carrier concentration of the 2DEG for realistic simulations of Ga-face AlGaN/GaN HFETs in Comsol.

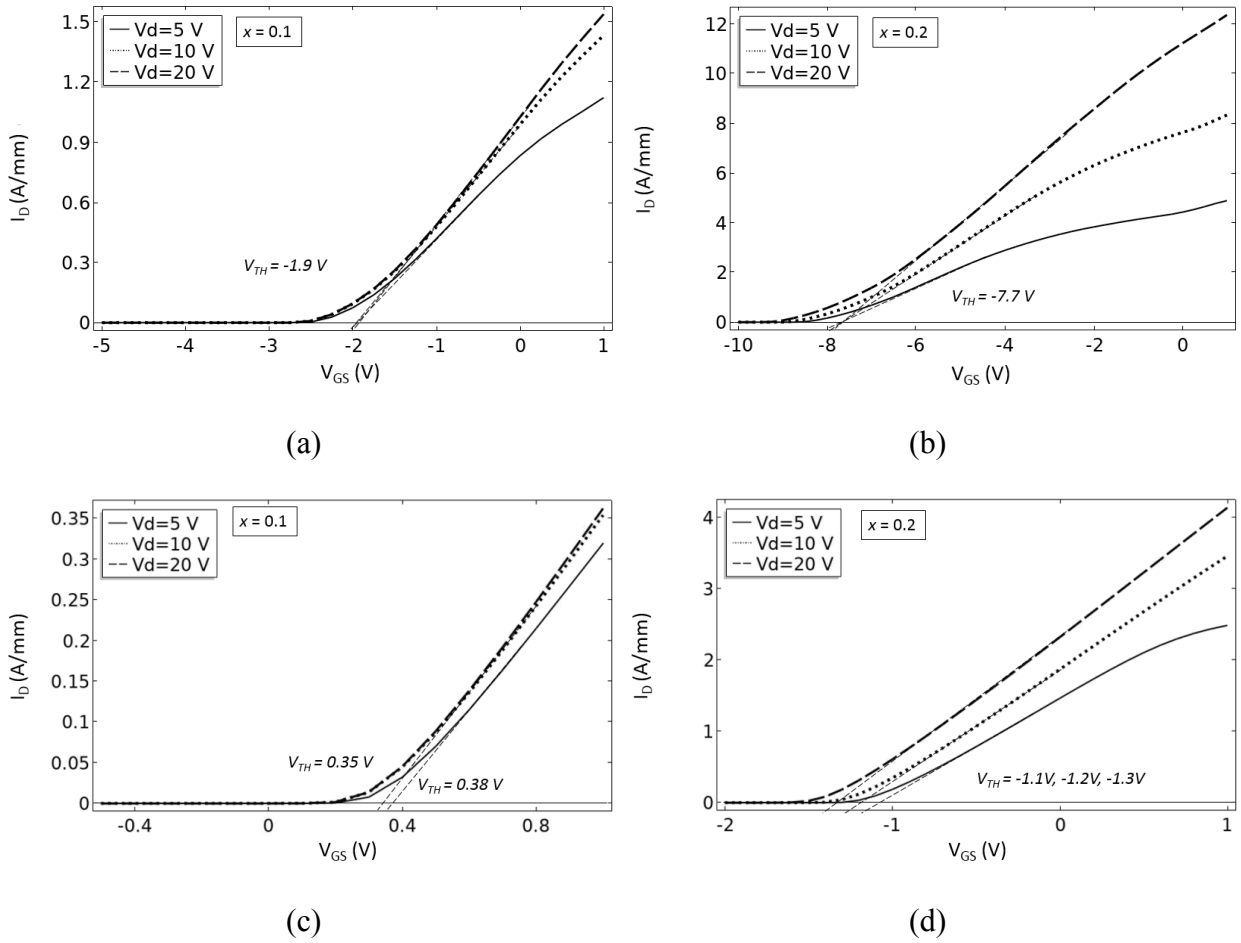

Figure 4.7 Transfer characteristics of (a)-(b) the laterally-controlled single-channel and (c)-(d) the top-gated single-channel Ga-face AlGaN/GaN HFETs for the two values of Al mole fraction of (a),(c) 0.1 and (b),(d) 0.2.

The shift of V_{TH} to more negative values at higher Al mole fractions marks the important role that a third gate at the top of the AlGaN barrier may have to strengthen the effect of the E-field, which turns to be not only laterally but also vertically depleting the 2DEG, which is deemed

very effective when the channel width becomes wider, as it is described experimentally by Ma *et al.* [19] [21] and Nela *et al.* [20].

One interesting observation made at the time of running the simulations was that current density drops at higher values of V_{GS} as shown by Figure 4.8. To understand this phenomenon, the electron current density profile at 3-D (Figure 4.9) was studied for the entire structure in order to try to identify patterns of current restriction or the establishment of a predominant flow in places different than the 2DEG channel. The arrows in Figure 4.9 represent the direction of the current density below the heterojunction (at the 2DEG), through the GaN channel layer, and through the p-GaN buffer layer. The value of V_{GS} is changed gradually in order to see the impact on the arrows' direction while V_{DS} is kept constant, in this case at 5V.

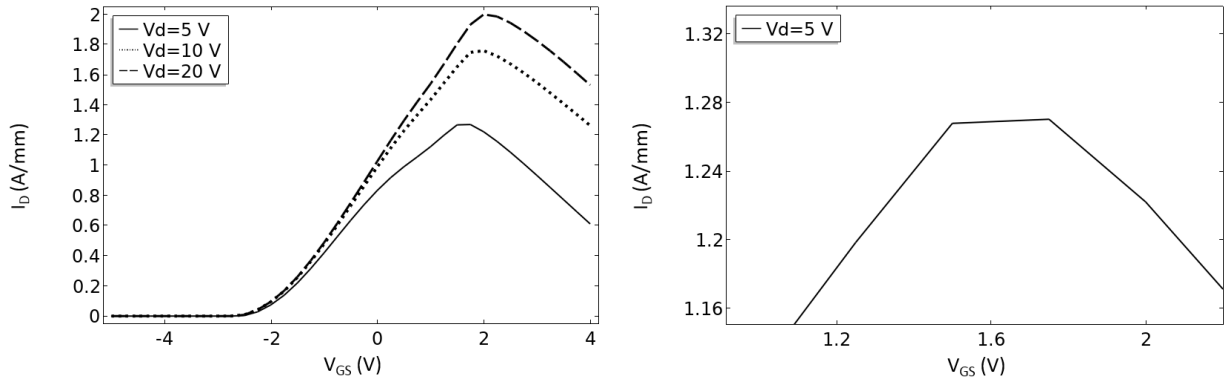

(a) (b)

Figure 4.8 (a) Transfer characteristics of the laterally-gated single-channel Ga-face AlGaN/GaN HFET for Al mole fraction of 0.1. (b) Zoom-in of (a) for V_{DS} = 5V at the region where I_D drops.

The drain current density's flow keeps the same direction on the GaN channel layer for $-5V \leq V_{GS} < 0.25V$. Then, at V_{GS} = 0.25V the current's flow starts changing its direction at the gates' edge of the source access region below the heterojunction (Figure 4.9(c)) and keeps the same pattern up to V_{GS} = 1.5V, when I_D reaches its maximum (Figure 4.8(b)). When V_{GS} = 1.75V,

again the current density's direction changes at the gates' edge of the source access region below the heterojunction (Figure 4.9(d)) and the value of I_D starts dropping (Figure 4.8(b)), keeping the same pattern for $V_{GS} > 1.75$V.

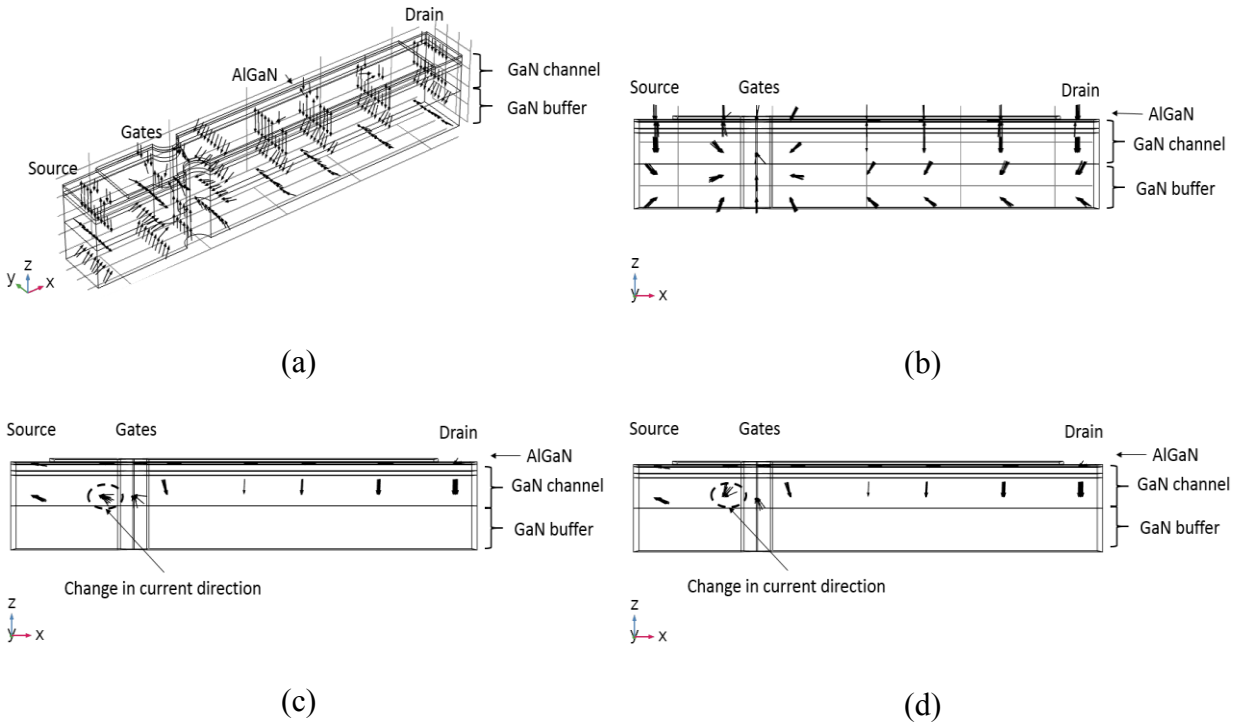

Figure 4.9 (a) 3-D profile and (b) 2-D profile of the current density at $V_{GS} = -5\,V$ and $V_{DS} = 5\,V$ for the single-channel laterally-gated Ga-face AlGaN/GaN HFET. (c) and (d) show the change in the flow of current density for 0.25V $\leq V_{GS} <$ 1.75 and $V_{GS} \geq$ 1.75V, respectively.

This drop in I_D may be caused by barrier lowering between the channel and the source. Apparently, one of the results of using simulation is that the software considers the source terminal as ideal, which implies a source of large amount of electrons, which produces a rush of charge carriers into the channel and therefore a reduction of the potential barrier, which is also related to the existence of a dynamic source access resistance, which may increase due to the negative feedback, resulting in a 3-D moving charge-carrier device rather than a 2-D charge-carrier confinement device. The presence of the mentioned dynamic source access resistance is supported

by the observation made by Palacios *et al.* [45] and also experimentally reported by Odabasi et al. [16].

In terms of the subthreshold performance, Figure 4.10 exposes the *Log* I_D vs V_{GS} for both device varieties: the laterally- and the top-gated Ga-face HFETs and for the two values of Al mole fraction (x). In the case of x = 0.1, the value of drain current density for V_{DS} in the linear regime when the device is OFF sets under 10^{-9} A/mm for the laterally-gated variety, whereas for the case of the top-gated device it sets below that value by almost one order of magnitude, which indicates less power consumption for the latter when it is not in operation. For the case of x = 0.2, although the usage of a higher Al mole fraction makes the current density to increase in both varieties, the same difference is present. This may happen because on the one hand the carrier concentration of the 2DEG at the gated area gets smaller in the top-gated variety and on the other hand the existence of the gate at the top keeps a constant distance to the 2DEG along the width of the channel, which makes the vertical E-field depletes the 2DEG uniformly. This is not the case for the lateral depletion, which becomes more challenging towards the middle of the channel ($\frac{W_{ch}}{2}$).

Regarding the drain-induced barrier lowering (*DIBL*), its value for each HFET variety and Al mole fraction (x) was calculated using equation (3.3), where $V_{DS}^{sat} = 20V$ and $V_{DS}^{lin} = 0.4V$. *DIBL* gets reduced by 45.6% when x = 0.1 and 33.72% when x = 0.2 in the top-gated variety compared to the laterally-gated one. This indicates an advantage for the former in terms of the V_{DS}'s impact on the electrostatic control of the gate, but with the cost of a lower current density. The degradation of *DIBL* in the laterally-gated variety gets worse in the Ga-face polarity compared to the case when polarization was not considered. This degradation may be explained by the stronger sheet carrier concentration of the 2DEG, which makes the lateral depletion of the channel more challenging and gives a more V_{DS} dependent device for channel control from the gates.

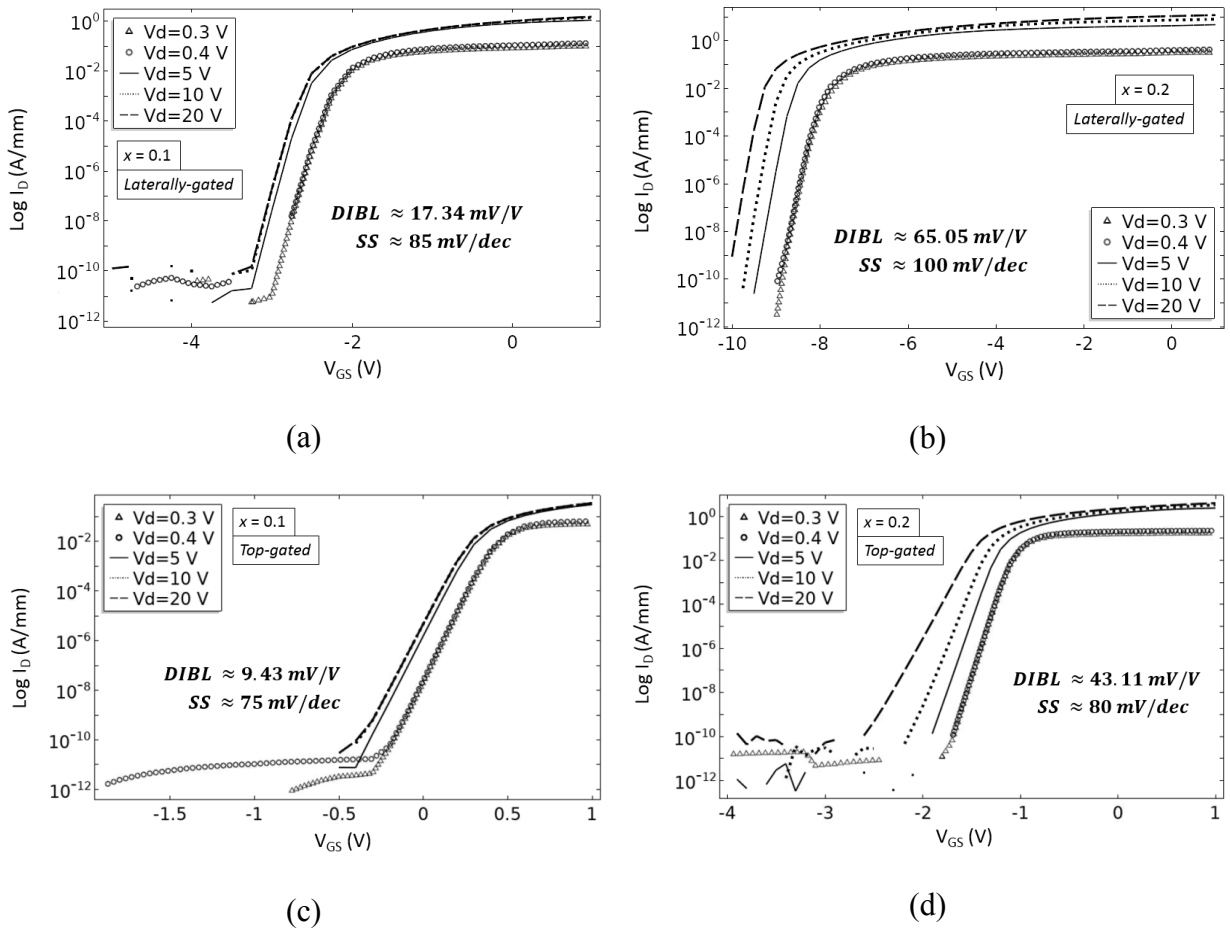

Figure 4.10 Subthreshold characteristics for (a)-(b) the single-channel laterally-gated and (c)-(d) the single-channel top-gated Ga-face AlGaN/GaN HFETs for V_{DS} in the linear and saturation regimes and for the two values of Al mole fraction of (a),(c) 0.1 and (b),(d) 0.2.

The subthreshold-swing (*SS*) obtained for the laterally-gated device is 13.3% and 25% higher when $x = 0.1$ and $x = 0.2$, respectively compared to the top-gated variety, but gets closer to the ideal value of *60 mV / dec* compared to the case of the laterally-gated HFET when polarization was neglected. The mentioned difference in *SS* between the laterally- and the top-gated varieties can be a representation of the effectiveness of the vertical vs lateral E-fields for switching the device between OFF and ON states, which may indicate a better controllability from the gate at the top rather than from the lateral gates. However, the I_{ON}/I_{OFF} ratios for both varieties are about the same value of 10^9.

Also, it is worth noting that *SS* degrades by a higher percentage at a higher Al mole fraction in the laterally-gated Ga-face AlGaN/GaN HEFT compared to the top-gated variety. However, the opposite happens for *DIBL*, which increases at a higher percentage in the latter, which shows a different sensitivity between varieties according to the parameter to be evaluated. Additionally, in contrast to the polarization-less laterally-gated HFET, whereas *SS* improves substantially, *DIBL* deteriorates in the laterally-gated Ga-face HFET. This can serve as a point of reference depending on applications' requirements such as fast switching and high current density.

4.2.2 Multi-channel laterally-gated Ga-face AlGaN/GaN HFET

The challenge of preserving the same threshold voltage of the single-channel device is also faced in this multi-channel structure. For achieving this goal, the thickness of the GaN channel layers at the middle and top channels were tuned to finally be set up at 100 nm. This symmetry in thickness of these GaN channel layers along with the doping concentration of the 1nm-thickness of the AlGaN barriers as indicated in Table 4.1 make the carrier concentrations of the multiple 2DEGs to be similar among them as shown by Figure 4.4, and allow the electric potential to be the same along the multiple channels as displayed by Figure 4.5. To summarize, the structure of this laterally-gated Ga-face AlGaN/GaN HFET is as follows:

4th channel (top):	***AlGaN (15nm) / n-GaN (100nm)***
3rd channel:	***AlGaN (15nm) / n-GaN (100nm)***
2nd channel:	***AlGaN (15nm) / n-GaN (100nm)***
1st channel (bottom):	***AlGaN (15nm) / n-GaN (200nm) / p-GaN (200nm)***

Figure 4.11 shows the transfer characteristics for the single-, dual-, triple, and quad-channel laterally-gated Ga-face AlGaN/GaN HFETs for the two values of Al mole fraction (0.1 and 0.2). For $x = 0.1$, V_{TH} can be preserved by each variety, whereas for $x = 0.2$ there is a shift on V_{TH} of

about 0.6 V for the triple- and the quad-channel varieties. This shift at $x = 0.2$ may have been caused by the fact that since the tuning of the GaN channel layers' thickness was made at $x = 0.1$, at higher Al mole fraction a thicker GaN channel layer would be required as additional channels are added, specifically for the case of the third and fourth channels.

Higher current densities are offered by every additional channel, obtaining an enhancement of 154% (~2.5x), 303.5% (~4x), and 452% (~5.5x) at $x = 0.1$ and 120% (~2.2x), 239% (3.4x), and 358% (4.5x) at $x = 0.2$ for the dual-, triple-, and quad-channel Ga-face HFETs, respectively, at V_{DS} = 5 V and V_{GS} = 1 V.

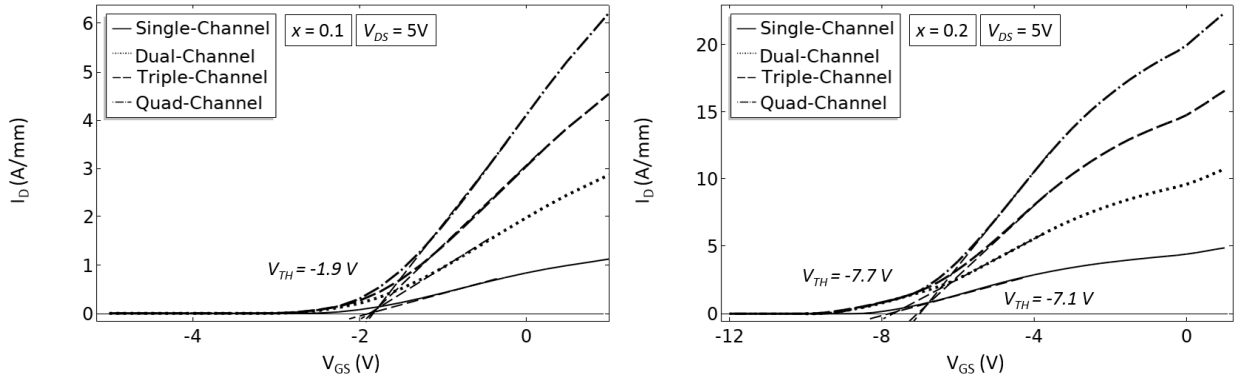

(a) (b)

Figure 4.11 Transfer characteristics from the single- to the quad-channel laterally-gated Ga-face AlGaN/GaN HFETs at V_{DS} = 5 V and for (a) $x = 0.1$ and (b) $x = 0.2$.

In terms of the subthreshold response, Figure 4.12 shows how *DIBL* is impacted by the incorporation of additional channels and change in the Al mole fraction. The more channels are added, the more dependent the DC response is on V_{DS} for drain-to-source voltages in the saturation region (e.g. 5V – 20V), which is confirmed by the change in *DIBL*, whose value increases with the number of channels almost linearly between the dual- and the quad-channel devices when the Al mole fraction is 0.1, but presents a saturation when Al mole fraction is 0.2 as shown by Figure 4.13. This dependence on V_{DS} may be caused by the distance between the additional channels and the GaN buffer layer positioned below the bottom channel heterojunction, making the effect of the

buffer to be progressively diminished with the number of channels and even more impacted at higher sheet carrier concentration of the multiple 2DEGs.

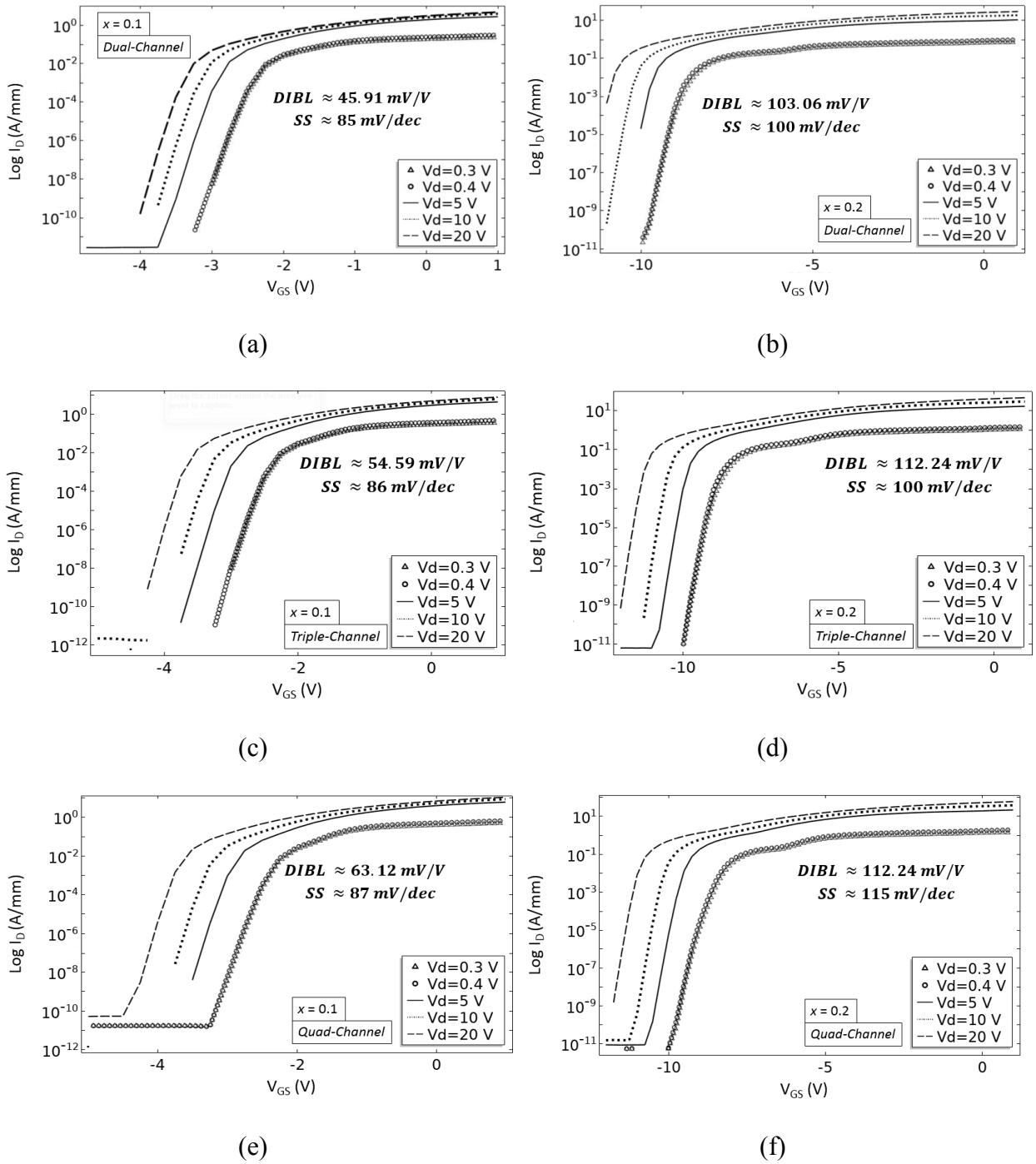

Figure 4.12 Subthreshold characteristics for the (a)-(b) dual-, (c)-(d) triple-, and (e)-(f) quad-channel laterally-gated Ga-face AlGaN/GaN HFETs at the two Al mole fractions: (a),(c),(e) x = 0.1 and (b),(d),(f) x = 0.2.

It is worth noting that a higher Al mole fraction has a considerable impact on the degradation of *DIBL* in the laterally-gated multi-channel Ga-face AlGaN/GaN HFETs, as it can be appreciated in Figure 4.12 for the cases between $x = 0.1$ and $x = 0.2$, where *DIBL* is more than 124%, 100%, and 77% degraded when Al mole fraction of 0.2 is used in the dual-, triple, and quad-channel laterally-gated Ga-face HFET varieties, respectively.

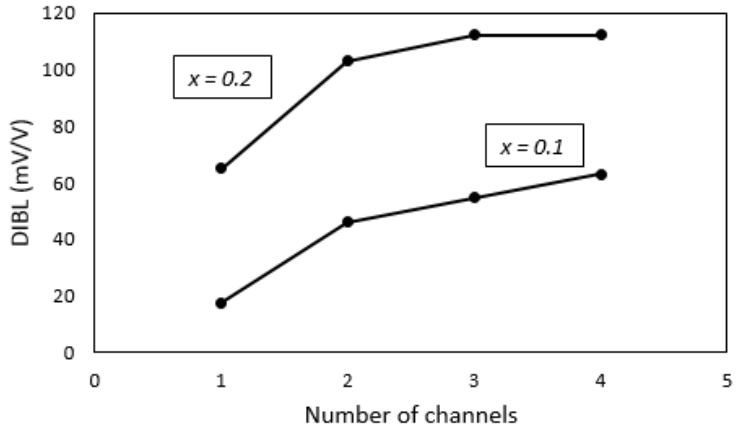

Figure 4.13 DIBL dependence on the number of channels for the laterally-gated multi-channel Ga-face AlGaN/GaN HFET at the two values of Al mole fractions under study.

Also, from Figure 4.12, the subthreshold swing (*SS*) can be evaluated with the number of channels and the different Al mole fraction. The multi-channel Ga-face HFETs show an almost identical *SS* compared to the single-channel device for both Al mole fractions. This demonstrates that little degradation is produced with the incorporation of additional channels while enhancement on current density, and as to be seen transconductance, is achieved. According to the presented data, the lowest *SS* that can be reached with these varieties of laterally-gated Ga-face AlGaN/GaN HFETs is 85 $mV\ /\ dec$ at $x = 0.1$ and 100 $mV\ /\ dec$ at $x = 0.2$ (Figure 4.14).

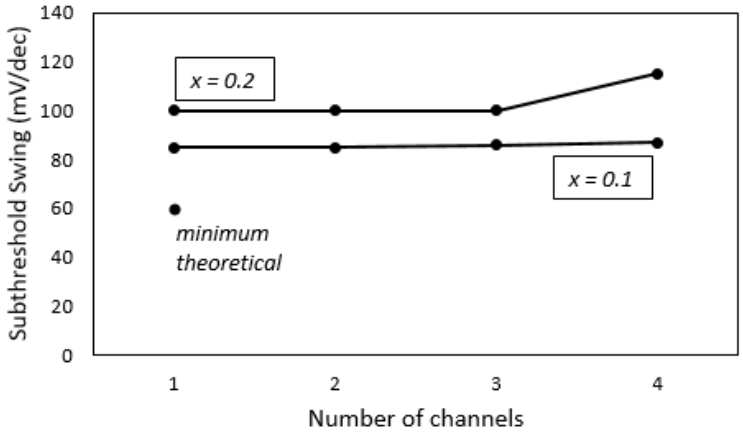

Figure 4.14 Subthreshold swing dependence on the number of channels for the laterally-gated multi-channel Ga-face AlGaN/GaN HFET at the two values of Al mole fractions under study.

Other two parameters to evaluate from Figure 4.12 are the off-current and the I_{ON}/I_{OFF} ratio, whose values are not deteriorated compared to the case of the single-channel variety, for the two different Al mole fractions. The off-current keeps its low values under 10^{-10} A/mm for V_{DS} in the linear regime, which means no degradation in terms of power consumption at the OFF state with the incorporation of additional channels. The I_{ON}/I_{OFF} is maintained at a relatively high value of $>10^9$ from the dual- to the quad-channel structure.

4.3 Output characteristics

4.3.1 Single-channel laterally-gated Ga-face AlGaN/GaN HFET

Figure 4.15 shows the output characteristics for the single-channel laterally- and top-gated Ga-face AlGaN/GaN HFETs with the same dimensions and for the two Al mole fractions under study (i.e. 0.1 and 0.2). The knee voltage (V_{knee}) is considerably impacted by changing the position of the gates from being at the top to be lateral, getting degraded in the laterally-gated variety and also by using a higher Al mole fraction. This degradation in V_{knee} may be explained by the less

uniform effect of the lateral E-field when gates are positioned laterally compared to a vertical one when the gate is at the top and cover the channel at the same distance along the channel width.

Different to what happen with V_{knee}, the ON resistance (R_{on}) gets improved in the laterally-gated variety by ~40% and ~47% at $x = 0.1$ and $x = 0.2$, respectively. This improvement in R_{on} can be attributed to the larger arear of the source and drain ohmic contacts than that of the effective channel width in the laterally-gated HFETs, as shown in chapter 3 for the case where polarization was excluded.

The output conductance (g_o) or slope in the saturation region at V_{GS} = 1V is higher in the laterally-gated HFET than in the top-gated variety. However, for smaller values of V_{GS}, the value of the slope is near zero as one may expect to obtain stability in radio frequency applications. The low output conductance along with a higher current density obtained in the laterally-gated variety compared to the top-gated HFET are possible because of the duality and the improved proximity of the gates to the channel and to both the AlGaN barrier and the GaN channel layers.

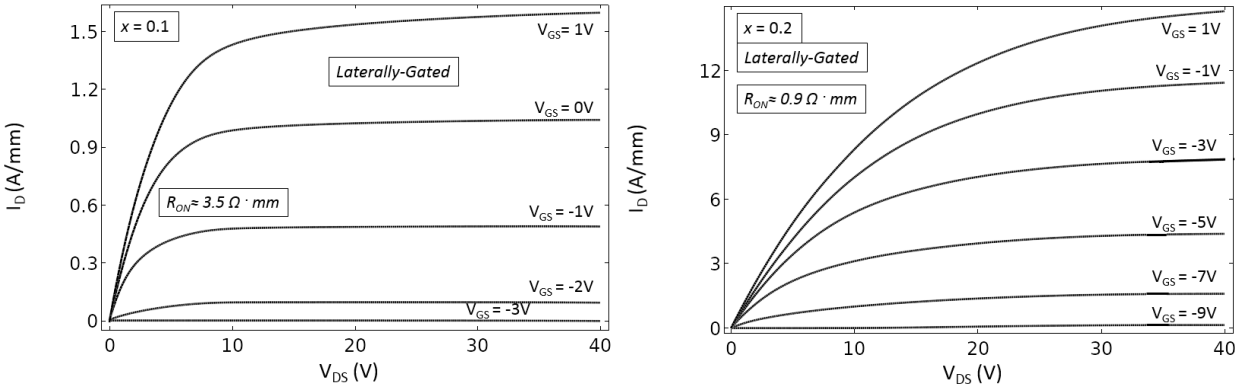

(a) (b)

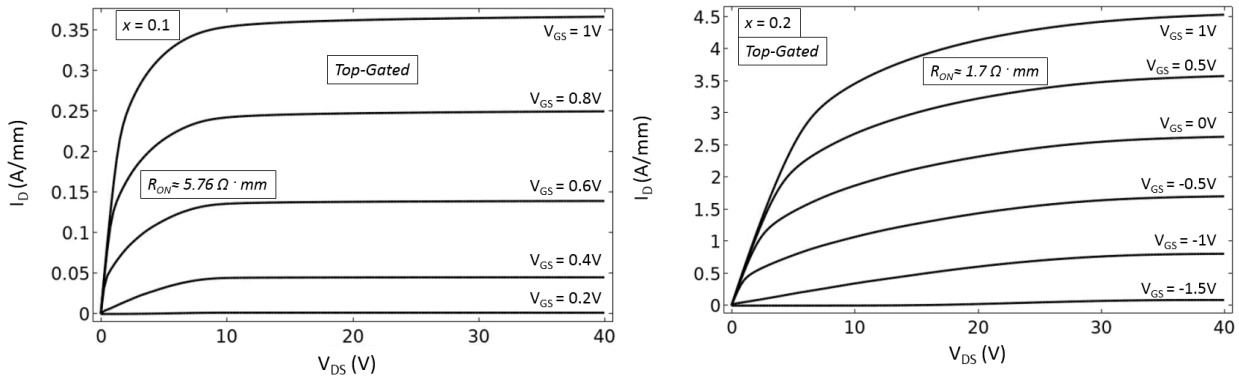

(c) (d)

Figure 4.15 Output characteristics of the single-channel (a)-(b) laterally-gated and (c)-(d) top-gated Ga-face AlGaN/GaN HFETs at the two Al mole fractions (a),(c) 0.1 and (b),(d) 0.2.

4.3.2 Multi-channel laterally-gated Ga-face AlGaN/GaN HFET

Figure 4.16 shows the output characteristics of the dual-, triple-, and quad-channel laterally-gated Ga-face AlGaN/GaN HFETs at the two Al mole fractions of 0.1 and 0.2, whereas Figure 4.17 shows the output characteristics at V_{GS} = 0V for the four device varieties (single- to quad-channel) and also at the two different Al mole fractions for comparison. The current densities are enhanced with the incorporation of additional channels, to the tune of ~3.2x, ~5.7x, and 8.2x higher than that of the single-channel variety when x = 0.1, and ~2.6x, ~4x, and ~5.4x higher than that of the single-channel variety when x = 0.2 (i.e. for the dual-, triple-, and quad-channel devices, respectively). The difference in current density enhancements from x = 0.1 to x = 0.2 is caused by the higher carrier concentration of the 2DEGs when a higher Al mole fraction of 0.2 is used, which affects the electric potential of the channels.

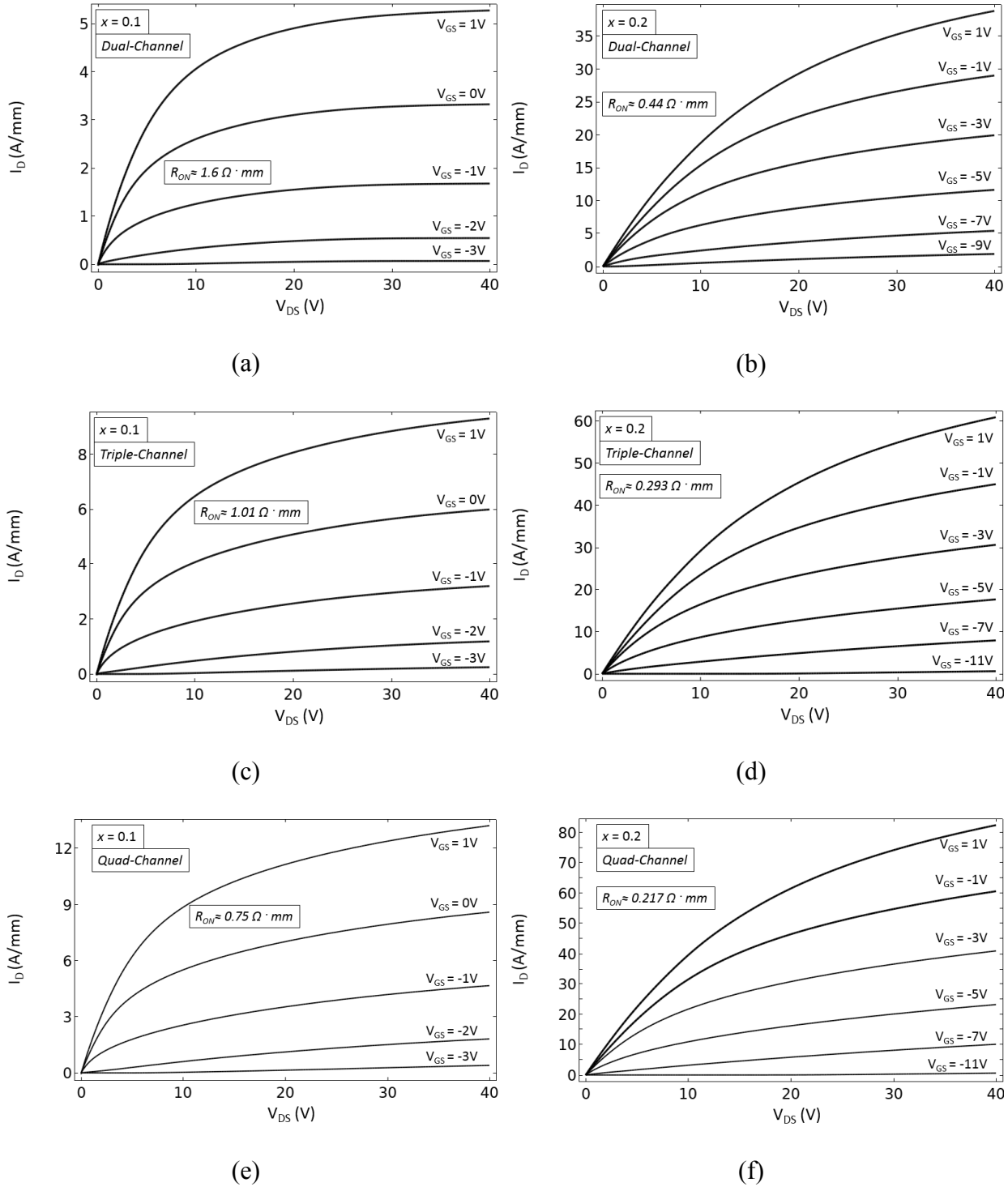

Figure 4.16 Output characteristics for the dual-, triple, and quad-channel laterally-gated Ga-face AlGaN/GaN HFETs modeled in this chapter at the two values of Al mole fraction of 0.1 and 0.2.

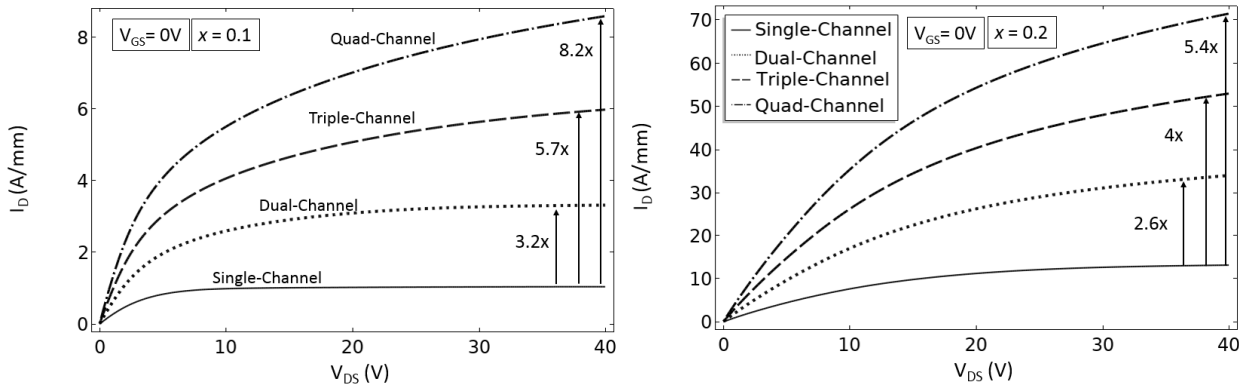

(a) (b)

Figure 4.17 Output characteristics at V_{GS} = 0 V for the single-, dual-, triple-, and quad-channel laterally-gated Ga-face AlGaN/GaN HFETs modeled in this thesis and for the two Al mole fractions of (a) 0.1 and (b) 0.2.

In terms of R_{on}, the value of this factor becomes smaller with increase in the number of channels. The reduction or attenuation in R_{on} per additional channel with respect to the single-channel HFET follows a linear characteristic for both Al mole fractions of 0.1 and 0.2 as shown in Figure 4.18.

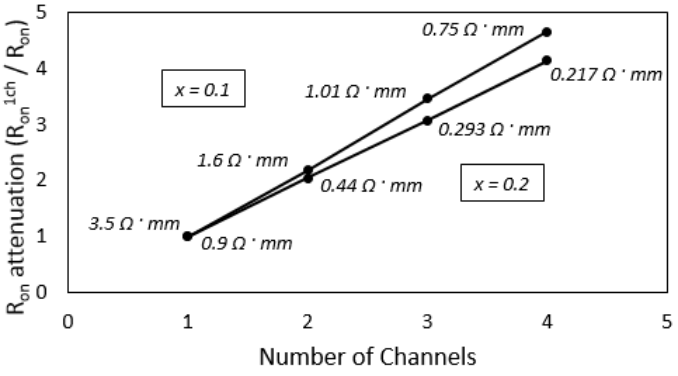

Figure 4.18 R_{on} attenuation dependence on the number of channels for the multi-channel laterally-gated Ga-face AlGaN/GaN HFETs.

Regarding the knee voltage (V_{knee}), its value tends to increase with the increase in the number of channels when using the same Al mole fraction; however, its change is much more

evident when higher Al mole fraction is used. This may indicate a draw back for the implementation of the laterally-gated HFET technology in power amplifier applications that require low voltage operation [46] despite the promising current density gain.

Another parameter that may raise concern is the output conductance (g_o) or slope at saturation region, which increases with the number of channels, specially for the triple- and quad-channel HFETs when x = 0.1. The situation is worsened when x = 0.2, where g_o at $V_{GS} = -1\,V$ is ~96x, ~16x, and ~12x larger than the case when x = 0.1 for the dual-, triple, and quad-channel devices, respectively. This increase in output conductance at higher Al mole fractions marks the impact of higher carrier concentrations of the multiple 2DEGs on the electrostatic control of the gates at higher values of V_{DS}.

4.4 Gate transconductance

4.4.1 Single-channel laterally-gated Ga-face AlGaN/GaN HFET

Figure 4.19 shows the transfer characteristics in terms of the gate transconductance (G_m) vs V_{GS} for the single-channel laterally- and top-gated Ga-face AlGaN/GaN HFETs. Not only from one variety to another but also from a value of Al mole fraction to a higher one, the gate transconductance becomes higher and broader. The laterally-gated HFET offers a ~60% and ~93% improvement in the gate voltage swing (GVS) FOM over the top-gated variety for V_{DS} = 5V when x = 0.1 and 0.2, respectively. This represents a more linear device for being implemented in amplifier applications with low distortion requirements [44]. In the case of a higher Al mole fraction (i.e. x = 0.2), an enhancement in GVS FOM of ~67% is obtained at V_{DS} = 5V. However, it should be noted that even if a higher current density and a broader gate transconductance are obtained with this laterally-gated Ga-face AlGaN/GaN HFET, when Al mole fraction is higher, a

higher induced 2DEG also comes along with a more negative threshold voltage, and the degradation in the drain-induced barrier lowering and V_{knee}.

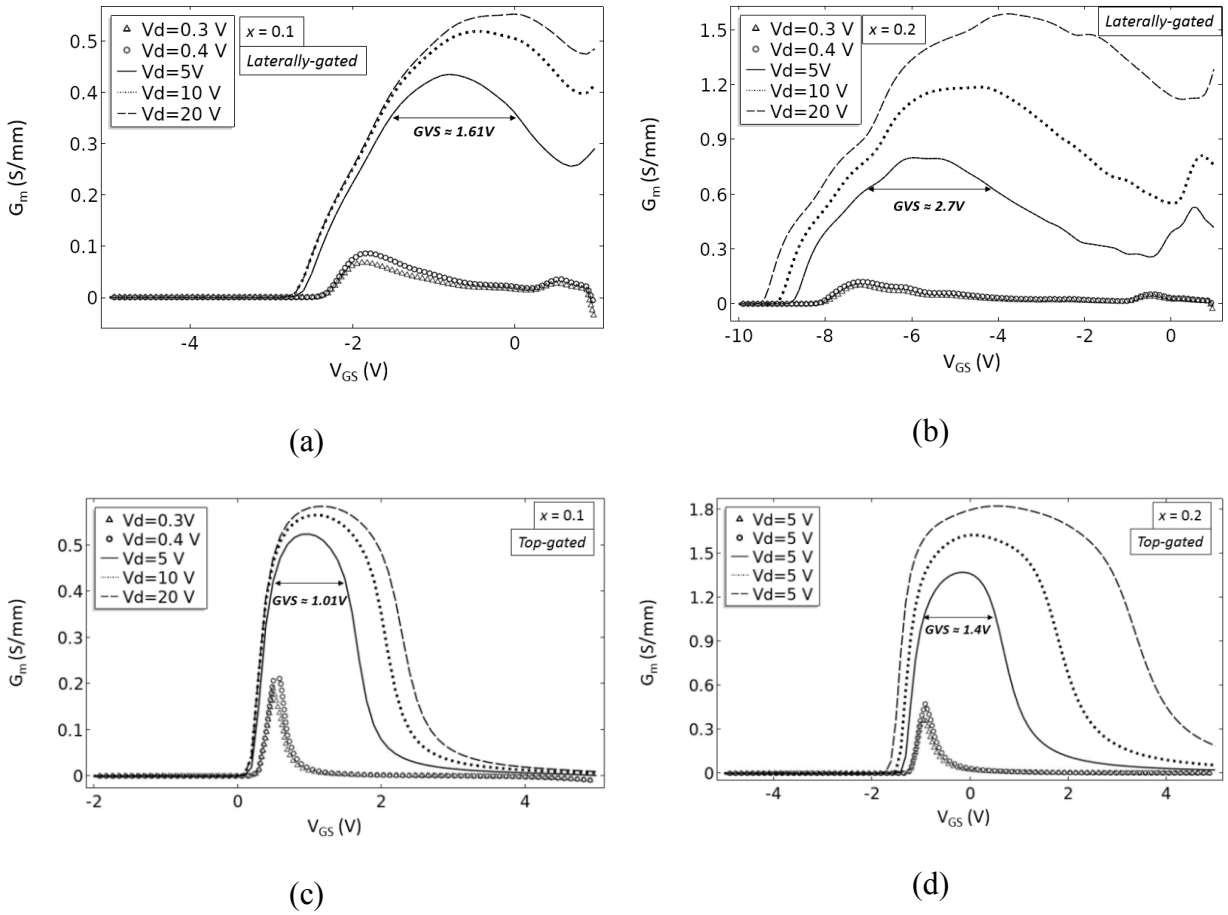

Figure 4.19 Gate transconductance (G_m) vs V_{GS} of the single-channel (a)-(b) laterally-gated and (c)-(d) top-gated Ga-face AlGaN/GaN HFETs for V_{DS} in the linear and saturation regimes and for Al mole fractions of (a),(c) 0.1 and (b),(d) 0.2.

4.4.2 Multi-channel laterally-gated Ga-face AlGaN/GaN HFET

Figure 4.20 shows the gate transconductance (G_m) vs V_{GS} for the dual-, triple-, and quad-channel laterally-gated Ga-face AlGaN/GaN HFETs for V_{DS} in the linear and saturation regimes. Although there is a constant increase in the peak of the gate transconductance with the increase in

the number of channels at both values of Al mole fraction, this is not always the case for GVS FOM, which still shows a slow increase for the case when the Al mole fraction is 0.1, but it seems to reach its maximum value of ~3V when x = 0.2 regardless the number of channels. This limit imposed at x = 0.2 may be caused by the higher induced carrier concentration of the multiple 2DEGs, which produces a higher current density with the number of channels as shown in Figure 4.17.

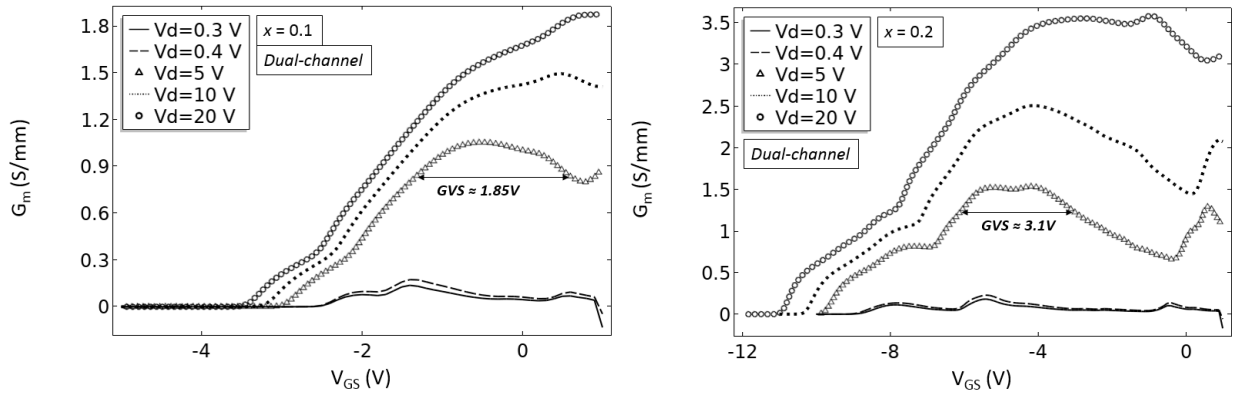

(a)

(b)

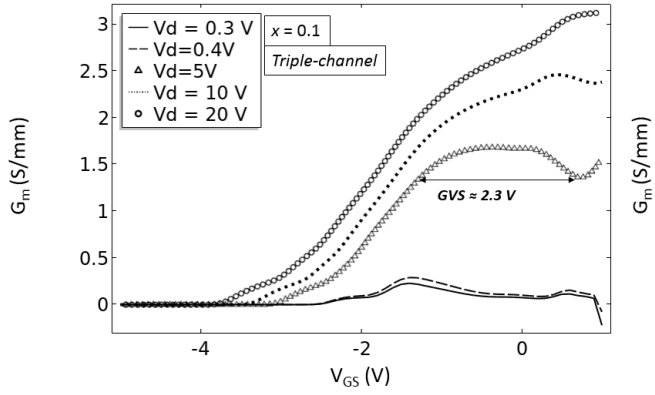

(c)

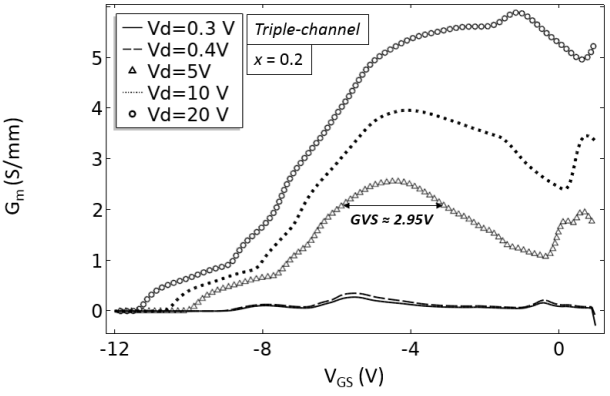

(d)

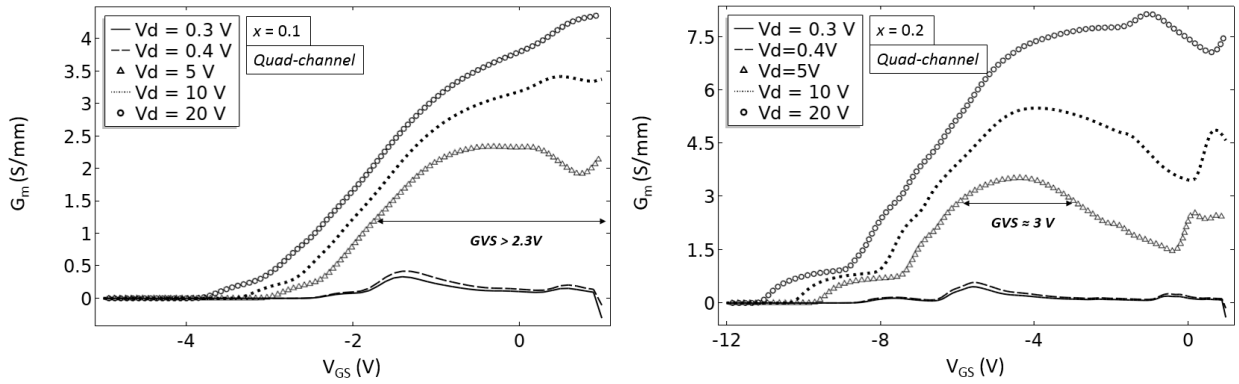

(e) (f)

Figure 4.20 Gate transconductance (G_m) vs V_{GS} for several V_{DS} in the linear and the saturation region of the (a)-(b) dual-, (c)-(d) triple-, and (e)-(f) quad-channel laterally-gated Ga-face AlGaN/GaN HFETs and for the two Al mole fractions of (a),(c),(e) 0.1 and (b),(d),(f) 0.2.

A more detailed illustration about the enhancement in the peak of gate transconductance is provided in Figure 4.21, where the curves for G_m vs V_{GS} are plotted for the four varieties of the laterally-gated Ga-face AlGaN/GaN HFETs (from single- to quad-channel) and for the two values of Al mole fraction under study.

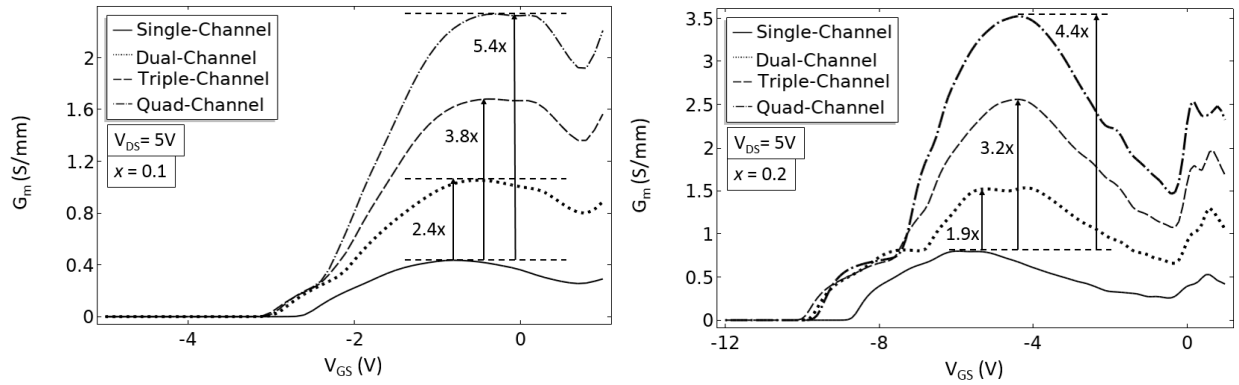

(a) (b)

Figure 4.21 Gate transconductance vs V_{GS} at V_{DS} = 5 V for the single-, dual-, triple-, and quad-channel laterally-gated Ga-face AlGaN/GaN HFET and for the two values of Al mole fraction of (a) 0.1 and (b) 0.2.

It is worth noting that the enhancement in gate transconductance has an almost linear dependence with the number of channels for both cases of Al mole fraction. This dependence is presented by Figure 4.22.

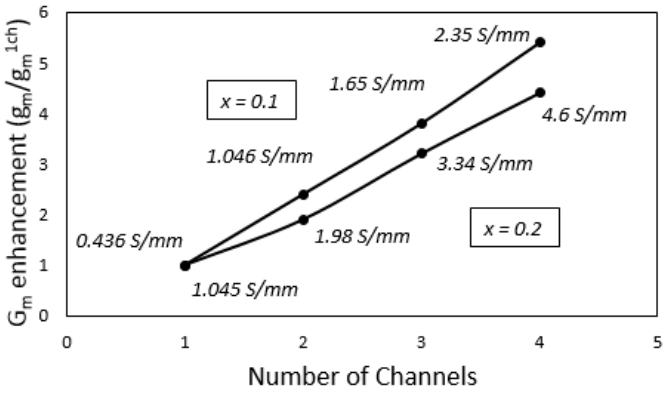

Figure 4.22 Gate transconductance enhancement dependence on the number of channels in the multi-channel laterally gated Ga-face AlGaN/GaN HFET for Al mole fractions of 0.1 and 0.2.

4.5 Chapter conclusions

- The V_{TH} is considerably more impacted by both the Al mole fraction and the W_{ch} in the laterally-gated Ga-face variety than in the top-gated one.
- The control of the multiple 2DEGs stacked vertically is also achieved in the multi-channel laterally-gated Ga-face variety by assuring electric potentials of close values among the channels.
- The alleviation of the peak of the electric field close to the gate in the single- and multi-channel laterally-gated Ga-face varieties compared to the top-gated ones promises a solution to obtain higher breakdown voltages while offering higher current densities.
- The multi-channel laterally-gated Ga-face AlGaN/GaN HFETs offer also current density and gate transconductance enhancements along with larger gate voltage swing figure of merit for their implementation in high power applications that require low

distortion. Also, the attenuation in ON resistance with the number of channels indicates an improvement in power management at higher current densities.

- The degradation of drain-induced barrier lowering with the increase in both the number of channels and values of Al mole fraction in the multi-channel laterally-gated Ga-face varieties should be evaluated with caution for high voltage applications despite the benefits of current density enhancement, ON resistance attenuation, and higher linearity.
- The multi-channel laterally-gated Ga-face varieties show a subthreshold swing closed to that of the laterally-gated single-channel varieties, indicating little degradation with the number of channels. However, the single-channel top-gated variety outperforms the laterally-gated one regarding this characteristic.
- As in the case of the polarization-less laterally-gated AlGaN/GaN HFETs, both the gate transconductance enhancement and the ON resistance attenuation follow an almost linear relationship with the number of channels in the Ga-face variety.

Chapter 5

Conclusion and future work

5.1 Conclusion

- This thesis has presented the steps to properly model single- and multi-channel laterally-gated AlGaN/GaN heterojunction field effect transistors (HFETs) with and without the appreciation of polarization.
- Analysis of their DC characteristics and comparisons against the top-gated varieties were also performed, showing that the laterally-gated devices outperform the top-gated ones in terms of gate voltage swing figure of merit and also in terms of current density.
- In addition, it is demonstrated that the controllability of multiple 2DEGs is quite efficiently achieved using lateral gates thanks to the closeness and presence of double Schottky contacts not only to the channel but also to the AlGaN and GaN layers.
- This controllability of the multiple channels stacked vertically is achieved in both varieties (in absence and presence of polarization) using the same technique of maintaining similar potentials between channels. However, the thicknesses of the GaN channel layers of the middle and top channels are different between the two device varieties due to the difference in sheet charge densities of the channels.
- We have shown that the threshold voltage is considerably more impacted by both the channel width and the Al mole fraction in the laterally-gated Ga-face AlGaN/GaN HFETs than in the polarization-less varieties, which indicates a challenge for the lateral E-field to effectively deplete the 2DEG at higher carrier concentrations of the channel.

This may make one look at other alternatives such as adding a gate at the top as a third mechanism to deplete the channel faster.

- It has also been observed that V_{knee} becomes considerably degraded in the laterally-gated varieties in absence and presence of polarization, and with the increase in both the number of channels and Al mole fraction for the case of the Ga-face varieties, setting a point of evaluation for power amplifier applications at low voltages.
- The gate voltage swing figure of merit (GVS FOM) demonstrates to have an improvement in the multi-channel laterally-gated varieties in absence and presence of polarization. However, when a higher Al mole fraction of 0.2 is used in the Ga-face varieties, the GVS FOM keeps approximately the same value regardless of the number of channels and the G_m enhancement.
- A linear relationship between the G_m enhancement and the number of channels has been reported for both cases: with the assumption of no polarization and when polarization was realistically incorporated.
- In addition, R_{on} is observed to reduce in the laterally-gated multi-channel device varieties in absence and presence of polarization, representing an improvement in power consumption at the offered higher current densities. This reduction of R_{on} with the number of channels also exhibits a linear relationship.
- Additionally, *DIBL* has been observed in the single-channel top-gated variety to be smaller than that of the laterally-gated variety in absence and presence of polarization, where its value tends to degrade with the increase in the number of channels and with higher Al mole fractions, which may mark a draw back for the laterally-gated devices in terms of the V_{DS} dependence of the controllability of the gates over the channels.

This should be looked with attention because the device may be more sensitive to short channel effects despite the promising results in terms of linearity, R_{on}, and higher current densities.

- It has also been observed that considering the device structures studied in this thesis, the subthreshold swing (*SS*) in the laterally-gated varieties is not as good as in top-gated ones, but in Ga-face polarity it is smaller than that of the polarization-less device, getting closer to the ideal value of 60 mV/dec.

5.2 Contributions

- This thesis makes up for the lack of information regarding the modeling and in-depth analysis of thermal equilibrium observations and DC characteristics of single- and multi-channel laterally-gated AlGaN/GaN HFETs with the assumption of no polarization resembling the N-face polarity and with the incorporation of the realistic Ga-face polarity.
- Detail explanations about the calculations of AlGaN alloy parameters and polarization parameters as well as the method used to implement them for realistic modeling scenarios are provided.
- Reports about the exploration of the incorporation of multiple channels in laterally-gated AlGaN/GaN HFETs along with their benefits and cons against single-channel laterally- and top-gated varieties is very limited. This research helps clarify steps on their implementation and provide results that serve to evaluate their behavior in DC.
- The techniques developed in the software tool to speed up the time of convergence in computations and achieve reliable results are not evident or documented in manuals.

This thesis offers the knowledge that help optimize the time of design and simulations in 3-D modeling of semiconductor devices.

5.3 Future work

5.3.1 Incorporation of non-idealities

The current densities obtained by simulation of the laterally-gated multi-channel Ga-face AlGaN/GaN HFETs are very high compared to experimental reports on GaN HFETs. This difference might be caused by secondary effects built into Comsol, such as a large amount of electrons caused by an ideal ohmic contact at the source, the lack of consideration of both the quantum effect and the change of the properties of the material at higher temperatures product of the self-heating of the transistor at higher current densities, and the involved scattering mechanisms in our simulations. All these issues, which are also product of the immaturity of this technology, impact the current density, among other things. For a more thorough study I suggest taking those into account.

5.3.2 Breakdown and RF Characteristics

Only DC characteristics were modeled and analyzed in this thesis. Now that the process of software tuning to achieve convergence in every variety of the laterally-gated AlGaN/GaN HFETs at different Al mole fractions has been completed, the same models can be used to continue the investigation on their performance at high frequencies and also at voltages close to breakdown. This exploration along with the incorporation of non-idealities described in the previous section

offers a very interesting opportunity to continue learning about this new technology that seems to be promising for the latest applications in telecommunications and power electronics industries.

5.3.3 Microfabrication

After exposing the intricacies of modeling laterally-gated single- and multi-channel AlGaN/GaN HFETs, a next phase on the exploration of these devices can be marked by their fabrication in order to not only compare the reliability of the simulations but also to continue improving the modeling techniques and applying again the new changes in the physical device according to new simulation results. This cycle is what finally gives the possibility to propose a real device that could be tested in a lab.

Bibliography

[1] M. Asif Khan, A. Bhattarai, J. N. Kuznia, and D. T. Olson, "High electron mobility transistor based on a GaN-AlxGa1-xN heterojunction," *Applied Physics Letters,* vol. 63, no. 9, pp. 1214 - 1215, 1993.

[2] O. Ambacher, J. Smart, J. R. Shealy, N. G. Weimann, K. Chu, M. Murphy, R. Dimitrov, L. Wittmer, M. Stutzmann, W. Rieger, and J. Hilsenbeck, "Two-dimensional electron gases induced by spontaneous and piezoelectric polarization charges in N- and Ga-face AlGaN/GaN heterostructures," *J. Appl. Phys.,* vol. 85, no. 6, pp. 3222-3233, 15 March 1999.

[3] P. Valizadeh, Field Effect Transistors, A Comprehensive Overview: From Basic Concepts to Novel Technologies, Wiley, February 2016.

[4] O. Ambacher, B. Foutz, J. Smart, J. R. Shealy, N. G. Weimann, K. Chu, M. Murphy, A. J. Sierakowski, W. J. Schaff, L. F. Eastman, R. Dimitrov, A. Mitchell, and M. Stutzmann, "Two dimensional electron gases induced by spontaneous and piezoelectric polarization in undoped and doped AlGaN/GaN heterostructures," *J. Appl. Phys.,* vol. 87, no. 1, pp. 334-344, 2000.

[5] T. Palacios, A. Chakraborty, S. Rajan, C. Poblenz, S. Keller, S. Denbaars, J. Speck, and U. Mishra, "High-power AlGaN/GaN HEMTs for Ka-band applications," *IEEE Electron Device Letters,* vol. 26, no. 11, pp. 781-783, 2005.

[6] M. Micovic, A. Kurdoghlian, A. Margomenos, D. F. Brown, K. Shinohara, S. Burnham, I. Milosavljevic, R. Bowen, A. Williams, P. Hashimoto, R. Grabar, C. Butler, A. Schmitz, P. J. Willadsen, and D. H. Chow, "92–96 GHz GaN power amplifiers," *EEE MTT-S Int. Microw. Symp. Dig.,* pp. 1-3, 2012.

[7] B. Romanczyk, M. Guidry, S. Wienecke, H. Li, E. Ahmadi, X. Zheng, S. Keller, and U. K. Mishra, "W-band N-polar GaN MISHEMTs with high power and record 27.8% efficiency at 94 GHz," *IEDM Tech. Dig.,* p. 3.5.1—3.5.4, 2016.

[8] K. Inoue, H. Yamamoto, K. Nakata, F. Yamada, T. Yamamoto, and S. Sano, "Linearity Improvement of GaN HEMT for RF Power Amplifiers," *Proc. IEEE Compound Semiconductor Integr. Circuit Symp. (CSICS),* pp. 1-4, 2013.

[9] S. Joglekar, U. Radhakrishna, D. Piedra, D. Antoniadis, and T. Palacios, "Large signal linearity enhancement of AlGaN/GaN high electron mobility transistors by device-level Vt engineering for transconductance compensation," *IEDM Tech. Dig.,* p. 25.3.1—25.3.4, 2017.

[10] D. S. Lee, H. Wang, A. Hsu, M. Azize, O. Laboutin, Y. Cao, J. W. Johnson, E. Beam, A. Ketterson, M. L. Schuette, P. Saunier, and T. Palacios, "Nanowire Channel InAlN/GaN

HEMTs With High Linearity of gm and fT," *IEEE Electron Device Letters,* vol. 34, no. 8, pp. 969-971, 2013.

[11] K. Zhang, Y. Kong, G. Zhu, J. Zhou, X. Yu, C. Kong, Z. Li, and T. Chen, "High-Linearity AlGaN/GaN FinFETs for Microwave Power Applications," *IEEE Electron Device Letters,* vol. 38, no. 5, pp. 615-618, 2017.

[12] J. Joh and J. A. del Alamo, "Mechanisms for Electrical Degradation of GaN High-Electron Mobility Transistors," *IEDM Tech. Dig.,* pp. 1-4, 2006.

[13] T. Fang, R. Wang, H. Xing, S. Rajan, and D. Jena, "Effect of Optical Phonon Scattering on the Performance of GaN Transistors," *IEEE Electron Device Letters,* vol. 33, no. 5, p. 709—711, 2012.

[14] S. Bajaj, O. F. Shoron, P. S. Park, S. Krishnamoorthy, F. Akyol, T.-H. Hung, S. Reza, E. M. Chumbes, J. Khurgin, and S. Rajan, "Density-dependent electron transport and precise modeling of GaN high electron mobility transistors," *Applied Physics Letters,* vol. 107, no. 15, pp. 153504-1 - 153504-2, 2015.

[15] K. Shinohara, C. King, A. D. Carter, E. J. Regan, A. Arias, J. Bergman, M. Urteaga, and B. Brar, "GaN-Based Field-Effect Transistors With Laterally Gated Two-Dimensional Electron Gas," *IEEE Electron Device Lett.,* vol. 39, no. 3, p. 417–420, March 2018.

[16] O. Odabası, D. Yılmaz, E. Aras, K. Asan, S. Zafar, B. Akoglu, B. Bütün, and E. Özbay, "AlGaN/GaN-Based Laterally Gated High-Electron-Mobility Transistors With Optimized Linearity," *IEEE Electron Device Letters,* vol. 68, no. 3, pp. 1016 - 1023, 2021.

[17] M. Samizadeh Nikoo, G. Santoruvo, C. Erine, A. Jafari, and E. Matioli, "On the Dynamic Performance of Laterally Gated Transistors," *IEEE Electron Device Letters,* vol. 40, no. 7, p. 1171—1174, July 2019.

[18] G. Santoruvo and E. Matioli, "In-Plane-Gate GaN Transistors for High-Power RF Applications," *IEEE Electron Device Lett.,* vol. 38, no. 10, p. 1413–1416, October 2017.

[19] J. Ma, C. Erine, P. Xiang, K. Cheng, and E. Matioli, "Multi-channel tri-gate normally-on/off AlGaN/GaN MOSHEMTs on Si substrate with high breakdown voltage and low ON-resistance," *Applied Physics Letters,* vol. 113, no. 24, pp. 242102-1 - 242102-5, 2018.

[20] L. Nela, J. Ma, C. Erine, P. Xiang, T. Shen, V. Tileli, T. Wang, K. Cheng, and E. Matioli, "Multi-channel nanowire devices for efficient power conversion," *Nature Electronics,* no. 4, p. 284–290, 2021.

[21] J. Ma, C. Erine, M. Zhu, N. Luca, P. Xiang, K. Cheng, and E. Matioli, "1200 V Multi-Channel Power Devices with 2.8 2.8 Ω·mm ON-Resistance," *IEEE IEDM,* p. 4.1.1—4.1.4, 2019.

[22] C. Erine, J. Ma, G. Santoruvo, and E. Matioli, "Multi-channel AlGaN/GaN in-plane-gate field-effect transistors," *IEEE Electron Device Lett.,* vol. 41, no. 3, p. 321–324, March 2020.

[23] https://www.comsol.com, accessed May 2019.

[24] F. Yun, M. A. Reshchikov, L. He, T. King, H. Morkoc, S. W. Novak, and L. Wei, "Energy band bowing parameter in AlxGa1-xN alloys," *Journal of Applied Physics,* vol. 92, no. 8, pp. 4837 - 4839, 2002.

[25] M. E. Levinshtein, S. L. Rumyantsev, and M. S. Shur, Properties of Advanced Semiconductor Materials, New York: John Wiley & Sons, 2011.

[26] M. A. Khan, J. M. Van Hove, J. N. Kuznia, and D. T. Olson, "High electron mobility GaN/AlxGa1−xN heterostructures grown by low-pressure metalorganic chemical vapor deposition," *Applied Physics Letters,* vol. 58, no. 21, pp. 2408-2410, 1991.

[27] W. H. Sun, J. W. Yang, J. P. Zhang, M. E. Gaevski, C. Q. Chen, J. W. Li, Z. Gong, M. Su, and M. A. Khan, "n-Al0.75Ga0.25N epilayers for 250 nm emission ultraviolet light emitting diodes," *physica status solidi (c),* vol. 2, no. 7, pp. 2083-2086, 2005.

[28] Y. Xi, K. Chen, F. Mont, J. Kim, E. Schubert, W. Liu, X. Li, and J. Smart, "Comparative study of n-type AlGaN grown on sapphire by using a superlattice layer and a low-temperature AlN interlayer," *Journal of Crystal Growth,* vol. 299, no. 1, pp. 59-62, 2007.

[29] T. Tanaka, A. Watanabe, H. Amano, Y. Kobayashi, I. Akasaki, S. Yamazaki, and M. Koike, "p-type conduction in Mg-doped GaN and Al0.08Ga0.92N grown by metalorganic vapor phase epitaxy," *Applied Physics Letters,* vol. 65, no. 5, pp. 593-594, 1994.

[30] S.-R. Jeon, Z. Ren, G. Cui, J. Su, M. Gherasimova, J. Han, H.-K. Cho, and L. Zhou, "Investigation of Mg doping in high-Al content p-type AlxGa1−xN (0.3<x<0.5)," *Applied Physics Letters,* vol. 86, no. 8, pp. 082107-1 - 082107-3, 2005.

[31] E. F. Schubert, "Delta doping of III-V compound semiconductors: Fundamentals and device applications," *J Vac Sci & Technol A,* vol. 8, no. 3, pp. 2980-2996, 1990.

[32] F. Bernardini, V. Fiorentini, and D. Vanderbilt, "Spontaneous polarization and piezoelectric constants of III-V nitrides," *Physical Review B,* vol. 56, no. 16, p. R10024—R10027, 1997.

[33] K. Shimada, T. Sota, and K. Suzuki, "First-principles study on electronic and elastic properties of BN, AlN, and GaN," *Journal of Applied Physics,* vol. 84, no. 9, pp. 4951 - 4958, 1998.

[34] K. Shimada, T. Sota, K. Suzuki, and H. Okumura, "First-Principles Study on Piezoelectric Constants in Strained BN, AlN, and GaN," *Japanese Journal of Applied Physics,* vol. 37, no. Part 2, No. 12A, p. L1421—L1423, 1998.

[35] H. R. Mojaver, Fabrication, and Physics-Based Modeling of Polar AlGaN/GaN and AlInGaN/GaN HFETs, Montreal: Concordia University, 2018.

[36] COMSOL Multiphysics® v. 5.4, Semiconductor Module User's Guide, Part number: CM024101, Stockholm, Sweden: COMSOL AB, 2018.

[37] J. Wong, K. Shinohara, A. L. Corrion, D. F. Brown, Z. Carlos, A. Williams, Y. Tang, J. F. Robinson, I. Khalaf, H. Fung, A. Schmitz, T. Oh, S. Kim, S. Chen, S. Burnham, A. Margomenos, and M. Micovic, "HEMTs, Novel Asymmetric Slant Field Plate Technology for High-Speed Low-Dynamic Ron E/D-mode GaN," *IEEE Electron Device Letters,* vol. 38, no. 1, pp. 95-98, 2017.

[38] M. Allaei, M. Shalchian, and F. Jazaeri, "Modeling of Short-Channel Effects in GaN HEMTs," *IEEE Transactions on Electron Devices,* vol. 67, no. 8, pp. 1-7, 2020.

[39] J. Chung, J. Roberts, E. Piner, and T. Palacios, "Effect of Gate Leakage in the Subthreshold Characteristics of AlGaN/GaN HEMTs," *IEEE Electron Device Letters,* vol. 29, no. 11, pp. 1196-1198, 2008.

[40] S. Arulkumaran, G. I. Ng, C. M. Manojkumar, K. Ranjan, K. L. Teo, O. F. Shoron, S. Rajan, S. B. Dolmanan, and S. Tripathy, "In0.17Al0.83N/AlN/GaN Triple T-shape Fin-HEMTs with gm=646 mS/mm, ION=1.03 A/mm, IOFF=1.13 μA/mm, SS=82 mV/dec and DIBL=28 mV/V at VD=0.5 V," *IEEE Electron Devices Society,* p. 25.6.1—25.6.4, 2014.

[41] C. C. Hu, Modern Semiconductor Devices for Integrated Circuits, Upper Saddle River, NJ: Prentice Hall, 2010.

[42] S. Havanur, "Power MOSFET Basics: Understanding the Turn-On Process," VISHAY SILICONIX, 23 Jun 2015. https://www.vishay.com/docs/68214/turnonprocess.pdf, accessed 29 Jan 2021.

[43] D. A. Neamen, Semiconductor Physics and Devices, New York, NY: McGraw-Hill, 2012.

[44] Y.-W. Jo, D.-H. Son, C.-H. Won, K.-S. Im, J. H. Seo, I. M. Kang, and J.-H. Lee, "AlGaN/GaN FinFET with Extremely Broad Transconductance by Side-wall Wet Etch," *IEEE Electron Device Letters,* vol. 36, no. 10, pp. 1008-1010, 2015.

[45] T. Palacios, S. Rajan, A. Chakraborty, S. Heikman, S. Keller, S. DenBaars, and U. Mishra, "Influence of the dynamic access resistance in the gm and fT linearity of AlGaN/GaN HEMTs," *IEEE Transactions on Electron Devices,* vol. 52, no. 10, p. 2117—2123, 2005.

[46] Z. Zheng, W. Song, J. Lei, Q. Qian, J. Wei, M. Hua, S. Yang, L. Zhang, and K. J. Chen, "GaN HEMT With Convergent Channel for Low Intrinsic Knee Voltage," *IEEE Electron Device Letters,* vol. 41, no. 9, pp. 1304-1307, 2020.

[47] A. Ebbersa, D. Reutera, M. Heukenb, and A. Wiecka, "In-plane gate transistors in AlxGa1−xN/GaN heterostructures written by focused ion beams," *Superlattices and Microstructures,* vol. 33, p. 381–388, 2003.

[48] H. R. Mojaver, F. Manouchehri, and P. Valizadeh, "Theoretical evaluation of two dimensional electron gas characteristics of quaternary AlxInyGa1-x-yN/GaN hetero-junctions," *J. Appl. Phys.,* vol. 119, no. 15, pp. 154502-1–154502-7, April 2016.

[49] H. R. Mojaver, J. L. Gosselin, and P. Valizadeh, "Use of a bilayer lattice-matched AlInGaN barrier for improving the channel carrier confinement of enhancement-mode AlInGaN/GaN hetero-structure field-effect transistors," *J. Appl. Phys.,* vol. 121, no. 24, pp. 244502-1–244502-6, June 2017.

[50] K. Ohi and T. Hashizume, "Drain Current Stability, and Controllability of Threshold Voltage and Subthreshold Current in a Multi-Mesa-Channel AlGaN/GaN High Electron Mobility Transistor," *Jpn. J. Appl. Phys. ,* vol. 48, no. 8, pp. 081002-1 - 081002-5, 2009.

[51] R. S. Howell, E. J. Stewart, R. Freitag, J. Parke, B. Nechay, H. Cramer, M. King, S. Gupta, J. Hartman, M. Snook, I. Wathuthanthri, P. Ralston, K. Renaldo, H. G. Henry, and R. C. Clarke, "The Super-Lattice Castellated Field Effect Transistor (SLCFET): A novel high performance Transistor topology ideal for RF switching," *IEDM Tech. Dig.,* pp. 11.5.1-11.5.4, 2014.

[52] P. S. Park and S. Rajan, "Simulation of Short-Channel Effects in N- and Ga-Polar AlGaN/GaN HEMTs," *IEEE Transactions on Electron Devices,* vol. 58, no. 3, pp. 704-708, 2011.

[53] X.-H. Ma, M. Lü, L. Pang, Y.-Q. Jiang, J.-Z. Yang, W.-W. Chen, and X.-Y. Liu, "Kink effect in current—voltage characteristics of a GaN-based high electron mobility transistor with an AlGaN back barrier," *Chinese Physics B,* vol. 23, no. 2, pp. 027302-1 - 027302-5, 2014.

[54] M. Wang and K. J. Chen, "Kink Effect in AlGaN/GaN HEMTs Induced by Drain, and Gate Pumping," *IEEE Electron Device Letters,* vol. 32, no. 4, pp. 482-484, April 2011.

[55] S. Kasap and P. Capper, Springer Handbook of Electronic and Photonic Materials, Switzerland: Springer, 2017.

[56] H. R. Mojaver and P. Valizadeh, "Reverse Gate-Current of AlGaN/GaN HFETs: Evidence of Leakage at Mesa Sidewalls," *IEEE Transactions on Electron Devices,* vol. 63, no. 4, pp. 1444-1449, 2016.

[57] X. Chen, D. Lv, J. Zhang, H. Zhou, Z. Ren, C. Wang, Y. Wu, D. Wang, H. Zhang, Y. Lei, J. Zhang, and Y. Hao, "Model of Electron Population and Energy Band Diagram of Multiple-Channel GaN Heterostructures," *IEEE TRANSACTIONS ON ELECTRON DEVICES,* vol. 68, no. 4, pp. 1557-1562, 2021.

[58] J. Pinchbeck, K. B. Lee, S. Jiang, and P. Houston, "Dual metal gate AlGaN/GaN high electron mobility transistors with improved transconductance and reduced short channel effects," *Journal of Physics,* vol. 54, no. 105104, pp. 1-7, 2021.